

UNIVERSITY COLLEGE LONDON  
DEPARTMENT OF PHYSICS AND ASTRONOMY

DOCTORAL THESIS

---

**Modelling charge transport in organic  
semiconductors with a fragment-orbital  
based surface hopping method**

---

*Author:*  
Jacob SPENCER

*Supervisor:*  
Prof. Jochen BLUMBERGER

*A thesis submitted in fulfillment of the requirements  
for the degree of Doctor of Philosophy*

*from*  
University College London

January 15, 2017



## Declaration of Authorship

I, Jacob SPENCER, declare that this thesis titled “Modelling charge transport in organic semiconductors with a fragment-orbital based surface hopping method” and the work presented in it are my own. I confirm that this work was done wholly while in candidature for a research degree at University College London. Where I have consulted the published work of others, this is always clearly attributed, and where I have quoted from the work of others, the source is always given. With the exception of such quotations, this thesis is entirely my own work. I have acknowledged all main sources of help. Where the thesis is based on work done by myself jointly with others, I have made clear exactly what was done by others and what I have contributed myself.

Signed:

---

Date:

---



*“By the time you finish elementary school, you know a little. By the time you finish high school, you know a bit more. With a bachelor’s degree, you gain a specialty. A Master’s degree deepens that specialty. Reading research papers takes you to the edge of human knowledge. Once you’re at the boundary, you focus. You push at the boundary for a few years until one day, the barrier gives way: and that dent you’ve made is called a PhD. Of course, the world looks different to you now, so don’t forget the bigger picture. Keep pushing.”*

Matt Might (<http://matt.might.net>), *The Illustrated Guide To A Ph.D.*  
<http://matt.might.net/articles/phd-school-in-pictures/>



## *Abstract*

Charge transport in organic semiconductors is an important current topic of research, but the exact nature of the charge transport remains an unresolved question. Experimental evidence exists to support either of two common models (band-like transport or small polaronic hopping) and various computational simulations suggest that for the standard parameter ranges for organic semiconducting devices, both of these models are likely invalid, with temperatures too high for a band-like transport model and couplings too high relative to the reorganization energy for charge localization to be assumed.

There is potential for a non-adiabatic molecular dynamics method that partially separates classical and quantum degrees of freedom, such as surface hopping, to be applied to the problem. This is what I have begun with my fragment-orbital based surface hopping (FOB-SH) method. Based on Tully's famous fewest-switches surface hopping algorithm, FOB-SH simulates a condensed phase organic semiconductor with a classical molecular dynamics approach while solving the Schrödinger equation to directly model the behaviour of a single excess electronic charge. The latter is made computationally efficient by using an analytic overlap method to calculate the Hamiltonian off-diagonal elements.

In this thesis I discuss in detail the theory behind FOB-SH, along with my first implementation and validation of the method. I present results on two systems, of two and ten 'ethylene-like' molecules respectively. In the two-molecule system I calculate charge transfer rates and find that my method qualitatively agrees with standard charge transfer theory in regimes where agreement is expected, though questions are posed in regimes where standard theory becomes invalid. For the ten-molecule system I demonstrate that charge mobilities can be calculated from my simulations. I observe a thermal activation peak for low couplings and a crossover from activated hopping to band-like transport with increasing temperature, qualitatively agreeing with another similar surface hopping method. I show that FOB-SH has great potential to tackle the charge transport in organics problem.



## *Acknowledgements*

First and foremost I must acknowledge and thank my supervisor, Professor Jochen Blumberger. Without him and his support this project simply would not exist; I am grateful to him for the opportunities I have had while working in his group and for the assistance he has offered during the course of my PhD. Under his supervision I have been able to tackle the greatest challenge of my life so far and turn it into my greatest achievement, while also enjoying many opportunities to present my work in a number of high-profile situations.

I have also had the privilege of working with many dedicated and talented early-career researchers in the Blumberger group. I would like to particularly thank Fruzsina Gajdos, who has been a close collaborator for the entirety of my time at UCL, and whose work is mutually complementary with mine. Others who deserve special thanks include Dr. Antoine Carof (who provided many stimulating discussions which helped me solidify my understanding of my own work, and who now has the task of building on my work to continue this avenue of research) and Laura Scalfi (who offered a much-needed 'fresh pair of eyes' at a late stage and saved me from a few potential disasters). I additionally thank the other members of the Blumberger group that I have worked alongside: Dr. Adam Kubas, Dr. Ehesan Ali and Dr. Marian Breuer; Guido Falk von Rudorff, Hui Yang and Xiuyun Jiang; Jamie Sage, Felix Hoffmann, Siim Valner, Bastian Burger, Karina Chan, Benjamin Rosseau and Dr. Charles Goehry. I sincerely appreciate all the assistance that they have lent me in the past four years and hope that I have been able to repay it in kind.

I wish to thank my family for their unwavering support, kindness and understanding. My parents, themselves both PhDs, presumably appreciate all too well the challenges, the hard work and long hours, the highs and the lows that go into a doctorate. My mother taught me patience, showed boundless compassion, and made me believe that it is okay to risk failure when pursuing one's ambitions. My father gave me my scientific enthusiasm, supported me as I unintentionally followed his path through life, and taught me how to ride a bicycle (a surprisingly essential skill for my PhD, as it turned out). This project would possibly have not

seen completion without their continuing willingness to assist in any way possible. I would accordingly like to dedicate my thesis to them, Patrick and Dorothy Spencer.

Last but not least, I want to acknowledge the friendships I have relied upon and sought joy in for four years. They are an eclectic bunch: friends from my childhood, friends from my undergraduate years, friends who moved to London and friends I made in London. There are honestly too many for me to individually name everyone who deserves it, but worthy of special mention are four of my fellow PhD students and my unofficial 'Fellow PhD support crew': Sam Fayer, Rachel Tilling, Charlotte Ridler and Matthew Barnbrook.

I have been supported by an IMPACT PhD studentship co-sponsored by University College London and the Department of Physics and Astronomy. In testing the methods and obtaining the results within this thesis, I acknowledge the use of the UCL High Performance Computing Facility 'Legion' and associated support services.

# Contents

<b>Declaration of Authorship</b>	<b>3</b>
<b>Abstract</b>	<b>7</b>
<b>Acknowledgements</b>	<b>9</b>
<b>Contents</b>	<b>11</b>
<b>List of Figures</b>	<b>15</b>
<b>List of Tables</b>	<b>21</b>
<b>1 Introduction</b>	<b>23</b>
1.1 Organic semiconductors: an overview . . . . .	23
1.2 Nature of the charge transport . . . . .	26
1.3 Computational evidence: are standard theories applicable? . . . . .	29
1.4 Non-adiabatic molecular dynamics (NAMD) . . . . .	31
1.5 Surface hopping in the literature . . . . .	34
1.6 This thesis . . . . .	37
<b>2 Theory and Derivation of FOB-SH</b>	<b>39</b>
2.1 Solving the electronic Schrödinger equation . . . . .	39
2.2 Site basis representation . . . . .	41
2.3 Nuclear gradients . . . . .	44
2.4 Special case: donor-acceptor complex . . . . .	46
2.5 Efficient calculation of matrix elements and derivatives . . . . .	46

<b>3</b>	<b>Implementation and Validation of FOB-SH</b>	<b>53</b>
3.1	Implementation details . . . . .	53
3.1.1	Molecular dynamics . . . . .	53
3.1.2	Charge dynamics and surface hopping . . . . .	55
3.1.3	Program flow . . . . .	57
3.2	Simulation details . . . . .	59
3.2.1	Model systems . . . . .	59
3.2.2	Force field parameters . . . . .	60
3.3	Tests . . . . .	62
3.3.1	Electronic behaviour and Rabi oscillations . . . . .	62
3.3.2	Nuclear forces and energy conservation. . . . .	64
<b>4</b>	<b>FOB-SH results from a donor-acceptor complex</b>	<b>69</b>
4.1	Simulation details . . . . .	69
4.1.1	Model system . . . . .	69
4.1.2	FOB-SH simulations . . . . .	71
4.1.3	Electron transfer rates . . . . .	72
4.2	Results . . . . .	75
4.2.1	$\lambda$ dependence . . . . .	77
4.2.2	$H_{ab}$ dependence . . . . .	80
4.2.3	$\Delta A$ dependence . . . . .	82
4.3	Discussion . . . . .	85
<b>5</b>	<b>FOB-SH results from a 10-molecule chain</b>	<b>89</b>
5.1	Simulation details . . . . .	89
5.1.1	Model system . . . . .	89
5.1.2	Procedure . . . . .	90
5.2	Results . . . . .	92
5.3	Discussion . . . . .	93
<b>6</b>	<b>Conclusions and Outlook</b>	<b>99</b>
6.1	Conclusions . . . . .	99

6.2 Outlook . . . . . 101

6.3 Final conclusion statement . . . . . 104



# List of Figures

- 1.1 Adiabatic (red) and diabatic (blue) potential energy surfaces for electron transfer, with  $A$  the free energy and  $\Delta E$  the vertical energy gap. The reorganization energy  $\lambda$  is indicated. The adiabatic surfaces are plotted for three different values of the electronic coupling  $H_{ab}$ . . . . . 30
- 3.1 A simplified version of the FOB-SH program flow. Abbreviations are as follows: FO (fragment orbital), DFT (density functional theory), SOMO (singly-occupied molecular orbital), AOM (analytic overlap method), TF (transformation), SH (surface hopping). . . . . 58
- 3.2 Visualizations of the two model systems used in this thesis. Panel A is the ELM dimer, with the molecules initially spaced  $4 \text{ \AA}$  apart. Panel B is the ten-molecule 1D chain, where the intermolecular spacing at initialization is again  $4 \text{ \AA}$ . . . . . 61
- 3.3 The population of each of two sites  $a$  (purple) and  $b$  (yellow) as a function of time. At time  $t = 0$ ,  $|u_a|^2 = 1$  and  $|u_b|^2 = 0$ . There are three sets of curves on this graph: one uses the Runge-Kutta method to propagate the electron, one uses the exponential solution, and one plots the analytic values of  $P_a$  and  $P_b$  as in Eq. 3.16. For each site, the three curves lie exactly on top of each other, showing that the Runge-Kutta method I have used agrees perfectly with exact theory in this simple case . . . . . 63

- 3.4 Nuclear forces obtained from the general  $N$ -site expression, Eq. 2.22, and from the 2-state expression, Eq. 2.36. The  $x$ ,  $y$  and  $z$  components of the nuclear forces in the ELM dimer are plotted as obtained from MD simulation (A) on the adiabatic ground state  $E_0$  with  $\langle |H_{ab}|^2 \rangle^{1/2} = 41$  meV, (B) on the adiabatic ground state  $E_0$  with  $\langle |H_{ab}|^2 \rangle^{1/2} = 8$  meV, (C) on the excited state  $E_1$  with  $\langle |H_{ab}|^2 \rangle^{1/2} = 41$  meV and (D) on the excited state with  $\langle |H_{ab}|^2 \rangle^{1/2} = 8$  meV. **Red crosses** refer to the full force calculation while **green circles** refer to the diagonal forces approximation as described in Table 3.2. . . . . 65
- 4.1 Visualization of the ELM donor-acceptor complex, used here as a test system to study charge transfer rates with respect to the parameters  $\lambda$ ,  $H_{ab}$  and  $\Delta A$ . The non-orthogonal localized site orbitals  $\varphi_1$  and  $\varphi_2$  are shown:  $\varphi_1$  corresponds to a hole fully localized on the left-hand molecule, and  $\varphi_2$  to a hole fully localized on the right-hand molecule. The arrow indicates the direction of hole transfer from ‘initial’ to ‘final’ charge localized states, though it should be noted that this is only intended as a guide to the ‘forward’ direction as the excess hole is never observed to fully re-localize. . . . . 70
- 4.2 A comparison of the population decay calculated with the three methods in Ref. 119: method 1 (circles), method 2 (plusses) and method 3 (diamonds). Each also has an exponential curve fitted to it: method 1 (dotted), method 2 (dashed) and method 3 (dot-dash). I have additionally plotted in red crosses a population decay calculated via method 2 with the decoherence correction, with an exponential fit as a solid red line. . . . . 74

- 4.3 An illustration of the behaviour of a typical trajectory. Panels A, B and C are time series of different properties during a typical FOB-SH simulation. Panel A shows the time evolution of the initial state amplitude  $|u_a|^2$ , including a transfer from initial to final state and back. Panel B shows the time evolution of the diabatic energy gap  $\Delta E$  and panel C shows the active adiabatic state of the system. . . . 76
- 4.4 ET rates for different  $\lambda$  values, obtained from SH simulations, via the population decay method (circle symbols) and transition count method (diamond symbols) against semi-classical ET theory (solid line). I additionally plot the rate of molecular transitions (plus symbols) against the adiabatic ET rate (dashed line) to understand the contribution of nuclear and electronic effects to the rate. . . . . 77
- 4.5 A comparison of the different electronic behaviour for two different values of reorganization energy  $\lambda$ . In panel A,  $\lambda = 0.1$  eV and within ten picoseconds I observe many large-amplitude oscillations, including a number of ‘successful’ transitions. In contrast, panel B has  $\lambda = 0.7$  eV and over the course of a nanosecond trajectory there are only a couple of successful transitions, while for long periods of time the population becomes stuck in a half-and-half state, contributing to the rate by exponential decay but not the rate by transition count. . . . . 79
- 4.6 ET rates calculated for different values of  $\langle |H_{ab}|^2 \rangle^{1/2}$  from the exponential fit method (circle symbols) and transition count method (diamond symbols). They are compared with the generalized semi-classical ET theory (solid line), adiabatic ET theory (dashed line) and Marcus theory (dotted line). . . . . 81

- 4.7 ET rates from FOB-SH MD simulation ( $k_p^{\text{SH}}$ , Eq. 4.5) against average diabatic electronic coupling  $\langle |H_{ab}|^2 \rangle^{1/2}$  (circles). For comparison, the ET rates from semi-classical ET theory, Eq. 1.3 (solid lines), and the respective non-adiabatic limit Eq. 1.1 (dotted line) and adiabatic limit Eq. 1.2 (dashed lines) are displayed. For large electronic coupling, charge relaxation rates from FOB-SH MD simulation are shown ( $t_{\text{max}}^{-1}$ , diamonds). All FOB-SH MD simulations were carried out for  $\lambda=0.3$  eV and  $\Delta A=0$ . . . . . 83
- 4.8 ET rates calculated for different values of driving force  $\Delta A$  from SH simulations via the exponential fit method (circle symbols), plotted against rates obtained from the semi-classical ET theory (solid line). Additionally, a parabola has been fitted to the SH rates, and is denoted by a dot-dash line. . . . . 84
- 4.9 This is similar to Figure 4.8, but in this figure a parabola has instead been fitted to a subset of the SH values. The ‘anomalous’ points at  $\Delta A = -300, -350, -400$  meV have been omitted from this subset. In this case the fit much more closely fits the result of Marcus theory. . . 85
- 5.1 A schematic of the simulation system for charge mobility calculations. 10 ELMs are placed in a chain with intermolecular distances of 4 Å. The three chains in the picture demonstrate the system with a charge localized on ELM 1, 2, and 3. . . . . 90

- 5.2 Temperature dependence of charge mobilities along the 10-molecule ethene-like chain, for three different values of average coupling as displayed. Results from both surface hopping (SH) and kinetic Monte Carlo (KMC) simulations are shown, as are the results of power law fits to the region 300K to 1000K for each coupling regime. For the lowest value, a clear thermal activation peak is visible in the SH results with a maximum mobility at a temperature of around 200K. For higher coupling values, I see a continual decrease in mobility with temperature, corresponding to a band-like transport mechanism. The KMC results contrast with the FOB-SH results, showing a much shallower decrease with temperature after the crossover. . . . 92
- 5.3 Gaussian distributions of the site energy difference between neighbouring molecules in the ELM chain along an initial equilibrium trajectory, for three different values of the temperature within the range plotted in Figure 5.2, and for two different coupling values in two different panels. As the temperature increases, thermal fluctuations in the site energies broaden these distributions. For sufficiently high values of  $\langle |H_{kl}| \rangle$ , as shown in panel A, this reduces the area under the curve that is within the resonance region i.e. between the values  $\Delta E = \pm 2 \langle |H_{kl}| \rangle$  and the mobility thus decreases accordingly with temperature. For smaller values of  $\langle |H_{kl}| \rangle$ , as shown in panel B, this broadening instead allows the area under the curve in the resonance region to increase from zero and thus increasing temperature instead increases mobility - though as Figure 5.2 shows, at some point this behaviour is replaced by a decreasing mobility with temperature. . . 96

- 5.4 The probability of the first two molecules in the ELM chain being in resonance for charge transfer with each other, divided by  $k_B T$ , is plotted against the corresponding mobility value. The trends in the resonance probability for the lowest and highest coupling regimes clearly match with the mobilities. The intermediate coupling regime appears to contain a mixture of the two behaviours. . . . . 97

# List of Tables

3.1	Parameterization of reorganization energy $\lambda$ via the equilibrium charged length of the C=C bond . . . . .	62
3.2	Total energy conservation of FOB-SH simulations for different approximations and corresponding speed-up on a single compute core. The simulations were 1 ns and 0.1 ns in length for the 2 and 10 site simulations respectively. The ionic timestep was 0.5 fs. . . . .	66
4.1	Parameterization of electronic coupling $H_{ab}$ via the constant $C$ (Eq. 2.38). . . . .	71



# Chapter 1

## Introduction

### 1.1 Organic semiconductors: an overview

“Organic semiconductors” refers to a class of carbon-based materials which display semiconductor behaviour when charge carriers are injected or generated. This behaviour has been known for around half a century [1,2] and today organic semiconductors are still the subject of a significant amount of research interest and investment. One characteristic attribute of all organic semiconducting materials is a high degree of dynamic disorder, as unlike inorganic counterparts they are held together in the condensed phase by the relatively weak van der Waals interactions between molecules [3].

Charge transport in organic semiconducting materials attracts a great amount of interest from the scientific community at present [4–14] for a wide range of applications such as organic light-emitting devices [15,16], organic field effect transistors [17,18], thin film transistors [19,20] and organic photovoltaics [21–26]. The last application is particularly appealing from an environmental perspective, as sunlight is a readily-available and sustainable alternative energy source that avoids all the well-known disadvantages of fossil fuels. Inorganic solar cells, which are usually silicon-based, have the disadvantage of an expensive active material [27] so it is hoped, given the sheer variety of organic molecules [28], that a cheaper alternative can be developed. The power conversion efficiency of current-generation organic photovoltaic devices is improving but still limited [29,30] which provides another

motivation for further research. Even if the efficiency of organic photovoltaic devices never reaches that of silicon-based technologies, it is hoped that further research into organic materials will lead to much cheaper possible devices. The environmental advantages of organic electronic technology would be even greater if such devices could be made biodegradable, as is being suggested [31].

Organic electronic devices have various advantages over inorganic electronics: chief among these are that they can be made physically flexible [32, 33] and are relatively inexpensive to produce [34]. On the other hand, organic semiconductors typically have low charge mobilities compared to inorganic counterparts [35–38], which limits the efficiency of any such devices [39]. Progress on designing new organic materials to maximize the charge mobility could be greatly helped by a better theoretical understanding of the exact nature of the charge transport in these systems [4, 40].

From the computational point of view, the main characteristic that hampers the development of such theory and which is common to most organic semiconducting systems (and related systems, such as large single biomolecules) is high simulation requirements. Put simply, organic systems are frequently extremely large - even individual molecules containing tens of atoms, if not more - and therefore any method such as density functional theory (DFT) which attempts to simulate a sufficiently large system (at least a few thousand atoms, and possibly more to properly investigate charge transport in the condensed phase) will correspondingly be extremely slow [41]. Furthermore, such systems display a great deal of dynamic disorder arising from the aforementioned relative weakness of the van der Waals intermolecular forces.

There are other specific challenges that organic semiconducting systems present to computational investigation. In contrast to inorganic semiconductors, the electron-phonon coupling in these systems is often sufficiently large to play a prominent role in the dynamics [42, 43]. In limits where this coupling dominates over the intermolecular electronic coupling, a small polaronic deformation can form to trap a

charge onto a single molecular site (as discussed in the next section). In the opposite case, where the electronic coupling is large compared with the electron-phonon coupling, these parameters take similar values to those in an inorganic semiconductor, such as amorphous silicon. One might therefore imagine that the electronic structure of the system is likely to resemble the band structure of an inorganic semiconductor, but the physical structure of the two types of systems is so different that this seems like an overly bold assumption. It is fair to say that these two limiting cases alone are insufficient to describe charge transport across the family of possible organic semiconducting materials, where the relative strengths of these two interactions are capable of taking a large range of values.

The strong connection between the nuclear and the electron dynamics throws up a difficult question regarding the relative timescales of different degrees of freedom. Both local (arising from intramolecular interactions) and non-local (arising from intermolecular interactions) electron-phonon coupling must be taken into account. These correspond to dynamic disorder in the diagonal and off-diagonal elements of the electronic Hamiltonian, respectively. The intramolecular nuclear vibrations in organic semiconductors, which are made of either polymers or pi-bonded molecules, can be associated with the stretch frequency of the carbon-carbon bond (which is on the order of  $10^{14} \text{ s}^{-1}$ ). The nature of the intermolecular behaviour is much more varied between different molecules, but is likely to include elements of both translational and rotational movement. An example that can be considered is the  $\text{C}_{60}$  molecule, which freely rotates within its crystal structure at room temperature [44] with a rotational relaxation time on the order of 10 ps [45]. Thus, simulations of organic semiconductors may need to cover long timescales (on the order of nanoseconds) but with a small timestep (on the order of femtoseconds), to capture a range of different molecular behaviours.

It is thus clear that a method which attempts to simulate the entire system in a quantum-mechanical framework will be impractical, and a further approximation (such as classical molecular dynamics) will have to be made for the sake of computational efficiency: nonetheless, as the crucial question is the behaviour of an

excess electron or electronic hole, quantum mechanics must still play a part in the simulation.

## 1.2 Nature of the charge transport

There are two traditional theoretical descriptions of the charge transport: one is based on a band-like conduction mechanism similar to inorganic semiconductors [46, 47], and the other on polaronic carriers hopping between molecules or fragments [4, 6, 48, 49]. While intuitive and simple, neither of these two limiting cases provides a generally satisfactory description, as has been noted in the literature [50–54]. Some more recent investigations specifically into organic semiconductors propose localization over a few molecules, induced by fluctuating electronic coupling between molecules [55, 56]. The search for materials that will be useful for the next generation of electronic devices is at present hampered by the lack of an adequate theory to fully explain the mechanism of charge transport in such systems.

One possible issue is that the sheer variety of possible organic molecular semiconductors makes it hard to apply any single theory to the problem of charge transport. This speaks both to the number of possible organic semiconducting molecules, and also to the different phases that they can take in physical devices [57–61]. Coropceanu et al. [3, 4] argue for a clear distinction between pure single molecular crystals and more disordered systems when looking at temperature dependence, finding that the former tends to display a behaviour  $\mu \propto T^{-n}$ , where  $n$  is usually 0.5–3.0 [62] while the latter are more likely to demonstrate thermally-activated hopping behaviour. This also fits with the argument of Troisi [47], who suggests that the eventual electronic behaviour is extremely sensitive to e.g. deposition conditions. Even within a single system, charge mobility and potentially even the nature of charge transport may be subject to strong anisotropy [63].

Karl [64] reviews the experimental evidence on charge transport and suggests that at low temperatures, the underlying process in organic semiconductors is band transport: as increasing temperature increases the electron-phonon coupling, charge

hopping becomes the dominant mechanism. This implies an intermediate temperature region during which both mechanisms co-exist in some way, and neither description of charge transport is an accurate depiction. More recently, Sirringhaus et al. [65] focus specifically on high-mobility organic semiconductors and similarly highlight conflicting experimental evidence. Podzorov et al. [66] observe a crossover with increasing temperature from trap-dominated charge hopping to bandlike charge transport on the surface of a rubrene crystal: it is important to distinguish between observed surface and bulk electronic behaviour, as there are reasons to believe that the charge behaviour can be very different between the two [67].

To give an example in a different system, Marumoto et al. [68] examine the spatial extent of the electronic wavefunction in a pentacene crystal and find it to be on the order of 10 molecules: this contradicts the small polaronic picture, which assumes a localization length of around a single molecule. The unexpectedly large extent of the wavefunction suggests that the charge is not at any point meaningfully 'trapped' by the environment and thus a polaron does not form: in the absence of this behaviour, band-like transport is assumed to take place.

In contrast, Tsao and Lin [69] conclude, from their observations of strong temperature dependence of charge mobility in pentacene, that the charge transport in pentacene must be dominated by hopping. At low temperatures they find that charge transport through the material takes place via tunnelling between nuclear sites, while increased temperature causes dynamic disorder between the molecules which allows for occasional charge 'escape' and thus charges hop between sites. These two studies cannot be simply reconciled: the most likely explanation is that differences in the experimental procedures have led to different charge transport behaviour in the two systems.

Sakanoue and Sirringhaus [70] study a pentacene derivative, TIPS-pentacene, and also suggest for this molecule that at room temperature the charge carrier is localized over more than one molecule. They note, however, that this localization length cannot be macroscopic. Additionally, the localization is not polaronic i.e. the

charge carrier is not localized as a result of environmental response, but due to dynamic disorder of the surroundings [71]. This interpretation supports the dynamic localization model of Troisi et al. [72,73].

Less direct evidence on the nature of charge transport comes from experimental studies on organic semiconductors which estimate the relevant parameters for charge transport, such as reorganization energy and electronic coupling. I present as an example a publication from Imahori et al. [74] studying charge transfer between porphyrins and fullerenes, finding that the reorganization energy for the process is small (on the order of 0.1 eV) and crucially of similar size to the electronic coupling. This close parity between these two parameters casts doubt on the certainty of charge localization and therefore on hopping as the mechanism for charge transport.

It seems likely from the experimental evidence that physical organic semiconductors see a variety of charge transport behaviours, determined by factors such as the degree of disorder, the nature of the molecules themselves, and the temperature of the system. This would suggest that experiment is limited in how much insight it can give us on the question, at least when compared to computational methods which in principle could be employed to simulate the full range of possible parameters that may effect different forms of charge transport. At present, however, such techniques are still in their infancy, in part because the polaronic model of charge transport is still sufficiently convenient (and gives results sufficiently close to experiment) that it is tempting to use it and ignore the question of whether or not it applies. The problems with this approach go beyond experiment, however, and I shall now explain how in many organic semiconductors a so-called 'hopping' picture simply cannot be truly accurate.

### 1.3 Computational evidence: are standard theories applicable?

The standard way to calculate a charge transfer rate still goes back to the celebrated Marcus equation [75,76]:

$$k_{\text{ET}} = \frac{2\pi}{\hbar} \langle |H_{ab}|^2 \rangle_{\text{TS}} (4\pi\lambda k_{\text{B}}T)^{-1/2} \exp\left(-\frac{\Delta A_{\text{na}}^\ddagger}{k_{\text{B}}T}\right). \quad (1.1)$$

where  $H_{ab}$  is the electronic coupling between initial and final states,  $\lambda$  the reorganization energy,  $T$  the temperature and  $\Delta A_{\text{na}}^\ddagger$  is the activation energy for charge transfer, which depends on  $H_{ab}$  and the reorganization energy  $\lambda$ . This equation assumes a non-adiabatic charge transfer from initial to final state: in other words, that the charge is localized at a given time in either the initial or final well. Other equivalent expressions exist for the cases in which this assumption is invalid: there is the adiabatic rate expression [77],

$$k_{\text{ad}} = \nu_{\text{n}} \exp\left(-\frac{\Delta A^\ddagger}{k_{\text{B}}T}\right), \quad (1.2)$$

and a generalized semi-classical rate expression which interpolates between the two [78,79]

$$k_{\text{sc}} = \kappa_{\text{el}} \nu_{\text{n}} \exp\left(-\frac{\Delta A^\ddagger}{k_{\text{B}}T}\right). \quad (1.3)$$

where  $\kappa_{\text{el}}$  is the Landau-Zener electronic transmission coefficient and  $\nu_{\text{n}}$  is the nuclear attempt frequency. In the literature, Eqs. 1.2 and 1.3 generally contain a nuclear tunnelling factor, which I have assumed to be unity.

Eq. 1.3 most straightforwardly illustrates the three components of each of these equations. The assumption is that there is some barrier to charge transfer, given by  $\Delta A^\ddagger$ : then the rate equation consists of the Boltzmann probability of climbing that barrier, a nuclear attempt frequency  $\nu_{\text{n}}$ , and an electronic transmission coefficient  $\kappa_{\text{el}}$ . Obviously this picture - of charge transfer from initial to final states, modulated by a barrier - breaks down in the absence of a barrier. As

the barrier height  $\Delta A^\ddagger$  is a function of the parameters reorganization energy  $\lambda$  and electronic coupling  $H_{ab}$ , it is possible for this barrier to be zero, as illustrated in Figure 1.1.

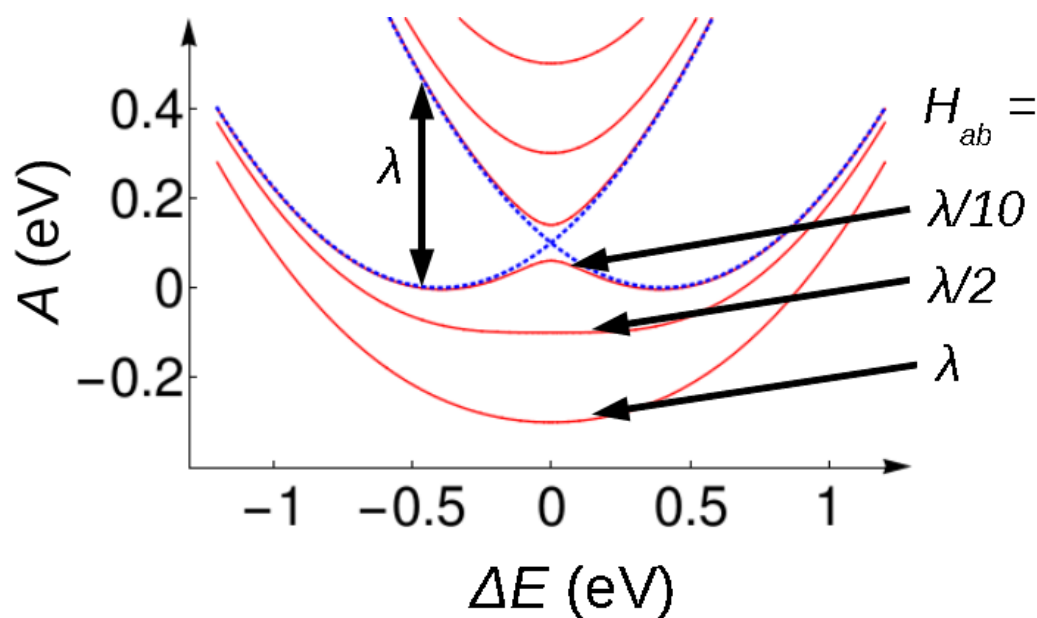


FIGURE 1.1: Adiabatic (red) and diabatic (blue) potential energy surfaces for electron transfer, with  $A$  the free energy and  $\Delta E$  the vertical energy gap. The reorganization energy  $\lambda$  is indicated. The adiabatic surfaces are plotted for three different values of the electronic coupling  $H_{ab}$ .

Organic semiconductors are often characterized by reorganization energies similar to or not much larger than the intermolecular coupling [80], and thus individual intermolecular configurations within condensed phase organic systems may frequently display a non-existent barrier to charge transport. Within my own research group, simulations have been published demonstrating this problem on C60 [51] and its derivative molecule PCBM [52]. Other researchers have suggested similar issues with organic molecules, such as Cheung and Troisi [53] and Ide et al. [81], both also with PCBM.

The problem with organic semiconductors is broadly stated thus: the nuclear and the electronic dynamics are too strongly coupled to assume polaronic transport, and the dynamic disorder is too high to assume band-like transport. There is a clear need for methods which do not rely on either assumption. Various such methods have been developed in the scientific community, or more broadly to tackle the

problem of charge transport in organic semiconductors through simulation. These include, for example, the work of Troisi et al. on a 1D model of harmonic oscillators [55,82,83]; a similar 1D model by Wang and Beljonne [84,85]; a method from Ren et al. [8] that atomistically simulates a pentathiophene layer, although neglecting the effects of the excess charge carrier on the nuclear system; the approach of Kubar and Elstner, based in SCC-DFTB, which has been successfully applied to biomolecules as well as to organic semiconductors [50,86–88]; the generalized nonadiabatic transition state theory of Zhao et al. [89]; and the PYXAID program from Akimov and Prezhdo [90–92]. This last is an example of an implementation of a non-adiabatic molecular dynamics approach, a family of methods which I shall now explain in more detail.

## 1.4 Non-adiabatic molecular dynamics (NAMd)

The starting assumption in standard molecular dynamics (MD) for modelling most chemical reactions is the Born-Oppenheimer approximation [93], in which the system evolves on a single adiabatic potential energy surface and the electronic motion is sufficiently fast that they can be assumed to instantaneously react to nuclear motion. In practice, this state is most usually the ground state of the system. There are many physical and chemical problems of interest where the Born-Oppenheimer approximation is invalid [94], and in such cases one needs to move beyond the separation of classical and quantum degrees of freedom by accounting for the effect of each on the other.

It is perhaps intuitive that one possible way of overcoming the difficulties inherent with treating a system at multiple different timescales would be to use a method which combines some aspects of both quantum mechanical theory and classical mechanics. The family of methods which use this approach are known as non-adiabatic molecular dynamics (NAMd) [95,96] or alternatively mixed quantum-classical dynamics (MQCD) [97,98] The typical picture [99] is to consider a ‘quantum subsystem’ which is embedded within a larger, classically treated system: for example, a single electron or fast-moving ion within a molecular framework.

The simplest version of a NAMD method is known as the classical path approximation, as used in e.g. the PYXAID program [90]. In this instance, the influence of the quantum subsystem on the classical system is assumed to be negligible: meanwhile the quantum subsystem evolves in a time-dependent potential which arises from the classical system. This approximation is valid in systems where the energy of quantum transitions is very small compared to the thermal energy of the classical particles, and breaks down if this is not the case [100]. In such cases, both quantum and classical parts must see the other as a time-dependent potential.

The majority of NAMD methods therefore treat both directions of feedback (the classical system on the quantum subsystem, and also vice versa) I shall broadly discuss them in terms of two categories: mean-field (MF) dynamics, and surface hopping methods. There are, however, alternative methods which do not fit into either of these two, such as the exact factorization approach published by e.g. Abedi et al. [101–103] and a combination of the two from Prezhdo and Rossky [104].

The most common form of MF dynamics is known as the Ehrenfest method [105–107], which has a related method known as time-dependent self-consistent field (TDSCF) dynamics. As TDSCF is a method where the entire system is treated in a quantum mechanical fashion, and I am only concerned in this thesis with situations where the majority of the system is treated classically, I shall restrict my discussion to the Ehrenfest method, although my descriptions apply analogously. The Ehrenfest method separates classical and quantum subsystems, and as in the classical path approximation the electronic (quantum) degrees of freedom are dependent on the positions and movements of the nuclei (classical). When it comes to the feedback from the electronic subsystem to the nuclei, the forces on the nuclei are not derived purely from any individual electronic state. Rather, the nuclei evolve on an adiabatic potential energy surface which corresponds to a weighted average of the energy surfaces associated with each electronic state. The weightings are by the instantaneous quantum populations of the electronic states. Although a typical Ehrenfest dynamics trajectory will begin on an energy surface that is associated with the system's initial quantum state, as time passes the surface which the nuclei

are on will deviate more from this initial potential as additional electronic states are 'mixed' in.

MF methods often work well in situations where all such surfaces are broadly similar [108]: conversely, it is well understood [84, 88, 109] that MF methods fail to capture the qualitative physical behaviour associated with events where separate trajectories on different potential energy surfaces would strongly diverge. An example commonly given is to consider a scattering event of a particle approaching a surface, which could (depending on criteria such as the initial energy of the particle and the nature of energy transfer during the scattering event) potentially become trapped near to the surface, or rebound and move away. A single average potential for the nuclei will be unable to describe either of these events satisfactorily. Since my goal is partially to better understand the qualitative nature of charge transport in organic semiconductors, a similar possibility arises. It is easy to imagine that certain potential energy surfaces may present large energetic barriers to charge transfer, thus localising charge onto a single site, whereas others would present smaller or minimal barriers and thus charge delocalization would be observed. A single MF trajectory on a single averaged potential energy surface cannot adequately describe both possible behaviours. Other known flaws include the failure of the Ehrenfest method to obey detailed balance [109]. These shortcomings partly explain the lasting popularity of an alternative NAMD method, known as surface hopping.

With surface hopping [110], rather than constructing an average potential energy surface, each possible potential energy surface arising from all the possible quantum states is considered. As in the mean-field case, a surface hopping trajectory starts on the energy surface corresponding to the initial quantum state. Whereas in the mean-field case this surface gradually becomes a more mixed one, in surface hopping the nuclei always evolve on a surface that corresponds to one of the possible quantum states of the system. The surface hopping enters because at fixed intervals (which can logically correspond to molecular dynamics time steps) probabilities are calculated for the trajectory to hop to a different potential energy

surface. These hops occur stochastically - in theory, a surface hop is never guaranteed, but is assigned a probability that is derived from the relative populations of the electronic states - and so along a single surface hopping trajectory, the nuclei will switch between potential energy surfaces multiple times. Crucially, though, at any individual point along the trajectory the nuclei will feel the potential from a single electronic state of the system.

This choice of stochastic hops between discrete surfaces comes with some immediate drawbacks which must be addressed. The hop from one surface to another changes the total energy of the system, requiring e.g. velocity rescaling to conserve energy along the trajectory. On a more conceptual level, a single surface hopping trajectory now has limited physical meaning: each surface hop is not necessarily directly associated with a physical reaction. Nonetheless, a statistical ensemble of trajectories can be used to calculate physical properties and make computational predictions, as well as overcome one failing of the Ehrenfest method, which is that multiple trajectories can demonstrate divergent behaviours within the same system. Surface hopping is currently a popular NAMD method due in part to its relative simplicity.

The potential for a surface hopping molecular dynamics method to be used to model charge transport is clear: a group of organic molecules in the condensed phase can evolve on a potential energy surface that arises from an excess electronic charge, but crucially this evolution is treated entirely classically and therefore can be calculated extremely quickly. Meanwhile, the excess charge is handled with a fully quantum mechanical approach in the time-dependent potential arising from the molecular motion.

## 1.5 Surface hopping in the literature

Surface hopping methods have received much attention in the literature over the past few decades [95,96,98,109,111–117]. Much use has been made of the influential algorithm published by Tully, known as fewest-switches surface hopping [110], which has been extensively reviewed [118–121]. Surface hopping has been used

to study e.g. photoinduced processes [122–124] including photoinduced charge transfer and catalysis [125], vibrational dissociation [126], exciton deactivation in oligothiophenes [127] as well as charge transport in very simple model systems [84,85,128].

There are known shortcomings of the surface hopping method. The nuclei are treated entirely classically, which is of course an approximation that may not always be valid. FSSH in particular overestimates electronic coherence after a surface crossing event [129,130], a flaw that can cause many problems when modelling long-term behaviour [131–136]. The ‘trivial crossing problem’ [137,138] needs to be accounted for. The stochastic nature of individual SH trajectories means they are no longer time-reversible, though the algorithm as a whole may be considered approximately equivalent in the forwards and backwards directions [139–141]. In the hope of overcoming some or all of these and other issues, there are presently many proposed altered versions of the method in the literature: examples include global flux surface hopping [142,143] to fix the trivial crossings problem and model superexchange reactions; and flexible surface hopping [85] which also solves the trivial crossings problem while massively reducing computational costs.

An example of another group’s surface hopping implementation is the PYXAID (PYthon eXtension for Ab Initio Dynamics) method developed by Oleg Prezhdo and coworkers [90,91,144]. The aims of the PYXAID program are similar to mine, seeking to develop a sufficiently efficient approach to simulate the hundreds or thousands of atoms required to model charge transport in condensed phase systems. This program was optimized for the study of photoexcited dynamics, but the principles are general enough that this method could be used to study more general charge transport problems in organic semiconductors. However, in order to achieve a desired level of computational efficiency while still using a DFT-based framework, the PYXAID program makes the ‘classical path’ approximation. As mentioned earlier, this neglects the feedback of the electronic subsystem onto the nuclei, which is an approximation that is likely acceptable if the classical kinetic energy of the nuclei is large compared to the energy splitting of the electronic

states i.e. there is little difference between the trajectories of the nuclei on different electronic surfaces. The PYXAID method is therefore likely not well suited to modelling systems where, for example, the reorganization energy is large or the electron-phonon coupling is particularly strong. In contrast, my FOB-SH method abandons the classical path approximation and accounts for feedback from the electronic subsystem onto the nuclei through the nuclear forces: this should ensure its applicability to all types of organic semiconductors.

For comparison, I also shall briefly examine another surface hopping method implemented by the research group of Marcus Elstner to the related problem of charge transport in DNA, as reported in e.g. Ref [88]. A relatively straightforward surface hopping scheme was compared to a mean-field approach, and there is some discussion about the relative merits of each to study this problem. In this particular work, the computational simplicity of the fewest-switches surface hopping algorithm is considered to be one of its greatest strengths. Unfortunately, while comparisons between these two approaches are important, I feel the presented surface hopping method is flawed in crucial ways which may call the findings into question. Although the rescaling of nuclear velocities in order to conserve the total energy of the system is mentioned as a vital step in Ref. [110], this is entirely neglected in Ref [88], which does not allow for energy conservation along a simulation and also means no treatment of possible ‘forbidden hops’. Similarly, there is no correction applied to the problem of electronic overcoherence. Kubar & Elstner both understand that these are issues that should ideally be addressed in future versions of their surface hopping method, but as it stands the method is lacking. The FOB-SH method both conserves energy at surface hops due to a velocity rescaling step at each hop, and has implemented a preliminary decoherence correction, though there is discussion in Chapter 6 about how each of these could be further improved.

I believe that the FOB-SH method developed and discussed within this thesis represents a step forward for the application of surface hopping to the problem of charge transport. There is a large body of work in the field already [84, 119, 145]

which generally deals with very simple ‘toy models’, such as a spin-boson Hamiltonian in the work of Wang et al. [84]. Other surface hopping methods simulate more realistic molecules [88, 122, 126, 146, 147]: an example is a recent paper by Plasser et al. [148] using 9H-adenine as a case study for their surface hopping method. Looking at the current state of the surface hopping field, I believe that there is scope for a method that applies surface hopping to study charge transport, but which simulates a physical organic semiconductor system rather than a simple toy model. This is the major original contribution that I hope to make with FOB-SH.

## 1.6 This thesis

The goal of this work has therefore been to develop a non-adiabatic molecular dynamics formulation which is capable of exploring the nature of charge transport in the family of organic semiconducting materials. To this end I have devised and implemented a method, based on Tully’s fewest switches surface hopping algorithm and the analytic overlap method from Gajdos et al. [149], which is specifically designed to model large organic semiconducting systems with a classical molecular dynamics approach while treating a single excess charge with a fully quantum-mechanical approach. This method is what I have called fragment-orbital based surface hopping, or FOB-SH. A large part of this thesis is devoted to explaining in detail the theoretical underpinnings of FOB-SH (Chapter 2), the particular implementation I have done during my project, and a series of tests which were carried out with the aim being to validate the correct behaviour of said implementation (both in Chapter 3). The derivation, implementation and validation were previously published in Ref. 150.

Once these validations have been presented and outlined, most of the remainder of the thesis (Chapters 4 and 5) will present the results which I have obtained from using FOB-SH on two different model systems. In Chapter 4 are values for an electron transfer rate between the two molecules of a donor-acceptor complex, presented in terms of their dependencies on key parameters. These results are compared with and discussed in the context of the equivalent curves from standard

electronic transfer theory. These results have been published in Ref. 151. Then in Chapter 5 there are results presented as a proof-of-concept on a larger system of ten molecules in a one-dimensional chain, where charge mobilities have been calculated for different temperatures and values of electronic coupling. These results carry some discussion although their main purpose is to demonstrate that the FOB-SH method is capable of calculating mobilities in large systems. These results were also published as part of Ref. 150.

I finally conclude in Chapter 6 that this implementation of FOB-SH demonstrates that it is 'fit-for-purpose' and shows promise for future investigations into charge transport in organic semiconductors. I will discuss what the results in this thesis suggest for these future investigations, and what we can perhaps already understand from them. I will also outline how I envisage the method may be expanded in further implementations in the near future.

## Chapter 2

# Theory and Derivation of FOB-SH

In this chapter I will go through the derivation of the fewest-switches surface hopping algorithm, showing how my method propagates the excess electronic charge in a site-orbital basis and transforms to the adiabatic basis for the calculation of adiabatic surface forces and probabilities of hops between surfaces, and arriving at the working equations for my particular implementation. The solution to the Schrödinger equation and the expression for the probability of surface hopping are both well known, but in order to fully explain the work done in this thesis I consider it important to review the derivations for both, particularly paying attention to the assumptions I have used. What is original to this work is the generalized force expression, which allows me to calculate the force arising on each atom from the current adiabatic potential energy surface for an arbitrary system, provided that I know the Hamiltonian and its gradient in some basis: this is the vital component allowing the FOB-SH method to be used on sufficiently large model systems to investigate condensed phase behaviour. I additionally include a much simpler force expression which can be easily derived ‘by hand’ and which is correct in the special and simplest case of a two-site system.

### 2.1 Solving the electronic Schrödinger equation

In order to calculate the time evolution of the electronic wavefunction, the electronic Schrödinger equation is solved for the time-dependent electronic potential

that arises from classical nuclear motion. The time-dependent electronic wavefunction  $\Psi(t)$  is usually expressed as a linear combination of adiabatic electronic wavefunctions  $\psi_n(\mathbf{R}(t))$  that depend parametrically on the nuclear coordinates  $\mathbf{R}(t)$ ,  $\Psi(t) = \sum_n c_n(t)\psi_n(\mathbf{R}(t))$ , and  $c_n$  are the time-dependent expansion coefficients. Insertion in the time-dependent electronic Schrödinger equation gives the time evolution of  $c_m$ ,

$$i\hbar\dot{c}_m(t) = \sum_n c_n(t) \left( H_{mn} - i\hbar d_{mn}^{\text{ad}} \right), \quad (2.1)$$

where  $H_{mn}$  are the matrix elements of the electronic Hamiltonian and  $d_{mn}^{\text{ad}}$  are the non-adiabatic coupling matrix elements (NACEs) between the adiabatic states,

$$d_{mn} = \left\langle \psi_m \left| \frac{d\psi_n}{dt} \right. \right\rangle. \quad (2.2)$$

The classical nuclei evolve on a single electronic potential energy surface at any given time according to Newton's equation of motion. For potential energy surface  $n=i$ ,  $E_i$ ,

$$m_I \ddot{\mathbf{R}}_I = -\nabla_{\mathbf{R}_I} E_i \quad (2.3)$$

where  $m_I$  is the mass and  $\mathbf{R}_I$  the position vector of nucleus  $I$ . The feedback from the electronic to the nuclear subsystem is incorporated in the ability of the system to undergo stochastic 'surface hops' i.e. switches from one potential energy surface to another. In the FSSH algorithm devised by Tully the probability  $g_{ji}$  of switching from the current electronic state  $i$  to another electronic state  $j$  is calculated from

$$g_{ji} = \frac{b_{ji}\Delta t}{a_{ii}} \quad (2.4)$$

$$b_{ji} = \frac{2}{\hbar} \text{Im}(a_{ji}^* H_{ji}) - 2\text{Re}(a_{ji}^* d_{ji}) \quad (2.5)$$

$$a_{ji} = c_j c_i^*, \quad (2.6)$$

where  $\Delta t$  is the MD time step and  $a_{ji}$  the elements of the density matrix. Crucially,

in the adiabatic electronic basis the Hamiltonian off-diagonal elements  $H_{ji}$  are zero and thus Eq. 2.5 becomes

$$b_{ji} = -2\text{Re}(a_{ji}^* d_{ji}) \quad (2.7)$$

Surface hopping is conventionally carried out in an adiabatic basis [152], although the derivation of the probabilities is general and applies in principle to any electronic basis.

## 2.2 Site basis representation

The purpose of this project was explicitly to simulate charge transport in an organic molecular semiconductor. It is therefore natural and intuitive to consider the electronic wavefunction  $\Psi(t)$  in a basis of molecular site orbitals. For this derivation I shall consider the case of an excess charge in a material made of  $M$  sites, where ‘site’ refers to a molecule or molecular fragment of the material. The formalism is analogous whether the charge is an excess electron or an excess electronic hole.

In this work I have treated the electronic behaviour exclusively as a one-particle problem. I consider only a single excess charge carrier, which moves in an effective time-dependent potential arising from the remainder of the system (the nuclei and other electrons). This means that valence and core electrons are not explicitly treated. The time-dependent wavefunction of the charge carrier,  $\Psi(t)$ , is expanded in a set of time-dependent orthogonal electronic site orbitals with the excess electron localized at site  $l$ ,  $\{\phi_l\}$ ,

$$\Psi(t) = \sum_{l=1}^M u_l(t) \phi_l(\mathbf{R}(t)). \quad (2.8)$$

In this derivation I assume the simplest case: each site contributes a single site orbital to the total electronic wavefunction. Physical organic molecules may well have degenerate molecular orbitals and thus a single molecule may contribute more than one orbital, but the derivation proceeds identically with  $M = kN$ , where

$N$  is the number of molecules and  $k$  some constant representing the number of site orbitals contributed by each molecule.

The site orbitals are obtained from the singly occupied molecular orbitals (SOMOs) of the isolated molecules, denoted  $\{\varphi_m\}$ , via Löwdin orthogonalization [153],

$$\phi_l = \sum_{m=1}^M T_{ml} \varphi_m, \quad (2.9)$$

where  $T_{ml}$  are the elements of the matrix  $\mathbb{T}$ ,  $T_{ml} = [\mathbb{T}]_{ml} = [\mathbb{S}^{-1/2}]_{ml}$  and  $\mathbb{S}$  the overlap matrix with elements  $S_{ml} = [\mathbb{S}]_{ml} = \langle \varphi_m | \varphi_l \rangle$ . Hence, while the  $\{\varphi_m\}$  are strictly localized on site  $m$  and have zero amplitude anywhere else, the  $\{\phi_m\}$  are strongly localized on site  $m$  and have small tails on the neighbouring sites to enforce orthogonality. The SOMOs  $\{\varphi_m\}$  can be obtained from gas phase calculations on the isolated molecules in vacuum for the same atomic configuration as in the material and for the charge state 1- (1+ for holes).

Insertion of Eq. 2.8 in the time-dependent electronic Schrödinger equation and multiplication from the left with  $\phi_k$  and integration gives, analogously to Eq. 2.1,

$$i\hbar \dot{u}_k(t) = \sum_l u_l(t) (H_{kl} - i\hbar d_{kl}), \quad (2.10)$$

where  $H_{kl}$  are the matrix elements of the electronic Hamiltonian  $H$  and  $d_{kl}$  the non-adiabatic coupling elements (NACEs) in the orthogonal site orbital basis, respectively,

$$H_{kl} = [\mathbb{H}]_{kl} = \langle \phi_k | H | \phi_l \rangle \quad (2.11)$$

$$d_{kl} = [\mathbb{D}]_{kl} = \langle \phi_k | \dot{\phi}_l \rangle. \quad (2.12)$$

The orthogonal site basis  $\{\phi_l\}$  is the most natural one for us to consider in the context of charge transfer between sites, and thus Eq. 2.10 is the main equation to determine the time evolution of the excess charge.

The matrix elements  $H_{kl}$  and  $d_{kl}$  can be expressed in terms of the non-orthogonal site orbital basis  $\{\varphi_l\}$  by substitution of Eq. 2.9,

$$H_{kl} = [\mathbb{T}^\dagger \mathbb{V}' \mathbb{T}]_{kl} = [\mathbb{T}^{-1} \mathbb{H}' \mathbb{T}]_{kl} \quad (2.13)$$

$$d_{kl} = [\mathbb{T}^\dagger \mathbb{D}' \mathbb{T}]_{kl} + [\mathbb{T}^\dagger \mathbb{S}' \dot{\mathbb{T}}]_{kl}, \quad (2.14)$$

where

$$V'_{kl} = [\mathbb{V}']_{kl} = \langle \varphi_k | H | \varphi_l \rangle \quad (2.15)$$

$$d'_{kl} = [\mathbb{D}']_{kl} = \langle \varphi_k | \dot{\varphi}_l \rangle, \quad (2.16)$$

and

$$\mathbb{H}' = \mathbb{S}^{-1} \mathbb{V}'. \quad (2.17)$$

is the electronic Hamiltonian in the non-orthogonal site orbital basis.

To calculate the forces arising from the adiabatic potential energy surface and the probability of hopping to a different surface, I require the adiabatic electronic wavefunctions  $\psi_n$  and the NACEs between the adiabatic states. The adiabatic wavefunctions can be easily obtained from the site orbital representation of the electronic wavefunction via a similarity transformation,

$$\psi_n(t) = \sum_l U_{ln} \phi_l(t), \quad (2.18)$$

where  $U_{ln} = [\mathbb{U}]_{ln}$  and  $\mathbb{U}$  diagonalizes  $\mathbb{H}$ ,

$$\mathbb{H}^{\text{ad}} = \mathbb{U}^\dagger \mathbb{H} \mathbb{U}. \quad (2.19)$$

The Hamiltonian in the adiabatic electronic basis (superscript “ad”) has the adiabatic potential energies  $E_n = [\mathbb{H}^{\text{ad}}]_{nn}$  on its diagonal,  $n = 0$  the electronic ground

state,  $n = 1$  the first excited state and so on. The off-diagonals are 0 by definition. For calculation of the NACEs, I insert the similarity transformation Eq. 2.18 in Eq. 2.2. This gives for  $n = j, i$

$$d_{ji}^{\text{ad}} = [\mathbb{U}^\dagger \mathbb{D} \mathbb{U}]_{ji} + [\mathbb{U}^\dagger \dot{\mathbb{U}}]_{ji}, \quad (2.20)$$

where  $\mathbb{D}$  is the matrix of NACEs in the site orbital basis, Eq. 2.12.

### 2.3 Nuclear gradients

The force on an atom  $I$  on the adiabatic potential energy surface  $E_i$  is given by

$$\mathbf{F}_{I,i} = -\nabla_I \langle \psi_i | H | \psi_i \rangle = -\langle \psi_i | \nabla_I H | \psi_i \rangle, \quad (2.21)$$

where I have used the Hellmann-Feynman theorem in the last equation. With an explicit expression for the Hamiltonian in the adiabatic electronic basis  $H$  in terms of the atomic coordinates  $R$ , I could therefore calculate these forces directly. I however do not have such an expression, as this Hamiltonian has been calculated from diagonalization of a Hamiltonian in a different basis set (the site orbital basis) and thus in general even if this Hamiltonian is known analytically in terms of  $R$ , the Hamiltonian in the adiabatic basis will not be. Instead I present here a general method that will allow me to calculate the forces in the adiabatic electronic basis from the forces in any other electronic basis (in this case, the site orbital basis).

Inserting Eq. 2.18 for  $n = i$  in Eq. 2.21, one obtains

$$\mathbf{F}_{I,i} = -[\mathbb{U}^\dagger \mathbb{G}_I \mathbb{U}]_{ii}, \quad (2.22)$$

with matrix elements  $[\mathbb{G}_I]_{kl} = \langle \phi_k | \nabla_I H | \phi_l \rangle$ . These elements can be written as

$$\langle \phi_k | \nabla_I H | \phi_l \rangle = \nabla_I \langle \phi_k | H | \phi_l \rangle - \langle \nabla_I \phi_k | H | \phi_l \rangle - \langle \phi_k | H | \nabla_I \phi_l \rangle \quad (2.23)$$

$$= \nabla_I H_{kl} - \langle \nabla_I \phi_k | \sum_m H_{ml} \phi_m \rangle - \langle \nabla_I \phi_l | \sum_m H_{mk} \phi_m \rangle^* \quad (2.24)$$

$$= \nabla_I H_{kl} + \sum_m (\mathbf{d}_{I,km} H_{ml} - H_{km} \mathbf{d}_{I,ml}), \quad (2.25)$$

where

$$\nabla_I H_{kl} = [\nabla_I \mathbb{H}]_{kl} = \nabla_I \langle \phi_k | H | \phi_l \rangle \quad (2.26)$$

$$\mathbf{d}_{I,kl} = [\mathbb{D}_I]_{kl} = \langle \phi_k | \nabla_I \phi_l \rangle \quad (2.27)$$

are the gradients of the Hamiltonian matrix elements and the non-adiabatic coupling vectors (NACVs) in the orthogonal site basis, respectively. In Eq. 2.25 I have made use of the identity

$$\mathbf{d}_{I,km} = -\mathbf{d}_{I,mk}^*, \quad (2.28)$$

which is valid for orthogonal wavefunctions. In matrix notation,

$$\mathbb{G}_I = \nabla_I \mathbb{H} + \mathbb{D}_I \mathbb{H} - \mathbb{H} \mathbb{D}_I. \quad (2.29)$$

I am only interested in the diagonal elements of the matrix  $\mathbb{U}^\dagger \mathbb{G}_I \mathbb{U}$ , as per Eq. 2.22. It can be easily shown that the diagonal elements of the latter two terms in Eq. 2.29 disappear after transformation to the adiabatic basis:

$$[\mathbb{U}^\dagger [\mathbb{D}_I \mathbb{H} - \mathbb{H} \mathbb{D}_I] \mathbb{U}]_{ii} = [\mathbb{U}^\dagger \mathbb{D}_I \mathbb{H} \mathbb{U} - \mathbb{U}^\dagger \mathbb{H} \mathbb{D}_I \mathbb{U}]_{ii}, \quad (2.30)$$

$$= [\mathbb{U}^\dagger \mathbb{D}_I \mathbb{U} \mathbb{U}^\dagger \mathbb{H} \mathbb{U}]_{ii} - [\mathbb{U}^\dagger \mathbb{H} \mathbb{U} \mathbb{U}^\dagger \mathbb{D}_I \mathbb{U}]_{ii}, \quad (2.31)$$

$$= [\mathbb{U}^\dagger \mathbb{D}_I \mathbb{U}]_{ii} E_i - E_i [\mathbb{U}^\dagger \mathbb{D}_I \mathbb{U}]_{ii}, \quad (2.32)$$

$$= 0 \quad (2.33)$$

Insertion of Eq. 2.29 in Eq. 2.22 and using Eq. 2.33 gives me the forces as in Eq. 2.21 and thus I now have a force expression that allows me to calculate the forces on the adiabatic electronic states on every atom in my system, as long as I know the electronic Hamiltonian in some basis set.

## 2.4 Special case: donor-acceptor complex

In the special case of charge transfer in a donor-acceptor complex (i.e. a system which can be approximated to two molecular sites only), the transformation from the site (or diabatic) basis to the adiabatic basis is analytic. For a  $2 \times 2$  matrix Eq. 2.19 can therefore be calculated 'by hand', giving

$$E_{0/1}(\mathbf{R}) = \frac{H_{11}(\mathbf{R}) + H_{22}(\mathbf{R})}{2} \pm \frac{1}{2} \sqrt{\Delta E^2(\mathbf{R}) + 4H_{12}^2(\mathbf{R})}, \quad (2.34)$$

where on the RHS of Eq. 2.34 the minus sign is for the adiabatic ground state energy,  $E_0$ , and the plus sign for the excited adiabatic state,  $E_1$ , and  $\Delta E$  is the vertical site (diabatic) energy gap,

$$\Delta E(\mathbf{R}) = H_{22}(\mathbf{R}) - H_{11}(\mathbf{R}) \quad (2.35)$$

Hence, the forces on the ions for each adiabatic surface can be directly obtained by differentiation of Eq. 2.34,

$$\mathbf{F}_{I,0/1} = -\frac{\nabla_I H_{11} + \nabla_I H_{22}}{2} \mp \frac{\Delta E(\nabla_I H_{22} - \nabla_I H_{11}) + 4H_{12}\nabla_I H_{12}}{2\sqrt{\Delta E^2 + 4H_{12}^2}} \quad (2.36)$$

The NACE required for the hopping probability between the two surfaces cannot be further simplified and needs to be calculated according to Eq. 2.20.

## 2.5 Efficient calculation of matrix elements and derivatives

The formulation of surface hopping in the site basis in sections 2.2-2.3 requires the calculation of a number of matrix elements and derivatives. For propagation of

the electronic subsystem according to Eq. 2.10 one needs to calculate the following matrix elements at each MD time step:  $H_{kl}$  and  $d_{kl}$  (requiring  $d'_{kl}$ ,  $S_{kl}$ ,  $T_{kl}$ ,  $\dot{T}_{kl}$ ). In addition, for propagation of the nuclear subsystem according to Eq. 2.29, one needs to calculate the nuclear gradients  $\nabla_I H_{kl}$ .

The diagonal elements of the Hamiltonian  $H_{kk} = \langle \phi_k | H | \phi_k \rangle$  are approximated here at the classical force field level. The corresponding site orbital basis functions  $\{\phi_k\}$  are strongly localized on site  $k$  and typically have only a very small contribution on neighboring sites  $l$  to enforce orthogonality. The element  $H_{kk}$  is calculated as the energy difference between two situations: the ‘charged’ system (site  $k$  carries the total excess electron whereas all other sites  $l \neq k$  are modelled in their neutral charge state) and the ‘neutral’ system (all sites are modelled in the neutral charge state).

The off-diagonal elements of the Hamiltonian  $H_{kl}$ ,  $l \neq k$ , are an intrinsically quantum mechanical property. For their calculation I turn to the analytic overlap method (AOM) of Gajdos et al. [149].

We consider at first the non-orthogonal site orbitals  $\{\varphi_k\}$ , where  $\varphi_k$  is the singly-occupied molecular orbital (SOMO) of molecule  $k$ , and the corresponding overlap matrix elements  $S_{kl}$ . The SOMO is obtained from standard electronic structure calculation on the isolated molecule in the charged state. The SOMO is then represented in a minimum basis of Slater-type atomic orbitals (STO) with optimized Slater decay coefficients. For  $\pi$ -conjugated systems it is usually sufficient to include only one optimized Slater  $p$ -orbital per atom contributing to  $\pi$ -conjugation. In this case

$$S_{kl} = \langle \varphi_k | \varphi_l \rangle = \sum_{i \in k}^{\text{atoms}} \sum_{j \in l}^{\text{atoms}} c_{p\pi,i}^* c_{p\pi,j} \langle p_{\pi,i} | p_{\pi,j} \rangle, \quad (2.37)$$

where  $i$  and  $j$  run over all  $\pi$ -conjugated atoms in molecules  $k$  and  $l$  respectively,  $p_{\pi,i}$  is the STO  $p$  orbital on atom  $i$  pointing along the direction of pi-conjugation and  $c_{p\pi,i}$  is the corresponding expansion coefficients. The latter is obtained from projection of  $p_{\pi,i}$  on the SOMO obtained from explicit electronic structure calculation with a standard basis set. (In our previous work we have denoted the double sum

on the right hand side of Eq. 2.37 by  $\bar{S}_{kl}$ .) The crucial advantage of the minimum STO representation is that the calculation of the overlap according to Eq. 2.37 is analytic and can thus be done extremely fast.

The overlap matrix elements of Eq. 2.37 are used to obtain  $H_{kl}$  according to the linear relationship

$$H_{kl} = CS_{kl}, \quad (2.38)$$

where  $C$  is a constant of proportion. Eq. 2.38 asserts that the off-diagonal Hamiltonian matrix element between the orthogonal site orbitals  $(\phi_k, \phi_l)$ ,  $H_{kl}$ , is proportional to the orbital overlap of the corresponding non-orthogonal site orbitals  $(\varphi_k, \varphi_l)$ ,  $S_{kl}$ , where the two orbital pairs are related by the Löwdin transformation Eq. 2.9.

In previous work my research group has investigated the linear relation in Eq. 2.38 (this relationship is also referred to as the analytic overlap method or AOM) for simple donor-acceptor pairs, for which  $H_{kl}$  is usually referred to as the electronic coupling matrix element or the transfer integral [149]. The linear relation Eq. 2.38 was calibrated against electronic coupling matrix elements obtained from wavefunction-theory validated fragment-orbital density functional theory (FODFT) calculations on a diverse set of  $\pi$ -conjugated organic donor-acceptor pairs ( $H_{kl}$ ,  $C$  and  $S_{kl}$  were denoted by  $H_{ab}$ ,  $\bar{C}$  and  $\bar{S}_{ab}$  in Ref. 149, respectively.). We found a very good linear correlation ( $R^2=0.974$ ) and transferability to  $\pi$ -conjugated compounds not included in the calibration. The mean error was only a factor of 1.9, translating into an error in the non-adiabatic ET rate by a factor of 3.6. This is considered to be an acceptable error when agreement between rates is often only within an order of magnitude. The difference between the donor-acceptor pairs investigated in this previous work and the multi-site systems (molecular materials) investigated here is that the  $\phi_k$  have small tails on all neighbouring sites, not only on site  $l$ . The influence of these tails on  $H_{kl}$  can be expected to be small and is neglected. The crucial advantage of the calibrated Eq. 2.38 is that it provides a way for ultrafast estimation of  $H_{kl}$  owing to the efficient calculation of the overlap via Eq. 2.37.

Eq. 2.37 is also used for rapid estimation of the NACEs. The time derivative of the site basis functions is replaced by a finite difference approximation that can be made arbitrarily accurate by reducing the MD time step  $\Delta t$ ,

$$d'_{kl}(t) = \left\langle \varphi_k(t) \left| \frac{d}{dt} \varphi_l(t) \right. \right\rangle \quad (2.39)$$

$$\begin{aligned} &\approx \frac{1}{\Delta t} (\langle \varphi_k(t) | \varphi_l(t + \Delta t) \rangle - \langle \varphi_k(t) | \varphi_l(t) \rangle) \\ &= \frac{1}{\Delta t} (S_{kl'}(t) - S_{kl}(t)), \end{aligned} \quad (2.40)$$

where  $S_{kl'}$  denotes the overlap between  $\varphi_k$  at time  $t$  and  $\varphi_l$  at time  $t + \Delta t$ . Both  $S_{kl'}$  and  $S_{kl}$  are calculated according to Eq. 2.37. The transformation matrix  $T_{kl}$  can be simply obtained from  $S_{kl}$  via matrix inversion and the time derivative  $\dot{T}_{kl}$  is similarly approximated by a finite difference calculation. The NACEs in the orthogonal site basis,  $d_{kl}$ , can then be obtained according to Eq. 2.14.

Here a note on the time evolution of the SOMOs,  $\varphi_k(t)$ , is in order. The time dependence is due to the classical dynamics of the nuclear subsystem with coordinates  $\mathbf{R} = \mathbf{R}(t)$ . Therefore  $\varphi_k(t) = \varphi_k(\mathbf{R}(t))$ . The projection coefficients  $c_{p\pi,i}$  in Eq. 2.37 are calculated only once, for the minimum energy structure of molecule  $k$  in vacuum. After every nuclear dynamics time step, the orientation of the atomic orbital  $p_{\pi,i}$  is updated so that it remains parallel to the direction of  $\pi$ -conjugation. This direction is orthogonal to the plane that minimizes the sum of the distances between the plane and atom  $i$  and the atoms covalently connected to  $i$ . The expansion coefficients of all atomic orbitals on molecule  $k$  are then scaled by the same factor (typically a small number close to 1) to normalize the SOMO at the new geometry. The expansion coefficients are not changed otherwise. Hence, the atomic orbitals comprising the SOMO follow the motion of the atoms but they are frozen otherwise. This means that possible electronic relaxation effects of the SOMO in response to nuclear motion are not included.

Turning to the calculation of the nuclear gradients, the diagonal contribution of the Hamiltonian,  $\nabla_I H_{kk}$ , is taken from the force field, consistently with my choice

for the diagonal energies. The off-diagonal contributions,  $k \neq l$ , are obtained from differentiation of Eq. 2.38,

$$\nabla_I H_{kl} = C \nabla_I S_{kl}. \quad (2.41)$$

The nuclear gradients of the overlap,  $\nabla_I S_{kl}$ , can be conveniently expressed in terms of the NACVs,

$$\nabla_I S_{kl} = \nabla_I \langle \varphi_k | \varphi_l \rangle = \langle \nabla_I \varphi_k | \varphi_l \rangle + \langle \varphi_k | \nabla_I \varphi_l \rangle = \mathbf{d}_{I,lk}^* + \mathbf{d}'_{I,kl}, \quad (2.42)$$

which are calculated numerically using the finite difference approximation,

$$\begin{aligned} \mathbf{d}'_{I,kl} &= \langle \varphi_k | \nabla_I \varphi_l(\mathbf{R}_1, \dots, \mathbf{R}_I, \dots, \mathbf{R}_M) \rangle \\ &\approx \begin{bmatrix} \frac{1}{\Delta s} (\langle \varphi_k | \varphi_l(\mathbf{R}_1, \dots, \mathbf{R}_I + \Delta s \mathbf{e}_x, \dots, \mathbf{R}_M) \rangle - \langle \varphi_k | \varphi_l(\mathbf{R}_1, \dots, \mathbf{R}_I, \dots, \mathbf{R}_M) \rangle) \\ \frac{1}{\Delta s} (\langle \varphi_k | \varphi_l(\mathbf{R}_1, \dots, \mathbf{R}_I + \Delta s \mathbf{e}_y, \dots, \mathbf{R}_M) \rangle - \langle \varphi_k | \varphi_l(\mathbf{R}_1, \dots, \mathbf{R}_I, \dots, \mathbf{R}_M) \rangle) \\ \frac{1}{\Delta s} (\langle \varphi_k | \varphi_l(\mathbf{R}_1, \dots, \mathbf{R}_I + \Delta s \mathbf{e}_z, \dots, \mathbf{R}_M) \rangle - \langle \varphi_k | \varphi_l(\mathbf{R}_1, \dots, \mathbf{R}_I, \dots, \mathbf{R}_M) \rangle) \end{bmatrix} \quad (2.43) \\ &= \begin{cases} \frac{1}{\Delta s} (\mathbf{S}_{I,kl'} - S_{kl} \mathbf{1}) & \text{if } I \in l \\ \mathbf{0} & \text{if } I \notin l \end{cases} \quad (2.44) \end{aligned}$$

In Eqs. 2.43-2.44,  $\Delta s$  is a small displacement and  $\mathbf{e}_x$ ,  $\mathbf{e}_y$ ,  $\mathbf{e}_z$  are the unit vectors in  $x$ ,  $y$  and  $z$  directions,  $\mathbf{S}_{I,kl'}$  is the vector of overlaps between  $\varphi_k$  at nuclear coordinates  $\mathbf{R} = (\mathbf{R}_1, \dots, \mathbf{R}_I, \dots, \mathbf{R}_M)$  and  $\varphi_l$  at nuclear coordinates of atom  $I$  displaced by  $\Delta s \mathbf{e}_x$ ,  $\Delta s \mathbf{e}_y$  and  $\Delta s \mathbf{e}_z$ , respectively (first vector in Eq. 2.43), and  $\mathbf{0}$  and  $\mathbf{1}$  are the null and unity vectors, respectively. Eq. 2.44 assumes that a displacement of a given atom  $I$  on a molecule  $l$  only leads to a change in the SOMO for that molecule, i.e.  $\varphi_l$ . The SOMOs of all other sites including site  $k$  remain unchanged. This is a consequence of the neglect of electronic relaxation effects due to nuclear motion.

With the derivation of all the equations required to propagate both atoms and charge within an SH scheme - crucially, the general force expression for the atoms, something unique to this work - it is now possible to implement such a method to begin carrying out simulations. In the next chapter I discuss the practical aspects of my implementation of FOB-SH and some of the validations I have carried out.



## Chapter 3

# Implementation and Validation of FOB-SH

In this chapter, I will present and discuss the practical details of my implementation of FOB-SH, with which I have calculated all the results in Chapters 4 and 5. I will discuss the program flow in this implementation, talk about some standard additions to the surface hopping algorithm, and show the outcome of some tests designed to verify that the method is working correctly.

### 3.1 Implementation details

#### 3.1.1 Molecular dynamics

In FOB-SH, the vast majority of the system consists of organic molecules which must be propagated with some form of classical force field. For this implementation, I have chosen to use the NAMD molecular dynamics package [154, 155] with the AMBER force field [156, 157]. The form of the AMBER force field is

$$E_{total} = E_{bonds} + E_{angles} + E_{dihedrals} + E_{nonbonded} + E_{elec} \quad (3.1)$$

with the following terms:

$$E_{bonds} = \sum_{bonds} \frac{1}{2} k_r (r - r_0)^2 \quad (3.2)$$

$$E_{angles} = \sum_{angles} \frac{1}{2} k_{\theta} (\theta - \theta_0)^2 \quad (3.3)$$

where in both cases the zero subscript denotes an equilibrium value;

$$E_{dihedrals} = \sum_{dihedrals, n} \frac{V_n}{2} (1 + [n\phi - \gamma]) \quad (3.4)$$

where the sum over  $n$  represents the fact that individual bonds may have more than one torsion term defined;

$$E_{nonbonded} = \sum_{i < j} 4\epsilon_{ij} \left[ \frac{\sigma^{12}}{r_{ij}^{12}} - \frac{\sigma^6}{r_{ij}^6} \right] \quad (3.5)$$

$$E_{elec} = \sum_{i < j} \frac{q_i q_j}{4\pi\epsilon_0 r_{ij}} \quad (3.6)$$

where  $i, j$  sum over all atoms in the system in all cases. This is the full form of the force expression for a ‘neutral’ system, and additional forces are applied that arise from the excess charge: as detailed in Section 2.3, these additional forces on the atoms arising from the excess charge can be calculated using either Equation 2.36 for a donor-acceptor complex, or more generally from Equation 2.22. Nearly all required parameters in the above equations were taken from the Generalized Amber Force Field (GAFF) parameterization. The only exceptions were when specific parameterization of the reorganization energy was required: this is detailed in Chapter 4.

My choice of NAMD was motivated by its `tclforces` functionality, which allows the user to write custom scripts to apply additional forces to the molecules. This is crucial to correctly propagate the atoms on the active adiabatic potential energy surface: the continual switching of surfaces makes it impossible to run simulations with a single topology file, but the `tclforces` functionality allowed me to set up and run simulations using an electronically-neutral topology file and then calculate and add the forces arising from the excess charge ‘on the fly’.

### 3.1.2 Charge dynamics and surface hopping

For the propagation of the excess charge, we first return to Eq. 2.10. If the coefficients  $u_k(t)$ ,  $k = 1, \dots, N$  are expressed as a column vector  $u(t)$  of dimension  $N$ , then Eq. 2.10 can be expressed as

$$\frac{d}{dt}u(t) = X(t)u(t) \quad (3.7)$$

where  $X(t)$  is a matrix with elements defined thus:

$$X_{kl} = \frac{-i}{\hbar}H_{kl} - d_{kl} \quad (3.8)$$

For my implementation, Eq. 3.7 is numerically integrated using the fourth-order Runge-Kutta method [158] with a timestep  $\delta t$ :

$$u(t + \delta t) = u(t) + \frac{\delta t}{6}(K_1 + 2K_2 + 2K_3 + K_4) \quad (3.9)$$

$$K_1 = X_t \quad (3.10)$$

$$K_2 = X_{t+\frac{1}{2}\delta t}(1 + \frac{1}{2}\delta t K_1) \quad (3.11)$$

$$K_3 = X_{t+\frac{1}{2}\delta t}(1 + \frac{1}{2}\delta t K_2) \quad (3.12)$$

$$K_4 = X_{t+\delta t}(1 + \delta t K_3) \quad (3.13)$$

In the above, the symbol  $X_t$  denotes the matrix  $X$  evaluated at timestep  $t$ . As detailed in Chapter 2, all elements of these matrices can be calculated from the analytic overlap method, with the exception of the diagonal Hamiltonian elements  $H_{ii}$  which I take from my classical force field.

At the end of the electronic propagation, the Hamiltonian  $H$  is diagonalized as detailed in Chapter 2 so as to calculate forces and surface hopping probabilities. A uniform random number between 0 and 1 is generated and used to calculate whether or not the system hops to a different surface. In an  $N$ -site system, the interval 0 to 1 is divided into  $N$  segments where the first  $N - 1$  segments have size  $g_{ji}$ , with  $i$  the current adiabatic state,  $j$  a different adiabatic state and  $g_{ji}$  the

probability of hopping (from Eq. 2.4): the  $N$ th segment is then considered to be the probability for not hopping.

It can be shown that for infinitesimal time step  $\Delta t$  the total sum of all surface hopping probabilities should be less than or equal to unity: in practice, the use of a finite time step in this implementation means that this is not guaranteed. To deal with the possibility that the probabilities might sum to a number greater than 1, the program is designed in this case to rescale all the probabilities by a factor  $\frac{1}{\sum g_{ji}}$  so that  $\sum g_{ji} = 1$ . In this case a surface hop is guaranteed, as the effective probability of remaining on the same surface is given by  $1 - \sum g_{ji} = 0$ .

### Velocity rescaling

As mentioned in Tully's original surface hopping paper, it is necessary to introduce some way of conserving the total energy of the system after a surface hop, as the energy splitting between adiabatic surfaces means that energy conservation does not happen automatically. The most common method is a rescaling of the atomic velocities of the system [110] though other suggestions exist [159]. This FOB-SH implementation uses a very straightforward approach. When the system undergoes a surface hop from  $i$  to  $j$ , all the atomic velocities of the system are rescaled at the point of a surface hop by a factor  $\kappa$  where

$$\kappa = \sqrt{\frac{T_i - (E_j - E_i)}{T_i}}, \quad (3.14)$$

where  $T_i$  is the total kinetic energy of the system in state  $i$  and  $E_i, E_j$  are the potential energies in states  $i$  and  $j$ , respectively. This procedure differs from the usual approach, where only the velocity component in the direction of the non-adiabatic coupling vector is rescaled. Unfortunately, the use of the NAMD package restricted me to a very limited ability to alter the system's velocities during a simulation, necessitating this approach. As the purpose of this work is to introduce and demonstrate the feasibility of a new methodology rather than report quantitative results, I have essentially disregarded any possible systematic errors due to this modified

velocity rescaling approach, although some discussion of their possible effects is included in Chapter 6.

### Decoherence correction

In response to the weight of literature discussing the electronic overcoherence problem that surface hopping methods suffer from [116,118,131–133,152,160,161] I have implemented a simple decoherence correction, which ensures that the overcoherence problem is accounted for in a similar fashion to Refs. [116] or [131]. There are two versions of the procedure, one of which is entirely general and one which is only applicable to a two-site system: I shall detail the latter first because it is more intuitive.

In a two-site simulation, after a surface hop from the excited to the adiabatic ground state I collapse the electronic wavefunction onto the adiabatic ground state the first time that the system passes through one of the ground state minima while moving away from the avoided crossing [116]. This is a simple and intuitive way to ensure that the wavefunction collapse only happens when the non-adiabatic coupling between the two states is negligible.

The exact same procedure is not available in a general system, where there is no corresponding analytic picture of the adiabatic states in terms of the diabatic states and thus no guarantee that a diabatic minimum will necessarily correspond to a region of low non-adiabatic coupling. In this case, the correction I have implemented takes the non-adiabatic coupling into account more directly. After any surface hop, the first time that the non-adiabatic coupling elements between the current state and each of the other system states all fall below a certain threshold, I collapse the electronic wavefunction onto the current adiabatic state. This procedure is judged to be essentially equivalent to that for the two-site case.

### 3.1.3 Program flow

To aid with understanding the flow of the FOB-SH program used for this work, Figure 3.1 is a flowchart that lays out a simplified version of the required calculations

prior to simulation start and during each timestep of a given simulation.

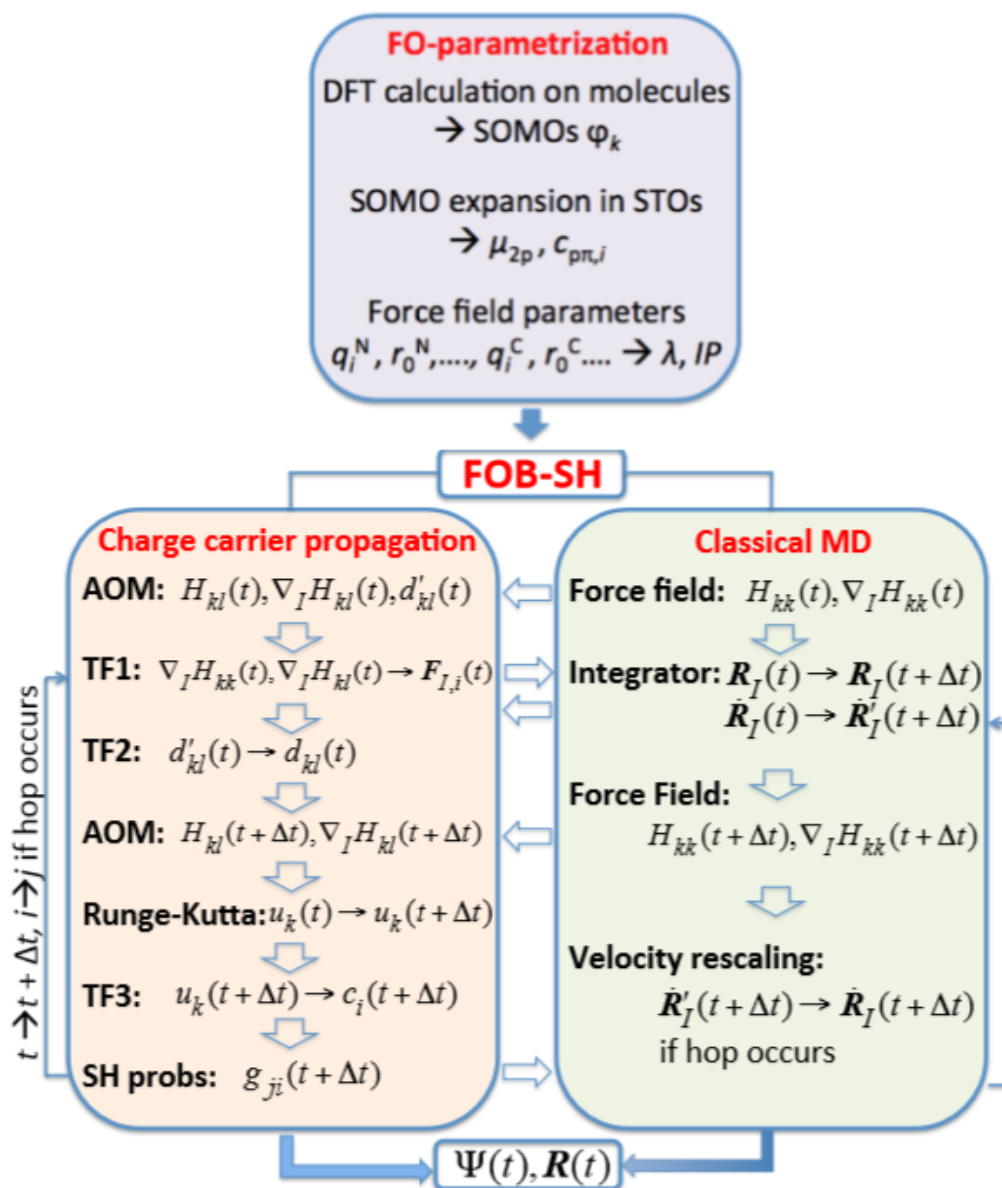


FIGURE 3.1: A simplified version of the FOB-SH program flow. Abbreviations are as follows: FO (fragment orbital), DFT (density functional theory), SOMO (singly-occupied molecular orbital), AOM (analytic overlap method), TF (transformation), SH (surface hopping).

The coupled equations of motion for the excess charge carrier, Eq. 2.10, and classical nuclei, Eq. 2.3, are integrated numerically using an electronic time step  $\delta t = 0.1$  fs and a nuclear time step  $\Delta t = 0.5$  fs for propagation of charge carrier and nuclei, respectively. These time steps were optimized to be the maximum possible without

introducing errors into the electronic propagation (in the case of  $\delta t$ ) and to improve the energy conservation of the method as much as possible while maintaining sufficient computational efficiency to make large-scale simulations practical (in the case of  $\Delta t$ ).

At the initial time  $t$  the electronic Hamiltonian  $H_{kl}(t)$  and the forces  $\nabla_I H_{kl}$  are calculated in the site basis as described above and transformed to the adiabatic basis according to Eqs. 2.19 and 2.22. The nuclei are then propagated on a given adiabatic surface  $i$  from time  $t$  to  $t + \Delta t$  according to Eq. 2.3 using the velocity Verlet algorithm. This is followed by calculation of the electronic Hamiltonian at time  $t + \Delta t$ ,  $H_{kl}(t + \Delta t)$ . In the next step, the charge carrier is propagated in the site basis according to Eq. 2.10 from time  $t$  to  $t + \Delta t$  in steps of  $\delta t$  using the fourth-order Runge-Kutta algorithm following Eqs. 3.9-3.13 [158]. At each electronic integration time step  $n$ , the electronic Hamiltonian is linearly interpolated between  $H_{kl}(t)$  and  $H_{kl}(t + \Delta t)$ ,  $H_{kl}(t + n\delta t) = H_{kl}(t) + [H_{kl}(t + \Delta t) - H_{kl}(t)](n\delta t/\Delta t)$ ,  $n = 1, \dots, (\Delta t/\delta t)$ .

The NACEs  $d_{kl}$  required for the carrier propagation are obtained from  $d'_{kl}$ , Eq. 2.40, via the transformation Eq. 2.14. The NACVs, and by virtue of Eqs. 2.41-2.42  $\nabla_I H_{kl}$  and  $\nabla_I S_{kl}$  respectively, are obtained by numeric differentiation using an increment for nuclear displacements of  $\Delta s = 10^{-4}$  Å. The surface hopping probabilities between the current adiabatic electronic state  $i$  and all other states  $j \neq i$ , according to Eq. 2.4, are calculated at every nuclear time step.

## 3.2 Simulation details

### 3.2.1 Model systems

In principle, the FOB-SH method as explained in this thesis can be applied to any organic semiconductor systems, as long as the molecular sites for the charge propagation are  $\pi$ -conjugated (as the analytic overlap method relies upon this assumption [149]). Early on in the project, tests of the method were carried out on fullerene molecules, specifically buckminsterfullerene ( $C_{60}$ ), derivatives of which are widely used in organic photovoltaic applications [162] due to their electronic acceptor

properties [163]. This choice of molecule was particularly motivated by previous work in my group on this molecule and derivatives, such as PCBM [51, 52, 164]. Although this molecule still presents interesting avenues for future research, I discovered while implementing FOB-SH that the computational cost of my method of estimating the NACVs - required for the calculation of the atomic forces - scales approximately as the square of the total number of atoms in the system. As fullerenes are among the largest non-polymeric organic molecules, they will correspondingly be some of the most expensive possible to simulate with the current set-up.

For reasons therefore of maximal computational efficiency, I have chosen to test and validate my FOB-SH implementation by simulation of electron hole transfer between ethylene-like molecules (ELMs). I call them “ethylene-like” because only their nuclear geometries correspond to real ethylene molecules: the reorganization energy  $\lambda$  and the constant  $C$  determining the magnitude of  $H_{kl}$  (Eq. 2.38) have been chosen freely to simulate charge transfer in different parameter regimes. This allows me to check my implementation on a very small system that does not directly correspond to a real, physical organic semiconductor but which nonetheless can demonstrate its suitability for such a purpose.

In this thesis I have carried out simulations on two systems of ELMs: a donor-acceptor complex of two molecules (the simplest system possible to study charge transfer) and a larger system, consisting of a 1-dimensional chain of 10 ELMs. Figure 3.2 is a visualization of the two systems in question: exact parameterization details for these systems are in Chapters 4 and 5 respectively.

### 3.2.2 Force field parameters

The site energies  $H_{kk}$  and corresponding forces  $\nabla_I H_{kk}$  are calculated with the AMBER classical force field. Specifically, I model intermolecular reorganization between neutral and charged geometries by a change in equilibrium distance  $R$  between the two carbon atoms, all other bonding parameters remaining unchanged. This means that the site energies and forces can be described by Eq. 3.2.

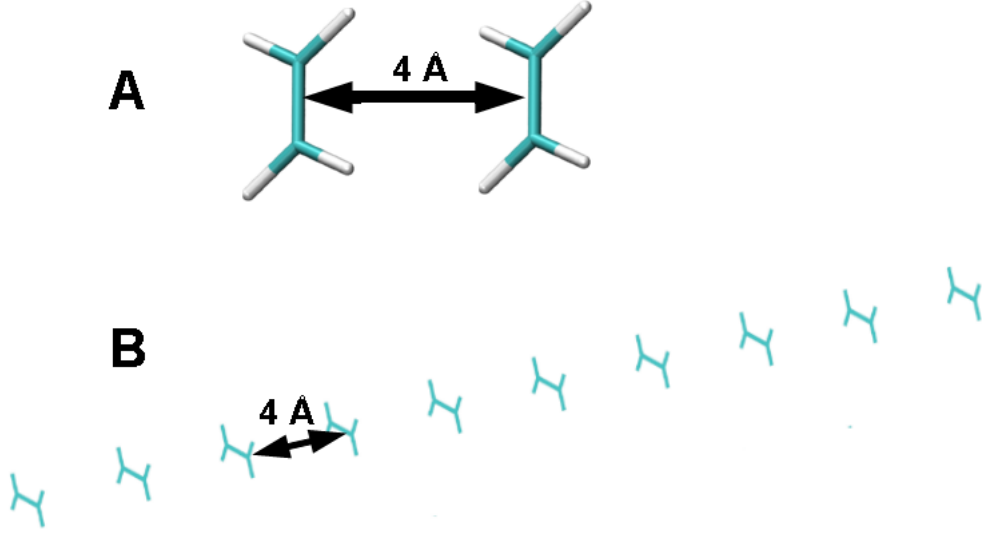


FIGURE 3.2: Visualizations of the two model systems used in this thesis. Panel A is the ELM dimer, with the molecules initially spaced 4 Å apart. Panel B is the ten-molecule 1D chain, where the inter-molecular spacing at initialization is again 4 Å.

The reorganization energy  $\lambda$  can be calculated from a standard fourpoint scheme [51],

$$\lambda = [E_C(\mathbf{R}_N) + E_N(\mathbf{R}_C)] - [E_C(\mathbf{R}_C) + E_N(\mathbf{R}_N)] \quad (3.15)$$

In Eq. 3.15,  $E_C(\mathbf{R}_N)$  is the total force field energy of the charged ELM (subscript C) at the minimum energy configuration of the neutral ELM,  $\mathbf{R}_N$ ,  $E_N(\mathbf{R}_C)$  is the total force field energy of the neutral ELM (subscript N) at the minimum energy configuration of the charged ELM,  $\mathbf{R}_C$ , and  $E_C(\mathbf{R}_C)$ ,  $E_N(\mathbf{R}_N)$  are the energies at the minimum energy configurations of the respective states. In Table 3.1, I demonstrate which values of  $R$  were used to give me different values of  $\lambda$  for the ELM.

The off-diagonal elements  $H_{kl}$ ,  $k \neq l$ , are calculated using the analytic overlap method, Eq. 2.38, with  $C$  treated as a parameter controlling the strength of electronic coupling. The calculation of the overlap integrals  $S_{kl}$  was carried out as described in Ref. 149 using a minimum Slater basis of  $p$  orbitals with Slater decay coefficients  $\bar{\mu}_{2p} = 1.0000 \text{ a.u.}^{-1}$ .

TABLE 3.1: Parameterization of reorganization energy  $\lambda$  via the equilibrium charged length of the C=C bond

Bond length (Angstroms)	$\lambda$ (meV)
1.324	0 (neutral molecule)
1.369	100
1.387	200
1.401	300
1.413	400
1.423	500
1.433	600
1.441	700

### 3.3 Tests

#### 3.3.1 Electronic behaviour and Rabi oscillations

One of the few analytically-known results that the electron propagation routine can be used to reproduce is the behaviour of a simple two-site system. From Nitzan [77], we know the following: given a  $2 \times 2$  Hamiltonian in the diabatic representation with diagonal elements  $H_{aa}$  and  $H_{bb}$  and off-diagonal  $H_{ab}$ , and assuming the system is initially in diabatic state  $a$ , the time-dependent probability of diabatic state  $b$  is

$$P_b = \frac{4|H_{ab}|^2}{(H_{aa} - H_{bb})^2 + 4|H_{ab}|^2} \sin^2 \left[ \frac{\Omega_R t}{2} \right] \quad (3.16)$$

$$P_a = 1 - P_b \quad (3.17)$$

$\Omega_R$  is known as the Rabi frequency, and is defined thus:

$$\Omega_R = \frac{1}{\hbar} \sqrt{(H_{aa} - H_{bb})^2 + 4|H_{ab}|^2} \quad (3.18)$$

This is directly applicable to the simplest conceivable application of the method. Consider a system of two molecules and a single excess electron. If the molecules are frozen in place, and do not react to the electron's presence i.e the coupling  $H_{ab}$  and the site energies  $H_{aa}, H_{bb}$  do not change in time, then the electronic population should oscillate between the two sites exactly as described above.

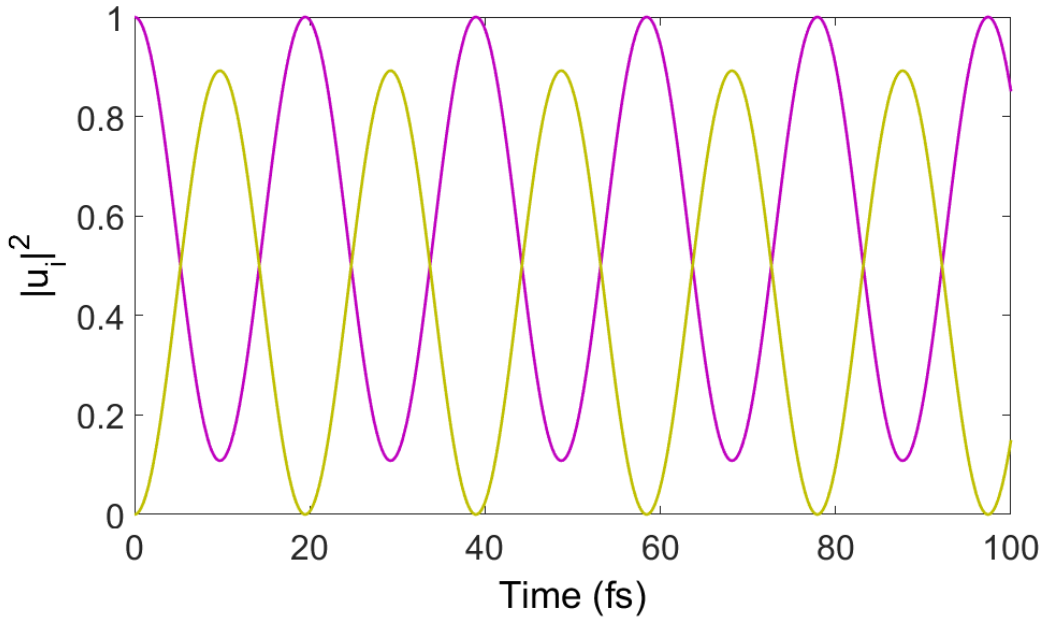


FIGURE 3.3: The population of each of two sites  $a$  (purple) and  $b$  (yellow) as a function of time. At time  $t = 0$ ,  $|u_a|^2 = 1$  and  $|u_b|^2 = 0$ . There are three sets of curves on this graph: one uses the Runge-Kutta method to propagate the electron, one uses the exponential solution, and one plots the analytic values of  $P_a$  and  $P_b$  as in Eq. 3.16. For each site, the three curves lie exactly on top of each other, showing that the Runge-Kutta method I have used agrees perfectly with exact theory in this simple case

Figure 3.3 plots curves of  $u$  for both sites, both those calculated from the Runge-Kutta routine and the analytic solutions. For further comparison, an alternative method was also used which solves the first-order differential equation 3.7 with a matrix exponential:

$$u(t) = \exp(Xt) \quad (3.19)$$

which is valid only for a time-independent  $X$  i.e. no molecular motion.

What we see in Figure 3.3 is that the Runge-Kutta method appears to have been correctly implemented, given its perfect (i.e. within numerical double precision) reproduction of the analytic equivalent. The diabatic populations of each site oscillate exactly according to Eq. 3.16. Obviously Eqs. 3.16 and 3.18 are strictly valid for a two-site time-independent system, but given the exact agreement between

my method and these equations in such a case I can extrapolate the qualitative behaviour of larger and time-dependent systems. It seems clear that the electronic population of sites in my systems will display similar oscillations, with the amplitude and frequency of these oscillations being controlled by the site energy difference  $\Delta E$  and the electronic coupling  $H_{ab}$ . This is indeed what I observe: see e.g. Figure 4.3 or Figure 4.5 for example electronic trajectories.

### 3.3.2 Nuclear forces and energy conservation.

As explained in Chapter 2, for a dimer system the nuclear forces on the active potential surface can be calculated using either Eq. 2.36 or the general  $N$ -site expression Eq. 2.22 for  $N=2$ . While both expressions are of course equivalent for a dimer, the implementation of the general  $N$ -site expression is more involved than the one for Eq. 2.36. A comparison between the numerical results obtained from the two expressions is therefore a good test for the validity of my implementation of Eq. 2.22. To achieve this, I carried out four MD simulations of 100 ps in length each, without surface hopping. Each simulation was carried out on a single adiabatic potential energy surface (ground or excited) and the scaling constant in Eq. 2.38 was chosen to be  $C = 88.7$  meV, 443.5 meV to produce two different values of the average intermolecular electronic coupling,  $\langle |H_{12}|^2 \rangle^{1/2} = 8$  meV and 41 meV respectively. Thus, for two different values of the coupling, I produced both a ground-state and an excited-state trajectory. For each trajectory, at 100 regularly-spaced configurations 1 ps apart, I calculated the forces on each atom according to both Eq. 2.36 and Eq. 2.22, as well as a version of Eq. 2.22 that sets the off-diagonal forces  $\nabla_I H_{kl}$ ,  $k \neq l$ , to 0. This last expression was chosen to demonstrate how the importance of these off-diagonal forces changes depending on the strength of the coupling.

The results are shown in Figure 3.4, which plots the forces from the full expression Eq. 2.22 (symbols in red) and from Eq. 2.22 with  $\nabla_I H_{kl} = 0$  for  $k \neq l$  (symbols in green) against the ones obtained from the full expression Eq. 2.36. I observe exact agreement between Eq. 2.22 and Eq. 2.36 for all four cases, validating the force calculation. In contrast, an error is made when neglecting the off-diagonal forces

in Eq. 2.22, which becomes pronounced in the larger coupling case (panels A and C) and also is greatest on the excited state trajectory, where the relative effect of the off-diagonal force terms is maximum (panel C, up to 0.1 Hartree/Bohr).

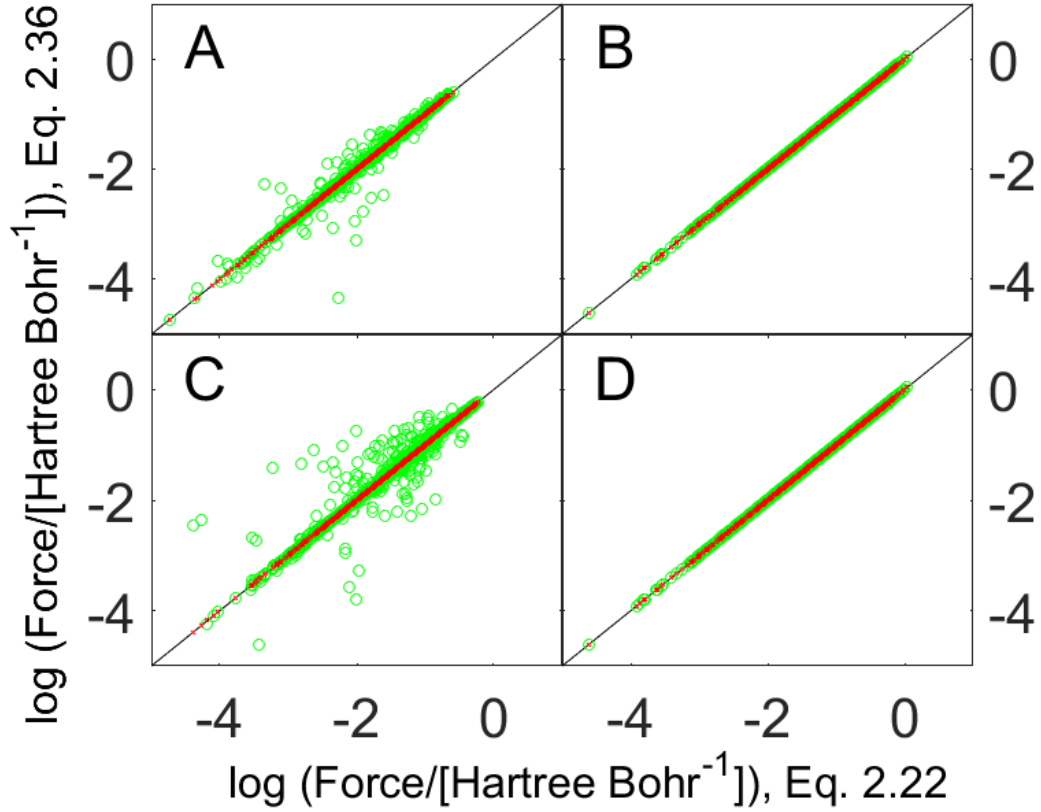


FIGURE 3.4: Nuclear forces obtained from the general  $N$ -site expression, Eq. 2.22, and from the 2-state expression, Eq. 2.36. The  $x$ ,  $y$  and  $z$  components of the nuclear forces in the ELM dimer are plotted as obtained from MD simulation (A) on the adiabatic ground state  $E_0$  with  $\langle |H_{ab}|^2 \rangle^{1/2} = 41 \text{ meV}$ , (B) on the adiabatic ground state  $E_0$  with  $\langle |H_{ab}|^2 \rangle^{1/2} = 8 \text{ meV}$ , (C) on the excited state  $E_1$  with  $\langle |H_{ab}|^2 \rangle^{1/2} = 41 \text{ meV}$  and (D) on the excited state with  $\langle |H_{ab}|^2 \rangle^{1/2} = 8 \text{ meV}$ . **Red crosses** refer to the full force calculation while **green circles** refer to the diagonal forces approximation as described in Table 3.2.

Having validated my force calculations and begun to understand the importance of the off-diagonal terms, I wanted to further investigate if my SH simulations would conserve total energy well, and to understand if the approximation  $\nabla_I H_{kl} = 0$  for  $k \neq l$  would cause a significant computational speedup. To see this, I performed individual SH simulations for the higher coupling strength model ( $C = 443.5 \text{ meV}$ ) of between 0.1 and 1 ns in length for five different simulation setups in the NVE ensemble. Three of these were on model ELM dimers, respectively

calculating the nuclear forces on the active potential energy surface using Eq. 2.36, Eq. 2.22 and the version of Eq. 2.22 that sets the off-diagonal forces to 0. The latter two force expressions were also applied to the 1D chain of 10 ELMs. Table 3.2 summarizes the energy conservation and computational cost of each of these simulations.

TABLE 3.2: Total energy conservation of FOB-SH simulations for different approximations and corresponding speed-up on a single compute core. The simulations were 1 ns and 0.1 ns in length for the 2 and 10 site simulations respectively. The ionic timestep was 0.5 fs.

Force expression	number of sites	total energy drift (Hartree/ps/atom)	CPU time (seconds/ps)
Eq. 2.36, no hops	2	$1.78 \times 10^{-9}$	0.6
Eq. 2.36	2	$1.18 \times 10^{-6}$	31.4
Eq. 2.22	2	$8.75 \times 10^{-7}$	44.5
Eq. 2.22, $\nabla_I H_{kl}=0$	2	$7.40 \times 10^{-6}$	32.9
Eq. 2.22	10	$5.45 \times 10^{-6}$	1027.9
Eq. 2.22, $\nabla_I H_{kl}=0$	10	$1.04 \times 10^{-5}$	674.9

I find that the energy drift is comparable when using Eq. 2.36 and Eq. 2.22 on the dimer system, which is expected as these two expressions are equivalent for  $N = 2$ . The energy drift when neglecting the off-diagonal forces, meanwhile, is an order of magnitude larger. For the 10-site system the energy drift also increases when neglecting the off-diagonal forces, but not by as much. This analysis suggests that despite the rather large errors in the forces (Figure 3.4), the total energy is still reasonably well conserved when the off-diagonal forces are neglected, at least for the chain of ELMs studied. Meanwhile, the computational time can be significantly decreased when using this approximation (by a factor of about 2 for the 10-site system).

Overall, the total energy drift of SH MD is reasonably small (on the order of  $10^{-6}$  Hartree/ps/atom), but about 3 orders of magnitude higher than for classical MD simulations on a single ground state or excited state surface without SH ( $10^{-9}$  Hartree/ps/atom). The higher energy drift in the SH runs is related to the discontinuity in the forces that comes from undergoing surface hops. Tully's original publication [110] discussed this to some extent, choosing to keep the sudden switches for

---

the sake of simplicity while noting suggestions for fictitious forces that would carry the molecules smoothly from one trajectory to another. I have also chosen to allow the system to hop suddenly between surfaces, both for reason of computational simplicity and also to avoid any possible outcome of the molecules being stuck on some interpolation between actual adiabatic surfaces while the system undergoes several surface hops. Finally, I highlight the computational efficiency of my implementation, allowing us to sample several picoseconds of SH dynamics per hour on a single CPU core for the 10 ELM model.

With the FOB-SH method now implemented and validated, I turn to a first attempt to use it to get some actual results and to begin to make comparisons with standard ET theory. In the following chapter, I present simulations on the simplest possible system - an ELM dimer - and outline how I used the FOB-SH method to calculate charge transfer rates and what results I found.



## Chapter 4

# FOB-SH results from a donor-acceptor complex

In this chapter I present the bulk of the results I have obtained using FOB-SH: calculating a charge transfer rate between the two molecules of an ethylene-like dimer; investigating the dependence of the rate on reorganization energy, electronic coupling, and driving force; and comparing these dependences with standard theory. I will discuss how the FOB-SH results diverge quantitatively from the theoretical values in regions with parameter values that suggest such theories should be valid, but qualitatively behaviour can still be reproduced.

### 4.1 Simulation details

#### 4.1.1 Model system

The system used to study charge transfer here is the ELM dimer. Figure 4.1 displays the system in question, along with a visualization of the non-orthogonal site orbitals  $\varphi_{1,2}$ .

As I am testing three different parameters in this chapter, I shall now briefly summarise their default values and how they were varied.

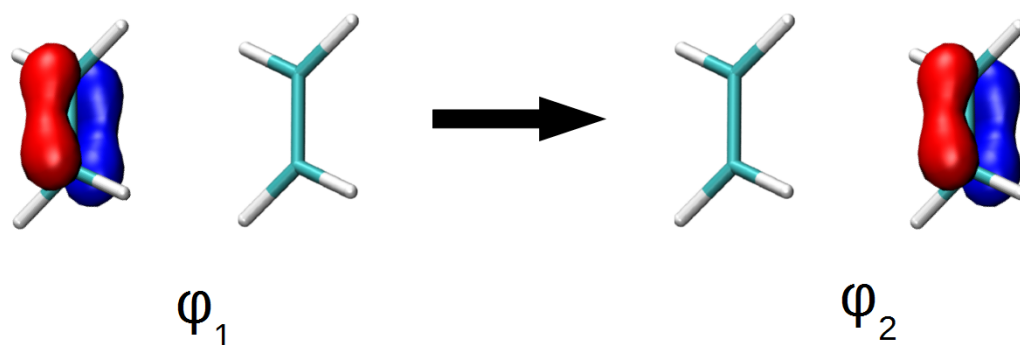


FIGURE 4.1: Visualization of the ELM donor-acceptor complex, used here as a test system to study charge transfer rates with respect to the parameters  $\lambda$ ,  $H_{ab}$  and  $\Delta A$ . The non-orthogonal localized site orbitals  $\varphi_1$  and  $\varphi_2$  are shown:  $\varphi_1$  corresponds to a hole fully localized on the left-hand molecule, and  $\varphi_2$  to a hole fully localized on the right-hand molecule. The arrow indicates the direction of hole transfer from ‘initial’ to ‘final’ charge localized states, though it should be noted that this is only intended as a guide to the ‘forward’ direction as the excess hole is never observed to fully re-localize.

### Reorganization energy

The default value is  $\lambda = 0.3$  eV, unless noted otherwise. The values of  $\lambda$  and  $r_0$  used for investigation of the ET rate dependence on  $\lambda$  are the same as already summarized in Table 3.1.

### Electronic coupling

Electronic coupling matrix elements,  $H_{ab}$ , are calculated using the analytic overlap method, Eq. 2.38, with  $C$  treated as a parameter controlling the strength of electronic coupling. The default value is  $C = 89$  meV giving  $\langle |H_{ab}|^2 \rangle^{1/2} = 8$  meV, unless noted otherwise. The values for  $C$  and the resulting values of electronic coupling used for investigation of the ET rate dependence on the coupling strength are summarized in Table 4.1.

### Driving force

The driving force  $\Delta A$  between the two ELMs is by default zero. Simulations at finite driving forces are modelled by simply adding a constant shift of  $\Delta A$  to  $H_{bb}$ .

TABLE 4.1: Parameterization of electronic coupling  $H_{ab}$  via the constant  $C$  (Eq. 2.38).

$C$ (meV)	$\langle  H_{ab} ^2 \rangle^{1/2}$ (meV)
89	8
177	15
355	30
532	44
710	57
887	68
1330	89
1774	109
2217	127
2661	144
3104	161
3548	180
4435	218

#### 4.1.2 FOB-SH simulations

Initial configurations for FOB-SH were generated from classical MD simulation of the ELM dimer on the initial diabatic state potential energy surface  $H_{aa}$ , i.e. with the hole fully localized on ELM 1. The dimer was initially placed in a stacked configuration at an intermolecular distance of 4 Å. A weak harmonic position restraint with force constant of 1.0 kcal mol<sup>-1</sup> Å<sup>-2</sup> was applied to each carbon atom to maintain a stable intermolecular separation while still allowing for rotational motion of the monomers.

FOB-SH simulations at zero driving force ( $\Delta A = 0$ ) are initiated from structures taken from the classical MD trajectory and propagated on the adiabatic ground state  $E_0$ , noting that  $H_{aa} \approx E_0$  in the initial state diabatic well. For increasingly negative driving forces the initial state becomes unstable against thermal fluctuations as the avoided crossing moves towards the initial state minimum. Here FOB-SH simulations are initiated from  $E_0$  when the energy gap between initial and final diabatic states  $\Delta E \geq 0$  and from the excited state  $E_1$  otherwise. For strongly negative driving forces deep in the Marcus inverted regime  $H_{aa} \approx E_1$ , hence FOB-SH simulations are initiated from  $E_1$ . Consistently to this, the initial conditions for hole propagation according to Eq. 2.10 are  $u_1(0) = 1$ ,  $u_2(0) = \dot{u}_1(0) = \dot{u}_2(0) = 0$ .

The simulations are all carried out in the NVT ensemble, with a Langevin thermostat applied at 300 K with a friction constant of  $\gamma = 10 \text{ ps}^{-1}$ .

### 4.1.3 Electron transfer rates

I have investigated two methods for the calculation of ET rates from SH based on two different observables. The first observable is the population decay of the initial charge-localized (diabatic) state and the other is the number of successful transitions between initial and final diabatic state per unit time. For a fully localized charge transferring between donor and acceptor, the ET rates from population decay and transition count will give the same result. However, in SH the charge is a quantum mechanical object and may delocalize over donor and acceptor. In this case the two definitions are no longer expected to give the same results. The population decay rate is the natural choice when comparing to experimental population decay measurements, whereas the transition count rate is arguably better suited for comparison to ET (Marcus) theory as the latter gives the rate for transfer from initial to final charge-localized (diabatic) state.

#### Population decay

To measure the population decay I monitor the population of the initial charge localized state,  $|u_a|^2(t)$ , and average over a large number of SH trajectories to obtain the electronic population

$$P_a(t) = \langle |u_a|^2 \rangle(t). \quad (4.1)$$

As we will see, the population decays obtained are to a good approximation exponential. I thus fit an exponential function of the form

$$P_a(t) = a \exp(-k_d t) + b, \quad (4.2)$$

which gives the population decay constant  $k_d$  (subscript “d”) while  $a$ ,  $b$  are constant fit parameters.

If I instead consider a reversible reaction of the form



I must take into account a forward rate  $k_f$  and a backwards rate  $k_b$  such that

$$P_a(t) = \frac{k_f}{k_f + k_b} \left[ \frac{k_b}{k_f} + \exp(-(k_f + k_b)t) \right]. \quad (4.4)$$

Comparing Eq. 4.4 with Eq. 4.2 I find  $k_d = k_f + k_b$  and  $a = k_f/k_d$ . Inserting the definition of the equilibrium constant  $K = k_f/k_b = \exp[-\Delta A/(k_B T)]$ , one obtains the SH ET rate from the population decay (subscript “p”),

$$k_p^{\text{SH}} \equiv k_f = k_d(1 + \exp(\beta \Delta A))^{-1}, \quad (4.5)$$

as well as the driving force,  $\Delta A = k_B T \ln(1/a - 1)$ . Subotnik and co-workers have suggested two more definitions of diabatic state population  $P_a$ , in addition to the one given in Eq. 4.1 which was denoted “Method 2” in their paper [119]. In the surface-based method (“Method 1” in Ref. 119) ET is measured by the time evolution of the projection of the active adiabatic electronic state  $\lambda$  on the initial charge localized electronic state. That is, the element of the matrix transforming between adiabatic and charge-localized states,  $P_a = \langle |U_{a\lambda}|^2 \rangle(t)$ . In “Method 3” the mixed quantum-classical density is used to describe the population,  $P_a = \langle \sum_{i=0}^1 |U_{ai}|^2(t) \delta_{i,\lambda} \rangle + \langle \sum_{i<j} 2\text{Re}(U_{ai}(t) \sigma_{ij}(t) U_{aj}^*(t)) \rangle$ , where  $\sigma_{ij} = c_i c_j^*$ .

For comparison, I have calculated and plotted the results of all three methods for one set of 500 SH trajectories, along with their respective exponential fits ( $\lambda = 0.1$  eV,  $\langle |H_{ab}|^2 \rangle^{1/2} = 8$  meV and  $\Delta A = 0$ ). As one can see in Fig. 4.2, the results are very similar for all three methods with ET rates falling in a narrow range of  $0.75 - 1.14 \times 10^{12}$  s<sup>-1</sup> (black lines). Moreover, I find that the decoherence correction leads to a slight decrease in the ET rate to  $1.05 \times 10^{12}$  s<sup>-1</sup> (red solid line) from  $1.14 \times 10^{12}$  s<sup>-1</sup> (black dashed line), improving the agreement with the rate from ET theory,  $8.83 \times 10^{11}$  s<sup>-1</sup>. Since I see little distinction between the three methods in my case, I have calculated all charge transfer rates with Method 2, and with a decoherence

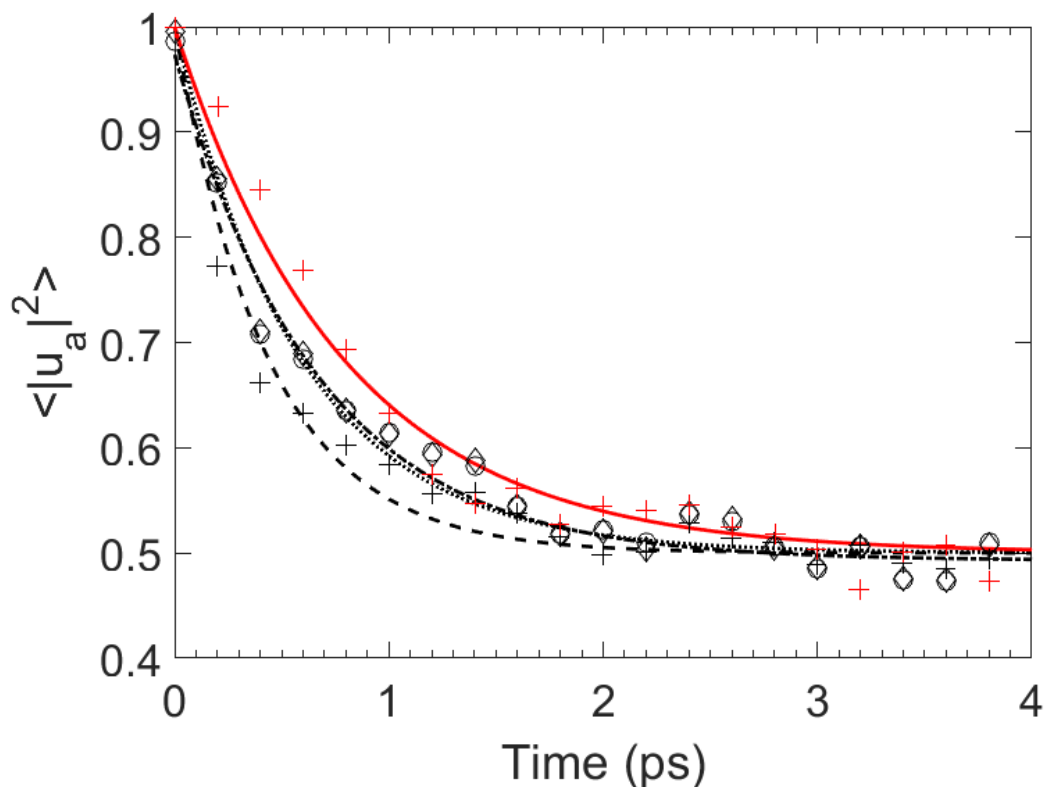


FIGURE 4.2: A comparison of the population decay calculated with the three methods in Ref. 119: method 1 (circles), method 2 (plusses) and method 3 (diamonds). Each also has an exponential curve fitted to it: method 1 (dotted), method 2 (dashed) and method 3 (dot-dash). I have additionally plotted in red crosses a population decay calculated via method 2 with the decoherence correction, with an exponential fit as a solid red line.

correction applied as detailed in Chapter 3.

### Transition count

Here I simply count the number of times,  $N_t$ , that a charge transfers from the donor to the acceptor per second and average over a large number of SH trajectories of length  $T$ ,

$$k_t^{\text{SH}} = \frac{1}{T} \langle N_t \rangle, \quad (4.6)$$

where the subscript  $t$  denotes transition count. Being a quantum mechanical object, the charge is never ‘fully’ located on either donor or acceptor (except at  $t = 0$ ). Hence I need to allow for some finite delocalization and consider a transfer from

donor to acceptor as successful when the amplitude changes from  $|u_a|^2 \geq 0.9$  to  $|u_a|^2 \leq 0.1$ . These ranges were found to adequately describe the transitions in the system. While reasonable changes to these ranges do not significantly affect results, their definition is to some extent arbitrary, which needs to be taken into consideration when making quantitative comparison to Marcus theory.

ET rates from SH are obtained according to Eqs. 4.5 and 4.6 by averaging over 500 FOB-SH runs of variable length in the range 2-500 ps depending on the decay rate. The population decays at zero driving force were found to fit well to a single exponential, Eq. 4.1, with  $R^2$  values of at least 0.92. For calculation of rates from ET theory, Eqs. 1.1, 1.2 and 1.3, values for  $\langle |H_{ab}|^2 \rangle_{\text{TS}}$ ,  $\lambda$ ,  $\Delta A$  and  $\nu_n$  are obtained as follows.  $H_{ab}$  was averaged over the MD trajectories used to initialize the FOB-SH simulations. The difference with the ensemble average at the transition state is expected to be very small and was neglected. Reorganization energies  $\lambda$  were also obtained from these MD runs by averaging over the energy gap,  $\lambda = \langle \Delta E \rangle_a$ . The numerical values were found to be virtually identical with the ones defined in Eq. 3.15 for 0 K at infinite donor-acceptor separation.

For  $\Delta A$  I used the same numerical values as applied in SH simulation. The frequency along the reaction coordinate,  $\nu_n$ , was obtained by calculating the spectral density function of the energy gap as obtained from above MD simulations (see e.g. Ref. 165 for details). The spectrum features a main peak at  $\nu_n = 1700 \text{ cm}^{-1}$ , representative of the C=C stretch vibration.

## 4.2 Results

Before I present my main findings I briefly illustrate a typical simulation in Fig. 4.3. Some properties along a typical FOB-SH run for this system ( $\lambda = 0.3 \text{ eV}$ ,  $\langle |H_{ab}|^2 \rangle^{1/2} = 8 \text{ meV}$  and  $\Delta A = 0$ ) are shown in panels A-C: the amplitude of the initial state,  $|u_a|$ , the time series of the energy gap  $\Delta E$ , and the active adiabatic electronic state. It can be seen that the system begins with the hole localized on the donor/initial diabatic state, with the site energy difference  $\Delta E$  oscillating around the corresponding ground state minimum ( $\Delta E \approx \lambda = 0.3 \text{ eV}$ ). As thermal oscillations bring  $\Delta E$  close

to 0, surface hops to the excited state and back occur and at the same time charge begins to transfer across to the other acceptor, until eventually the system settles down on the ground state with the excess charge now localized on the acceptor. In this example, the same process later occurs in reverse, returning the system to its initial state. In Panel A there are lines to denote the values of 0.9 and 0.1: these are the values I use in the transition-count method when considering if a hole transfer reaction has taken place.

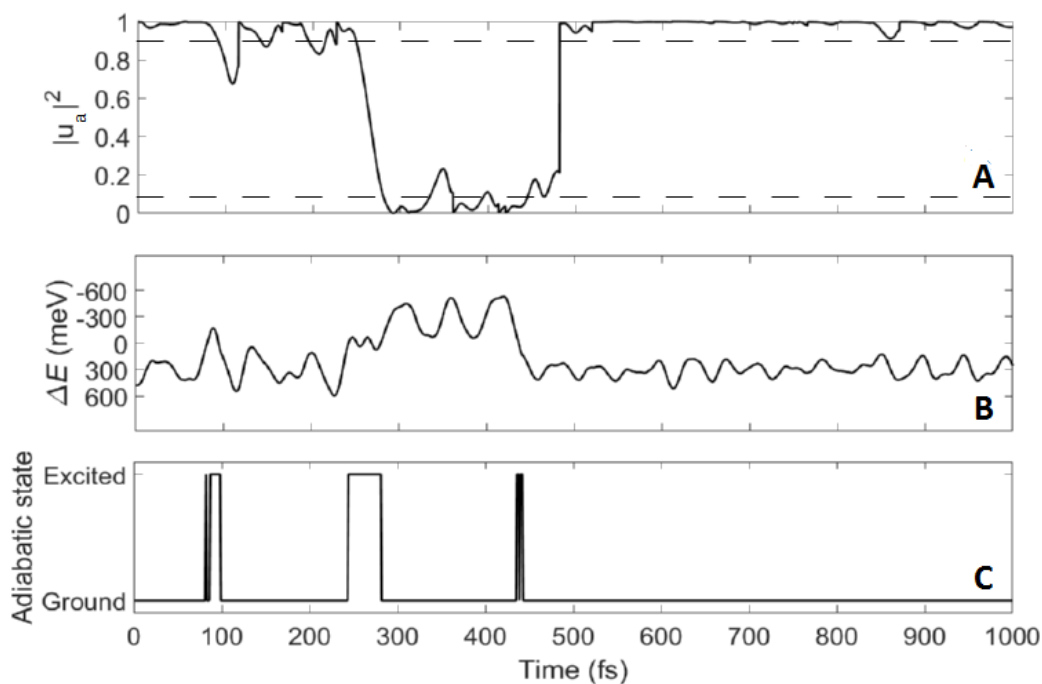


FIGURE 4.3: An illustration of the behaviour of a typical trajectory. Panels A, B and C are time series of different properties during a typical FOB-SH simulation. Panel A shows the time evolution of the initial state amplitude  $|u_a|^2$ , including a transfer from initial to final state and back. Panel B shows the time evolution of the diabatic energy gap  $\Delta E$  and panel C shows the active adiabatic state of the system.

This example trajectory in Fig. 4.3 gives us some idea of what to qualitatively expect from the rate dependencies. It is clear that large-scale charge transfer requires the system to be close to the crossing point at  $\Delta E = 0$ . For larger values of  $\lambda$ , the activation barrier will be higher and the initial state will be further from the crossing point, so I expect the rate to decrease with increased  $\lambda$ . Conversely, as

$H_{ab}$  increases the barrier height will decrease, so the system will reach the crossing region more easily and I expect to see rate increasing with  $H_{ab}$ . Both of these behaviours are also predicted by ET theory, suggesting my SH simulations can (at least) qualitatively reproduce standard results, and are also in agreement with the form of the Rabi equations (Eqs. 3.16 and 3.18).

#### 4.2.1 $\lambda$ dependence

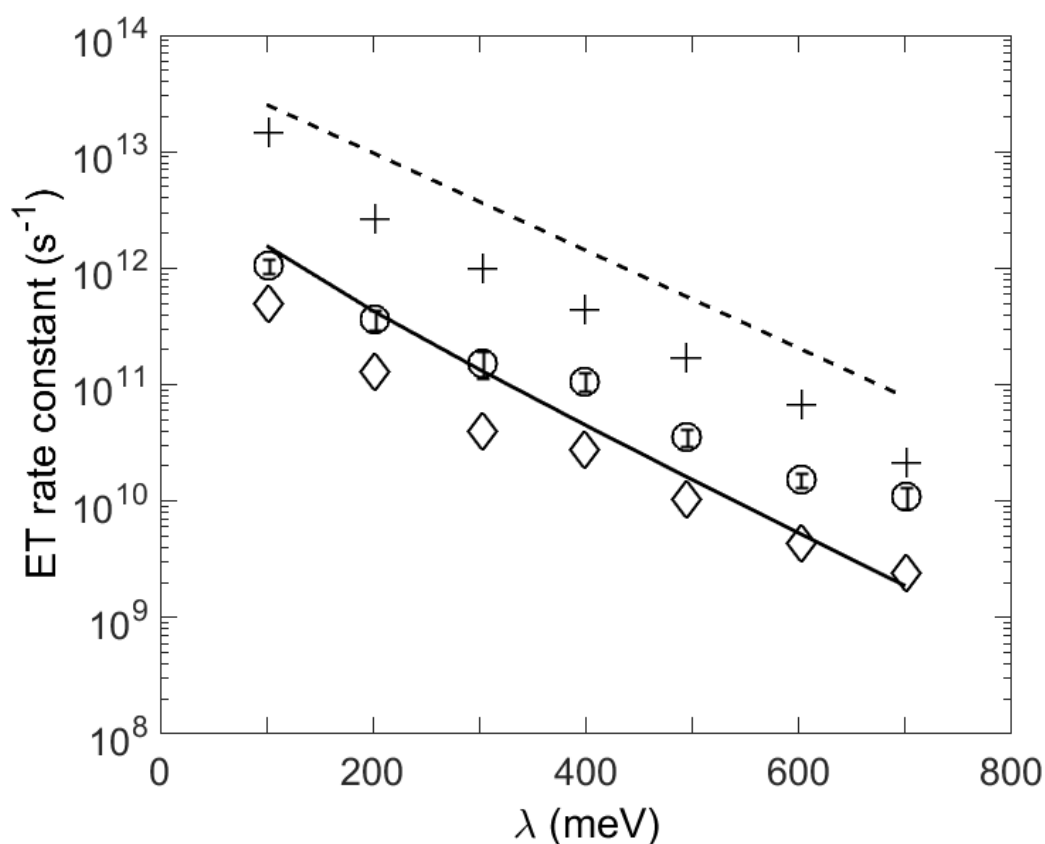


FIGURE 4.4: ET rates for different  $\lambda$  values, obtained from SH simulations, via the population decay method (circle symbols) and transition count method (diamond symbols) against semi-classical ET theory (solid line). I additionally plot the rate of molecular transitions (plus symbols) against the adiabatic ET rate (dashed line) to understand the contribution of nuclear and electronic effects to the rate.

In Fig. 4.4 I plot ET rates from SH transition count ( $k_t^{\text{SH}}$ , diamonds) and population decay ( $k_p^{\text{SH}}$ , circles) against reorganization energy  $\lambda$ . I compare these against results from semi-classical ET theory, Eq. 1.3 (solid lines). I immediately observe a

very good agreement between the transition count rates and ET theory, with absolute values differing by less than a factor of 2. Even for the lowest value of  $\lambda$ , where the activation barrier is on the order of  $k_B T$  and the ET is very fast, this excellent agreement consists. The population decay rates are also in good agreement with ET theory for small  $\lambda$  values, but there are significant deviations of up to a factor of 5 for larger  $\lambda$  values. Both the SH transition count and exponential decay rates appear to predict similar slopes for rate vs.  $\lambda$ , and these slopes are also slightly shallower than those predicted by ET theory. In the following I try to rationalize these findings.

Seeking to analyse at first the good agreement between ET theory and SH transition count rates, I consider the ET rate  $k$  ( $k_{SC}$  in Eq. 1.3 as a product of the rate in the adiabatic limit,  $k_{ad}$  (Eq. 1.2), which is a purely nuclear rate factor, and the electronic transmission coefficient  $\chi_{el}$ ,  $k = \chi_{el} k_{ad}$ . Similarly,  $k_t^{SH}$  is considered as a product of a purely nuclear rate obtained by counting nuclear crossings during SH simulation from initial to final state well,  $k_{t,ad}^{SH}$ , and a corresponding electronic transmission coefficient  $\chi_{t,el}^{SH} = k_t^{SH} / k_{t,ad}^{SH}$ . I can see in Fig. 4.4 that  $k_{t,ad}^{SH}$  (plus symbols) is smaller than  $k_{ad}$  (dashed lines), by a factor of up to 5. This can be attributed to frictional effects on the molecules, leading to unsuccessful crossings and recrossings at the barrier top, not taken into account by ET theory. Conversely, the electronic transmission coefficient in SH is by about the same amount larger than what is expected according to ET theory, more specifically Landau-Zener theory. Those two opposing effects largely cancel one another and lead to similar overall ET rates.

The increasing difference between the transition count ( $k_t^{SH}$ ) and population decay ET rates ( $k_p^{SH}$ ) with increasing  $\lambda$  can be understood by analysing the qualitative behaviour of the donor amplitude  $|u_a|^2(t)$ . In Fig. 4.5 I show  $|u_a|^2(t)$  for small  $\lambda$  (0.1 eV, panel A) and for large  $\lambda$  (0.7 eV, panel B). At 0.1 eV the barrier on the ground state is about  $k_B T$ . Barrier crossings, switches to the excited state and generation of resonant donor-acceptor structures (defined by  $-H_{ab} \leq \Delta E \leq H_{ab}$ ) occur very frequently, resulting in the oscillation of one full hole between donor and acceptor. With increasing  $\lambda$  the barrier increases and becomes more steep. Resonance

occurs infrequently and for shorter durations. This can lead to “interruption” of hole transfer by the system moving quickly away from the crossing point before the hole becomes fully localized on a single site.

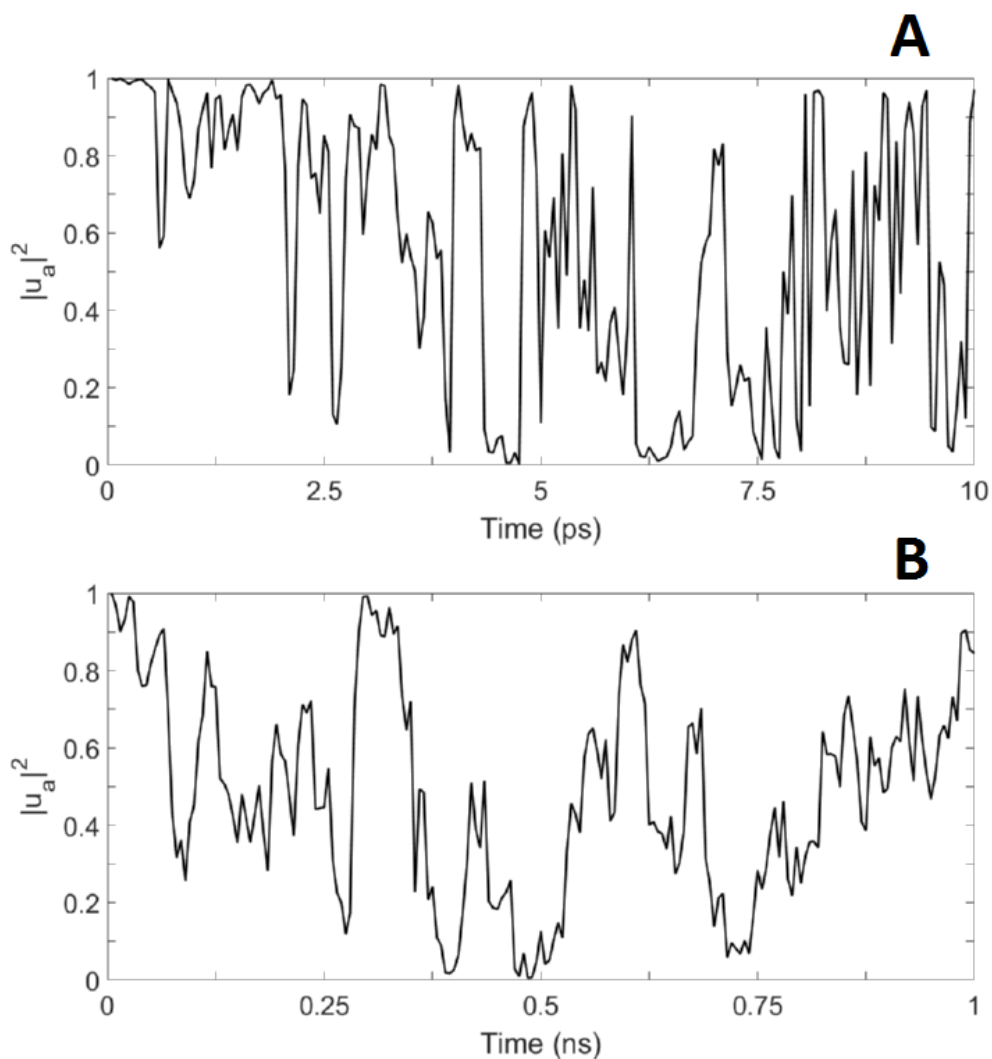


FIGURE 4.5: A comparison of the different electronic behaviour for two different values of reorganization energy  $\lambda$ . In panel A,  $\lambda = 0.1$  eV and within ten picoseconds I observe many large-amplitude oscillations, including a number of ‘successful’ transitions. In contrast, panel B has  $\lambda = 0.7$  eV and over the course of a nanosecond trajectory there are only a couple of successful transitions, while for long periods of time the population becomes stuck in a half-and-half state, contributing to the rate by exponential decay but not the rate by transition count.

The decoherence correction then causes  $|u_a|^2$  to attain values close to 0 or 1, depending on whether the system settles in the initial or final well. While each

interrupted transfer event contributes to the population decay and hence to  $k_p^{\text{SH}}$ , only the fraction of events that settle in the final well count towards  $k_t^{\text{SH}}$ . This explains the consistently higher  $k_p^{\text{SH}}$  compared with  $k_t^{\text{SH}}$ .

#### 4.2.2 $H_{\text{ab}}$ dependence

I now want to expand my parameter range to configurations where I expect the ET theory to be inadequate, due to high electronic coupling reducing the barrier to zero. For this reason, I plot in Fig. 4.6 the dependence of ET rates on average electronic coupling strength,  $\langle |H_{\text{ab}}|^2 \rangle^{1/2}$ . As before, I plot data from both SH transition count ( $k_t^{\text{SH}}$ , diamonds) and population decay ( $k_p^{\text{SH}}$ , circles) alongside results from ET theory (lines) - in this instance I plot the general ET rate Eq. 1.3 as well as both the non-adiabatic and adiabatic ET rates, Eqs. 1.1 and 1.2 respectively, to demonstrate how the former interpolates between the latter two expressions.

I observe some similar qualitative behaviour to that found in Fig. 4.4. The agreement between SH and ET theory (Eq. 1.3) is particularly good in the small coupling regime ( $0 - 60 \text{ meV} \leq 0.2\lambda$ ) with deviations of less than a factor of about 2. I fit a curve  $\log k_p^{\text{SH}} = a \log \langle |H_{\text{ab}}|^2 \rangle^{1/2} + b$  to the points in this range and obtain  $a = 2.0$ , in good agreement with the prediction for the non-adiabatic limit Eq. 1.1, for which  $a = 2$  (though for the larger couplings in this regime the non-adiabatic rate starts to deviate from Eq. 1.3). The SH rates begin to flatten in comparison to ET theory in the adiabatic regime where electronic coupling values are large ( $\geq 60 \text{ meV} = 0.2\lambda$ ).

At the point  $\langle |H_{\text{ab}}|^2 \rangle^{1/2} = \lambda/2$  (150 meV), the barrier for ET has completely disappeared and the SH rate is below the ET theory rate, though by no more than a factor of 5. The latter is maximal at this point and equal to the frequency of the effective nuclear mode coupling to ET,  $k = \nu_n = 5 \times 10^{13} \text{ s}^{-1}$  (Eq. 1.3,  $\kappa_{\text{el}} = 1, \Delta A^\ddagger = 0$ ). In this ultrafast regime, ET theory is no longer expected to be valid. It is therefore interesting to note the relatively good agreement with SH results. The SH rate continues to increase with increasing electronic coupling even after the ET theory rate has reached its maximum value.

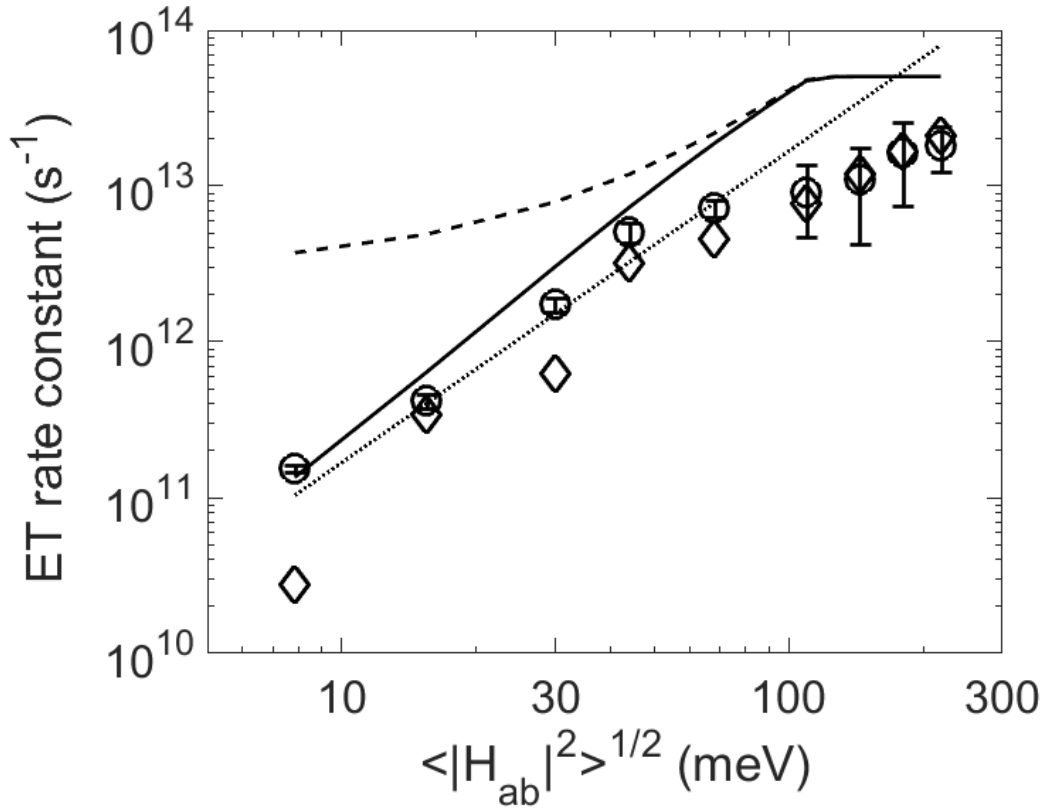


FIGURE 4.6: ET rates calculated for different values of  $\langle |H_{ab}|^2 \rangle^{1/2}$  from the exponential fit method (circle symbols) and transition count method (diamond symbols). They are compared with the generalized semi-classical ET theory (solid line), adiabatic ET theory (dashed line) and Marcus theory (dotted line).

Returning again to the difference between transition count and exponential decay rates, I find that the former are again generally lower than the latter. I ascribe this to the same reasons as in Fig. 4.4. As electronic coupling increases, the two methods appear to converge: I suggest that this is because for sufficiently large coupling, where the barrier is negligible, the charge is constantly oscillating between the two states and thus there is no real difference between the two methods of calculating the rate.

Further insight into this high-coupling regime comes from work that was done in my group as an extension of my investigation here, which was published in Ref. 151: although this particular finding is not my work, I include it here as it is relevant to the discussion. As  $\langle |H_{ab}|^2 \rangle^{1/2}$  increases past  $\lambda/2$ , the barrier to charge transfer entirely disappears and thus the charge becomes delocalized over both

sites. Laura Scalfi and Antoine Carof, my co-workers in Ref. 151, observed that in this region the exponential fit to the population decay appears to be less valid and came up with an alternative description, based on the Rabi frequency as in Eqs. 3.16 and 3.18. This description is rooted in the idea that for very high couplings, the first few electronic oscillations are well described by the initial Hamiltonian  $H(0)$ . With this in mind, a new description analogous to the electronic transfer rate (as the absence of a barrier negates actual transfer between sites) in this region was devised: a relaxation rate from localized to delocalized charge was defined as  $1/t_{max}$  where  $t_{max}$  is the time at which the damped oscillation of the electronic population reaches its first maximum after  $t = 0$ .

This new description of the rate for very high electronic couplings led to an updated figure for the dependence of rate with  $H_{ab}$ . This is Figure 4.7, reproduced with permission. The relaxation rate in the highest coupling regime is calculated as described in the previous paragraph: we observe an approximately linear increase in rate with  $H_{ab}$ , which fits with the form of Eq. 3.18 at  $\Delta E = 0$ .

### 4.2.3 $\Delta A$ dependence

Finally I investigate whether SH can reproduce the characteristic inverse power-law dependence of ET rates on driving force and the Marcus inverted region in particular. In Fig. 4.8 I plot the SH rate obtained from the population decay ( $k_p^{SH}$ , circles) alongside the ET theory rate Eq. 1.3 (lines). The driving force is varied from  $\Delta A = 0$  to more negative values well beyond the onset of the inverted regime at  $\Delta A = -\lambda$ . The reaction now becomes biased towards the final state and is in fact irreversible on the time scale of present simulations. Once the hole is localized on the acceptor I do not observe the reverse transfer. Therefore, the transition count method is no longer used for calculating rates.

In Fig. 4.8 I see that SH is capable of reproducing the inverse power law of ET theory in broad strokes. A fit  $\log k_p^{SH} = -(\Delta A + a)^2 / (4bk_B T) + c$  ( $R^2 = 0.64$ ) gives  $a = 282$  meV,  $b = 410$  meV, which should be compared to the result of Marcus theory,  $a = b = \lambda = 0.3$  eV. Consistent with simulations discussed above, the calculated SH

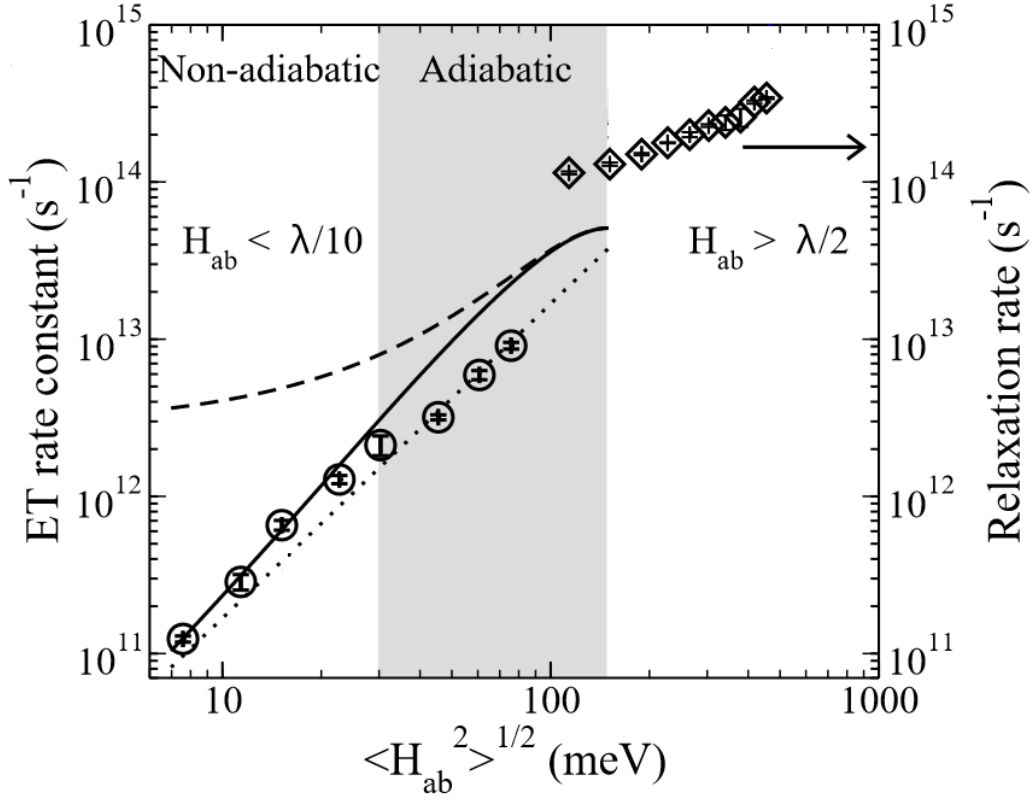


FIGURE 4.7: ET rates from FOB-SH MD simulation ( $k_p^{\text{SH}}$ , Eq. 4.5) against average diabatic electronic coupling  $\langle |H_{ab}|^2 \rangle^{1/2}$  (circles). For comparison, the ET rates from semi-classical ET theory, Eq. 1.3 (solid lines), and the respective non-adiabatic limit Eq. 1.1 (dotted line) and adiabatic limit Eq. 1.2 (dashed lines) are displayed. For large electronic coupling, charge relaxation rates from FOB-SH MD simulation are shown ( $t_{\text{max}}^{-1}$ , diamonds). All FOB-SH MD simulations were carried out for  $\lambda = 0.3$  eV and  $\Delta A = 0$ .

rates are generally higher than those predicted by ET theory, on average by a factor of 2-3. Again I think this is due to partial hole transfer and delocalization giving a faster population decay rate than that which would be given by the counting of transitions of a full hole between donor and acceptor.

I additionally observe that these rates qualitatively describe an increase and subsequent decrease in the rate with decreasing  $\Delta A$ , with my maximum value coming close to  $\Delta A = -\lambda$ . In Fig. 4.8 I again see, in agreement with the previous figures, that my calculated SH rates are generally higher than those predicted by standard ET theory, by up to an order of magnitude. Although my method

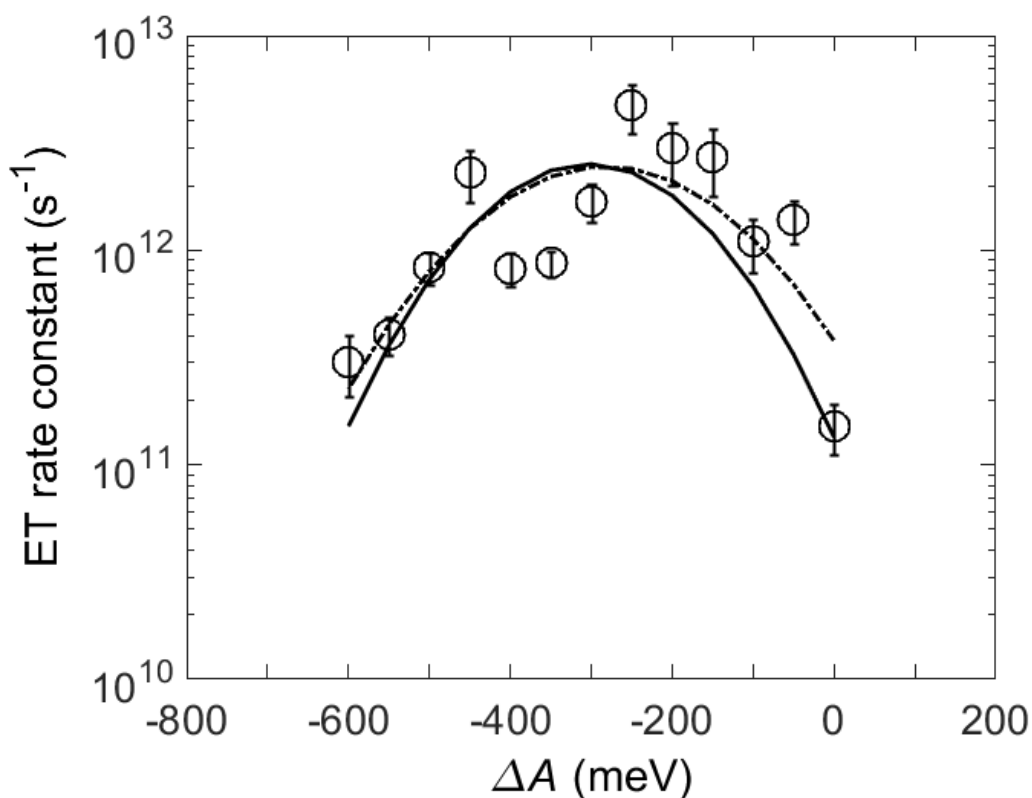


FIGURE 4.8: ET rates calculated for different values of driving force  $\Delta A$  from SH simulations via the exponential fit method (circle symbols), plotted against rates obtained from the semi-classical ET theory (solid line). Additionally, a parabola has been fitted to the SH rates, and is denoted by a dot-dash line.

is apparently capable of reproducing this behaviour in broad strokes, I notice one odd feature which is a 'dip' in the calculated rates shortly after the theoretical peak at  $\Delta A = -\lambda$ . An exact explanation for this feature is not understood at present. In general, despite the symmetric dependence on  $\Delta A$  in the generalized ET expression, I can expect that the continuously increasing irreversibility of the electronic transfer would give rise to qualitatively different behaviour on either side of  $\Delta A = -\lambda$ , but at present I do not have a fully satisfying explanation for this feature.

As my first step towards such an explanation, I have plotted in Figure 4.9 the same data as in Figure 4.8 but have compared the data against a slightly different fit. I still fit the expression  $\log k_p^{\text{SH}} = -(\Delta A + a)^2 / (4bk_B T)$ , but now I exclude the 'anomalous' points from the fit (the rates at  $\Delta A = -300, -350, -400$  meV). In this case the fit yields  $a = 294$  meV,  $b = 291$  meV, as well as an unsurprisingly much

higher  $R^2$  value ( $R^2 = 0.88$ ). The fact that this fit agrees much better with Marcus theory suggests that those three points are the result of some additional effect that does not fit in with the overall picture of the rest of the results.

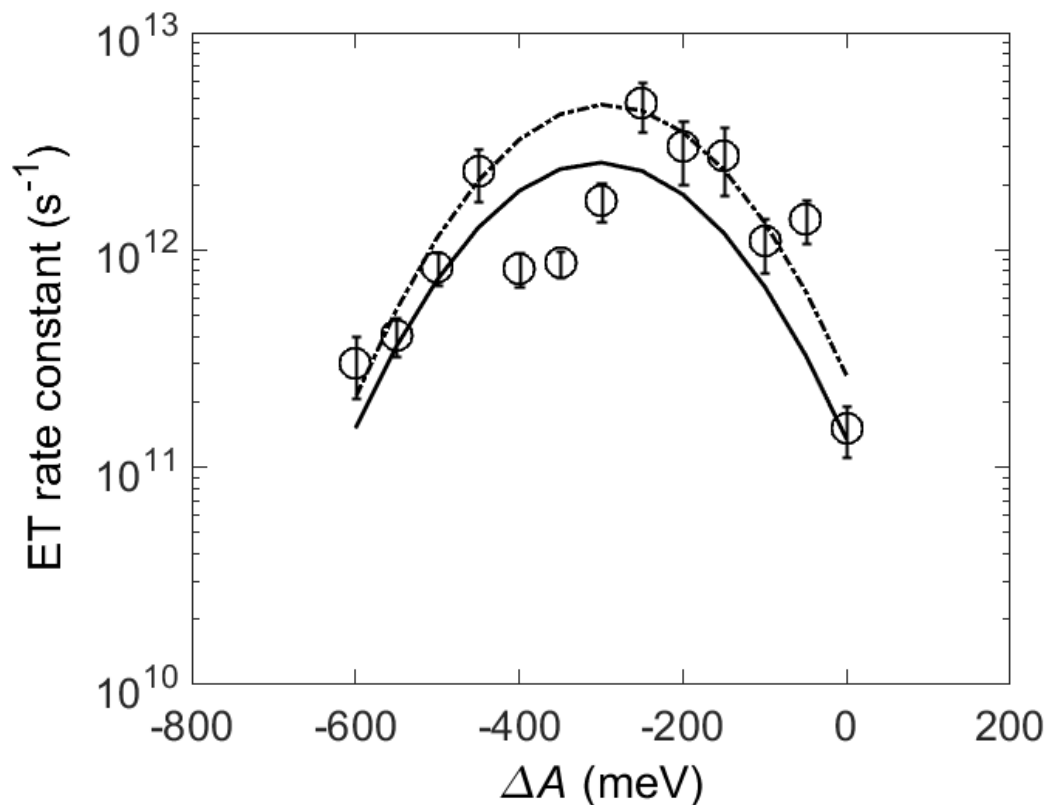


FIGURE 4.9: This is similar to Figure 4.8, but in this figure a parabola has instead been fitted to a subset of the SH values. The ‘anomalous’ points at  $\Delta A = -300, -350, -400$  meV have been omitted from this subset. In this case the fit much more closely fits the result of Marcus theory.

I nonetheless can conclude that my SH method can qualitatively show the existence of the inverted Marcus region.

### 4.3 Discussion

Although the results I present here come from a first implementation of FOB-SH, I think they still provide an interesting comparison to the standard ET theory rates. My method is able to quickly produce a statistically significant number of trajectories, meaning that for the first time I can investigate charge transfer rates on a

system that closely resembles a physical one. As this takes us beyond the realm of analytic solutions, my comparisons must consider both the validity or otherwise of standard ET theory and the known shortcomings of the SH method.

As discussed in section 4.1.3, there is a question over exactly how ET rates should be calculated from SH simulations. My two methods both have imperfections for comparison to standard ET theory. On the one hand, extracting a rate from an exponential fit is analogous to experimental measurements of population decay and, it can be argued, may not be directly comparable to e.g. Marcus theory. Such theories directly calculate a rate for transfer from initial to final state, which is also what my transition count method does. This method however depends on an arbitrary choice for the transition ‘threshold’ (chosen in my simulations as  $|u_a|^2$  dipping below 0.1): the calculated rate is dependent upon this choice; the most stringent definition possible ( $|u_a|^2$  reaching 0) is likely to give us spurious rates, as the quantum oscillations of the electronic populations make it unlikely for this point to actually be reached; and without a clear justification for any other particular choice, a quantitative comparison between standard ET theory and transition count rates should also be treated with caution. On the other hand, the fact that I can calculate these rates in two different methods, each corresponding to a different experimental technique, suggests that my method could eventually be useful for comparison to a wide range of experimental results.

The decoherence correction, specifically the choice of how to correct for electronic overcoherence, is a big feature of my (indeed of any) SH method, as the literature widely agrees that such a correction is vital to reproduce physical behaviour. Fig. 4.2 does suggest that this correction, among other effects, could alter the rates that I calculate from SH simulation, though at least in my case this does not seem to be a very significant effect. Thus far, the correction applied is a very simple one, simply collapsing the wavefunction at certain points during the trajectory, and it is equally possible that there could be an effect on the rate from choosing different corrections for the overcoherence. This is something that could be investigated with future uses of the FOB-SH method, as I discuss in Chapter 6.

My aim with the FOB-SH method was to begin to see if I could probe the regions of ultrafast ET transfer, where the electronic coupling  $H_{ab}$  becomes large and standard ET theory should become inapplicable. I see here that the semi-classical ET theory and my SH results diverge in this region, although the disagreement is still less than an order of magnitude. Perhaps a more striking feature is that the semi-classical theory reaches a maximum value where the activation barrier becomes zero, but beyond this point my SH rates apparently continue to increase. Although these results are not conclusive, this suggests that my FOB-SH method agrees well with standard ET theory in the regions where I expect it to be valid (large reorganization energy and/or small electronic coupling), while diverging more for large couplings. Nonetheless the agreement is still relatively good between SH and ET theory rates, with a difference of less than an order of magnitude. The fact that standard ET theory and my non-adiabatic molecular dynamics methods can produce rates that agree relatively closely suggests that, for some reason, ET theory is capable of coming close to the 'true' rates even when the assumptions underpinning it are invalid: this may also explain why hopping models of electron transport are capable of producing electron mobilities which agree well with experimental results, even when the hopping model itself may be an invalid assumption.

I lastly conclude that these results are promising for future applications of the FOB-SH method. I have used it to compare to standard ET theory over a wide parameter range in a system that closely models an idealized molecular donor-acceptor complex. The method is able to describe charge transport and produce comparisons to standard theory in the ultrafast ET regime, suggesting that it is well suited to investigating problems of electronic behaviour in physical systems where typical values of the reorganization energy and the electronic coupling are such that these standard theories may not be valid. In the next chapter, I will progress beyond the two-state system described in this chapter and will perform some preliminary investigations into a larger system.



## Chapter 5

# FOB-SH results from a 10-molecule chain

In this last chapter, I demonstrate that the FOB-SH method can be successfully applied to a system of sufficient size that the two-site force expression cannot be used. For the sake of relative simplicity in proving this, I have created a system of ten ethylene-like molecules in a chain and have calculated the temperature dependence of the charge mobility along this chain according to FOB-SH for three different values of the electronic coupling between molecules. I discuss what seems to influence this temperature behaviour and attempt to understand the different results in different regimes.

### 5.1 Simulation details

#### 5.1.1 Model system

Figure 5.1 displays the simulation system. 10 ELMs were placed along the  $x$ -axis with a distance of 4 Å separating each molecule. Similarly to the two-molecule system, a weak harmonic restraint was applied to the carbon atoms of each molecule with a force constant of 1.0 kcal/mol Å<sup>-2</sup> to keep them close to their starting positions and to keep the chain structure stable.

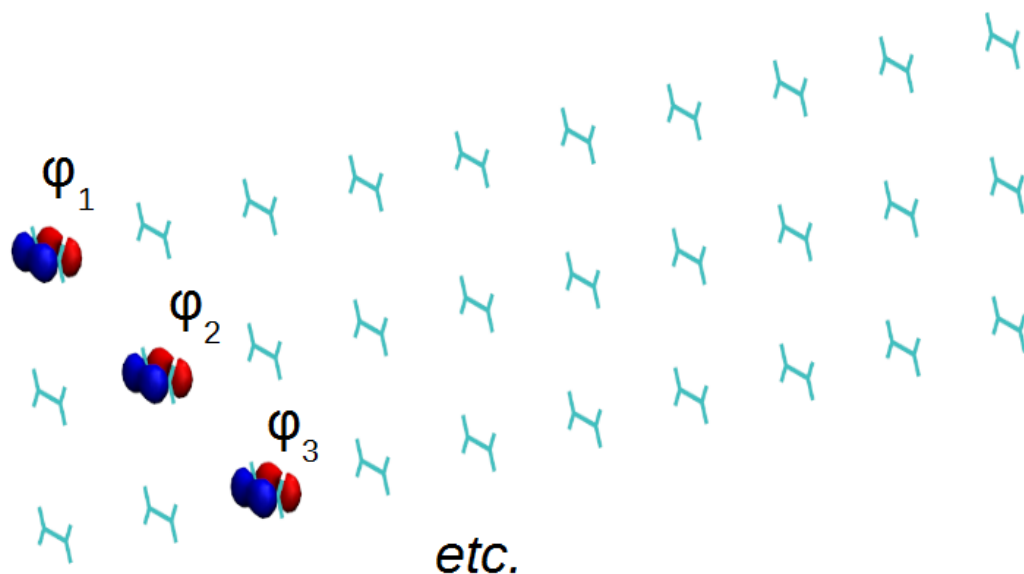


FIGURE 5.1: A schematic of the simulation system for charge mobility calculations. 10 ELMs are placed in a chain with intermolecular distances of 4 Å. The three chains in the picture demonstrate the system with a charge localized on ELM 1, 2, and 3.

### 5.1.2 Procedure

My intention was to demonstrate that, similarly to a recent investigation by Wang and Beljonne [85], my FOB-SH MD method is capable of reproducing the thermally-activated CT at low electronic coupling strength and its absence for higher coupling strength. I also sought to understand exactly what in my systems causes this difference in behaviours at low and high coupling.

To generate starting configurations from which to run mobility calculations, a similar procedure to that outlined in Chapter 4 was followed. First, a classical MD trajectory in the NVT ensemble at temperature  $T$  was run for 1 ns without surface hops, where the first/leftmost ELM was modelled in the positively charged state and the remaining 9 ELMs in the neutral state.  $N$  snapshots from that MD trajectory were taken as initial configurations and velocities for SH MD runs. For each SH MD trajectory the mean-squared displacement (MSD) of the centre of charge of the carrier, was obtained from the time evolution of the expansion coefficients in the site basis, Eq. 2.10, and averaged over all  $N$  SH MD trajectories thus:

$$R^2(t) = \frac{1}{N} \sum_{n=1}^N \langle \Psi_n(t) | x | \Psi_n(t) \rangle^2 \quad (5.1)$$

$$= \frac{1}{N} \sum_{n=1}^N \left[ \left( \sum_{l=1}^M |u_{l,n}(t)|^2 x_{l,n}(t) \right)^2 \right] \quad (5.2)$$

where  $x_{l,n}$  is the position of the centre of mass of molecule  $l$  in trajectory  $n$ , and  $\sum_{l=1}^M |u_{l,n}(t)|^2 = 1$ .

The SH trajectories were initiated with the charge carrier localized on the first site, hence  $R^2(0) = 0$ . When the MSD is linear, which was the case for the system investigated here, the Einstein diffusion constant  $D$  can be obtained from the MSD,

$$D = \frac{1}{2} \frac{dR^2(t)}{dt}. \quad (5.3)$$

The mobility  $\mu$  is then given by

$$\mu = \frac{eD}{k_B T}, \quad (5.4)$$

where  $e$  is the elementary charge and  $k_B$  the Boltzmann constant.

I kept the reorganization energy  $\lambda$  at a consistent value of 0.2 eV for all these simulations. I calculated mobilities along the chain for three values of  $C = 17.74, 177.4$  and 1419 meV and for a wide range of temperatures,  $T = 50, 75, 100, 150, 200, 250, 300, 500, 800, 1000$ K. The MSD was averaged over 500 SH MD trajectories to obtain  $R^2(t)$ . In each case, there was a clear linear regime in the time-evolution of  $R^2(t)$ , occurring before charge carrier amplitude was building up at the final site of the system (which would introduce artificial reflection effects).  $D$  was obtained from a linear fit to this region in each case. The statistical uncertainty of the mobility, obtained by block averaging of  $R^2(t)$ , is typically 10% of the mean value.

## 5.2 Results

The mobilities obtained from SH MD according to Eq. 5.4 are plotted against temperature in Figure 5.2. Straight away it is clear to see that, similarly to the aforementioned investigations by Wang et al. [85], the lowest coupling values display a thermally activated behaviour, with the mobility increasing with temperature to a point before decreasing again: and that this contrasts with the higher coupling behaviours, both of which broadly show a decrease in mobility with increasing temperature.

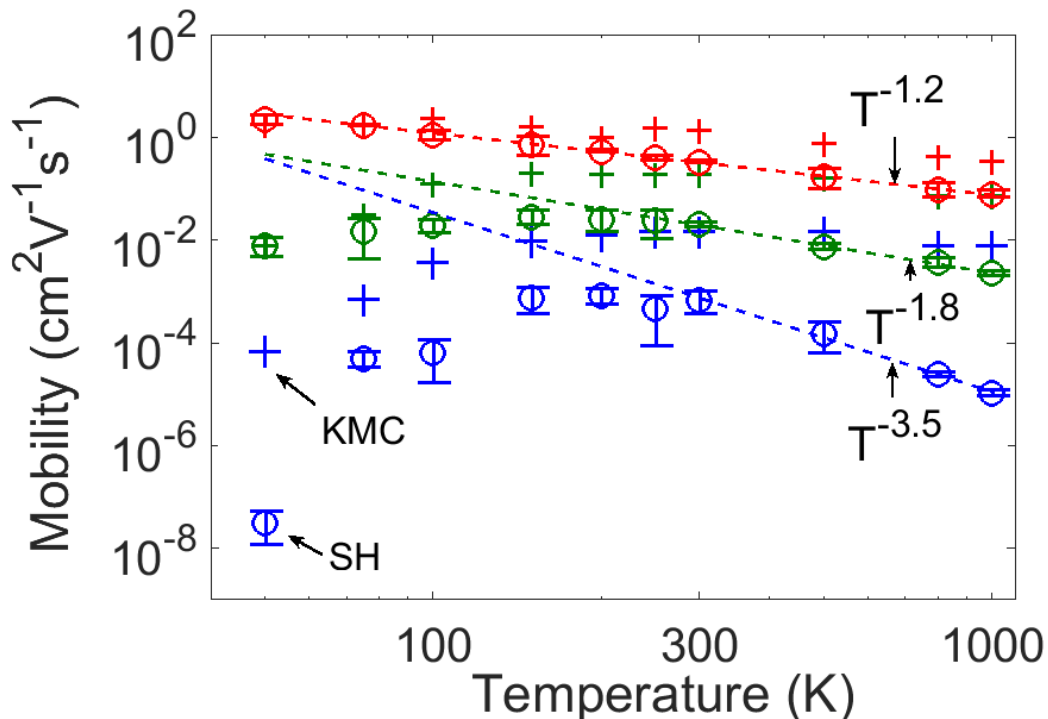


FIGURE 5.2: Temperature dependence of charge mobilities along the 10-molecule ethene-like chain, for three different values of average coupling as displayed. Results from both surface hopping (SH) and kinetic Monte Carlo (KMC) simulations are shown, as are the results of power law fits to the region 300K to 1000K for each coupling regime. For the lowest value, a clear thermal activation peak is visible in the SH results with a maximum mobility at a temperature of around 200K. For higher coupling values, I see a continual decrease in mobility with temperature, corresponding to a band-like transport mechanism. The KMC results contrast with the FOB-SH results, showing a much shallower decrease with temperature after the crossover.

For further analysis I fitted a simple power law-type temperature dependence to the higher temperature values (300 to 1000K) for each of the three coupling

regimes. This gives a range of exponents as follows:  $T^{-1.2}$  for the highest coupling,  $T^{-1.8}$  for the intermediate and  $T^{-3.5}$  for the lowest. These should probably be compared with the range of exponents suggested by Heck et al. [62], i.e. from -0.5 to -3.

For comparison, I have also plotted in Figure 5.2 mobilities calculated for the hopping model using a KMC simulation. These KMC simulations were carried out by Fruzsina Gajdos in our research group [150] to provide comparison and contrast between my FOB-SH method and a more frequently used method for modelling charge transport. In contrast to the SH results, the KMC simulations seem to underestimate the decrease in mobility with  $T$  relative to FOB-SH: I note that Eq. 1.3, which this method relies upon for rate calculations, is problematic for this regime of  $|H_{kl}|$  due to the absence of an energy barrier for charge transfer. For the lowest coupling regime, the KMC does appear to demonstrate a thermal activation, but still does not display the marked cross-over from thermally activated hopping to band-like transport.

### 5.3 Discussion

As I anticipated, we can see a thermally-activated charge transport for the smallest electronic coupling strength (blue symbols) at low temperatures. Around room temperature I observe a crossover from activated to band-like transport with the mobility decreasing for increasing temperatures according to  $\mu \propto T^{-3.5}$ . With increasing electronic coupling strengths, thermal activation gradually disappears. For the highest coupling strength investigated (red symbols), the mobility decreases steadily with  $T$  according to  $\mu \propto T^{-1.2}$ . A qualitatively very similar behaviour, i.e. crossover from activated to band-like transport at low coupling and disappearance of activated regime at high coupling regime, has been obtained from SH simulations of a simple 1D model Hamiltonian by Wang and Beljonne [85], as mentioned previously. Moreover, an inverse power law dependence of the mobility with temperature similar to the one observed here for the large coupling regime, has been reported by Troisi et al. [47, 55] and by Fratini et al [166].

To explain the steady decrease in mobility with increasing temperature in the high coupling regime, I return to the concept of resonance for charge transfer. In Figure 5.3 (panel A) I plot the probability distribution of the vertical energy gap between the first site where the charge is initially located and the second site,  $\Delta E_{12}$ , along an equilibrium MD simulation in that initial electronic state, for different temperatures. I also indicate an averaged resonance region arising from the mean electronic coupling along these trajectories,  $\langle |H_{12}| \rangle = 129.9$  meV, which remains rather insensitive on temperature. For low temperature, I find that the peak of the thermal equilibrium distribution of  $\Delta E_{12}$  is already well within the resonance region, which I define with the boundaries  $\Delta E_{12} = \pm 2\langle |H_{12}| \rangle$ , as at these boundaries the prefactor in Eq. 3.16 is exactly 0.5 and potentially allows half the charge to transfer to the second site. Therefore propagation of the charge carrier occurs instantly for the vast majority of initial configurations. A temperature increase will broaden the distribution for  $\Delta E_{12}$  and thereby reduces the probability for the system to be within the resonance region. Consequently, the time it takes for the charge to move from site 1 to site 2 and further along the chain will increase and hence the mobility will decrease.

The situation is strikingly different for the temperature-activated transport observed in the low coupling regime, Figure 5.3 (panel B). Here the peak of the equilibrium distribution of  $\Delta E_{12}$  is outside the very narrow resonance region ( $\langle |H_{12}| \rangle = 1.6$  meV). As the temperatures increases, the energy gap distribution becomes wider and the probability for resonance increases. Therefore the charge mobility increases with increasing temperature at low temperature. The reason for the crossover at about room temperature is less clear, though I think that the effect of increasing probability for resonance saturates at a sufficiently high temperature so that the  $T^{-1}$  term of Eq. 5.4 takes over. The observed  $T^{-2.1}$  dependence points to an additional effect that leads to a decrease of the diffusion constant with temperature in this regime, an observation that needs to be further analyzed in future work.

Our explanation of the  $T$ -dependence of mobility is further illustrated in Figure

5.4, where I plot the fraction of time that the system has spent in the resonance region  $\Delta E_{12}(t) = \pm 2|H_{12}(t)|$  (i.e. the probability to be in the resonance region) during the same equilibrium MD runs described above (first site in charged state, all other sites in neutral state). I assert that this resonance probability be proportional to the diffusion constant and in the spirit of Eq. 5.4 divide it by  $k_B T$  to correlate it with the mobility from SH. As one can see in Figure 5.4 the correlation is very good, in particular for the low and high electronic coupling regimes.

With this set of results from a relative large system of organic molecules, I consider that the aim of the project - being to develop a method, implement it, and demonstrate its suitability and applicability to the problem of charge transport in organic semiconductors - has been satisfactorily reached. Naturally, with these somewhat preliminary results not every question has been answered and in fact many more have been posed. In particular, the purpose of the FOB-SH method is to investigate charge transport in the regime where standard ET theory is not valid, but so far I have not provided any comprehensive answers as to the nature of charge transport in these regimes. I have instead enjoyed more success with showing agreement with known results in regimes where these results should be valid. In the next and final chapter, I will discuss how the method might be expanded and improved upon, and then applied in earnest to these questions in the hope of making further substantial contributions towards solving the problem.

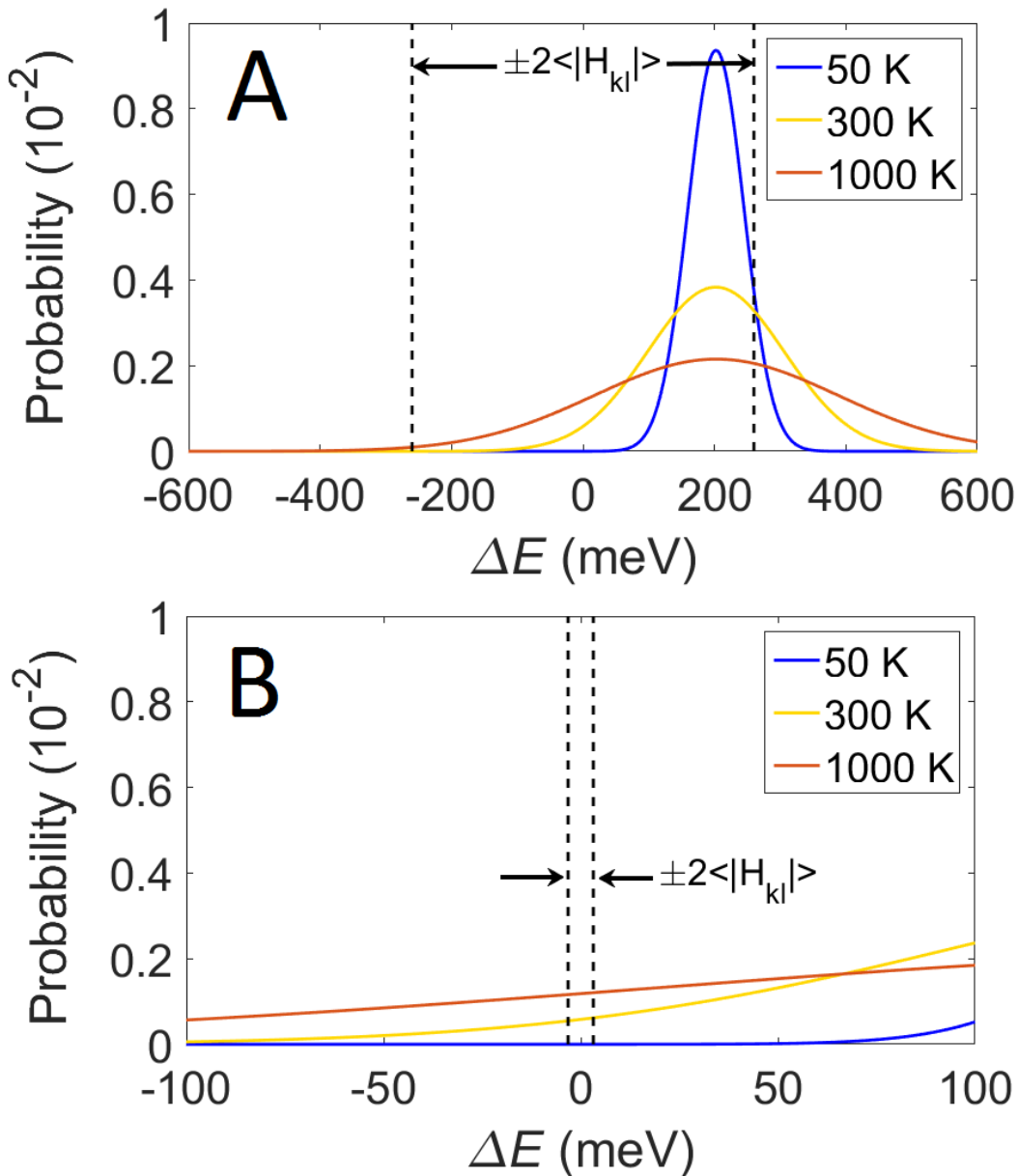


FIGURE 5.3: Gaussian distributions of the site energy difference between neighbouring molecules in the ELM chain along an initial equilibrium trajectory, for three different values of the temperature within the range plotted in Figure 5.2, and for two different coupling values in two different panels. As the temperature increases, thermal fluctuations in the site energies broaden these distributions. For sufficiently high values of  $\langle |H_{kl}| \rangle$ , as shown in panel A, this reduces the area under the curve that is within the resonance region i.e. between the values  $\Delta E = \pm 2\langle |H_{kl}| \rangle$  and the mobility thus decreases accordingly with temperature. For smaller values of  $\langle |H_{kl}| \rangle$ , as shown in panel B, this broadening instead allows the area under the curve in the resonance region to increase from zero and thus increasing temperature instead increases mobility - though as Figure 5.2 shows, at some point this behaviour is replaced by a decreasing mobility with temperature.

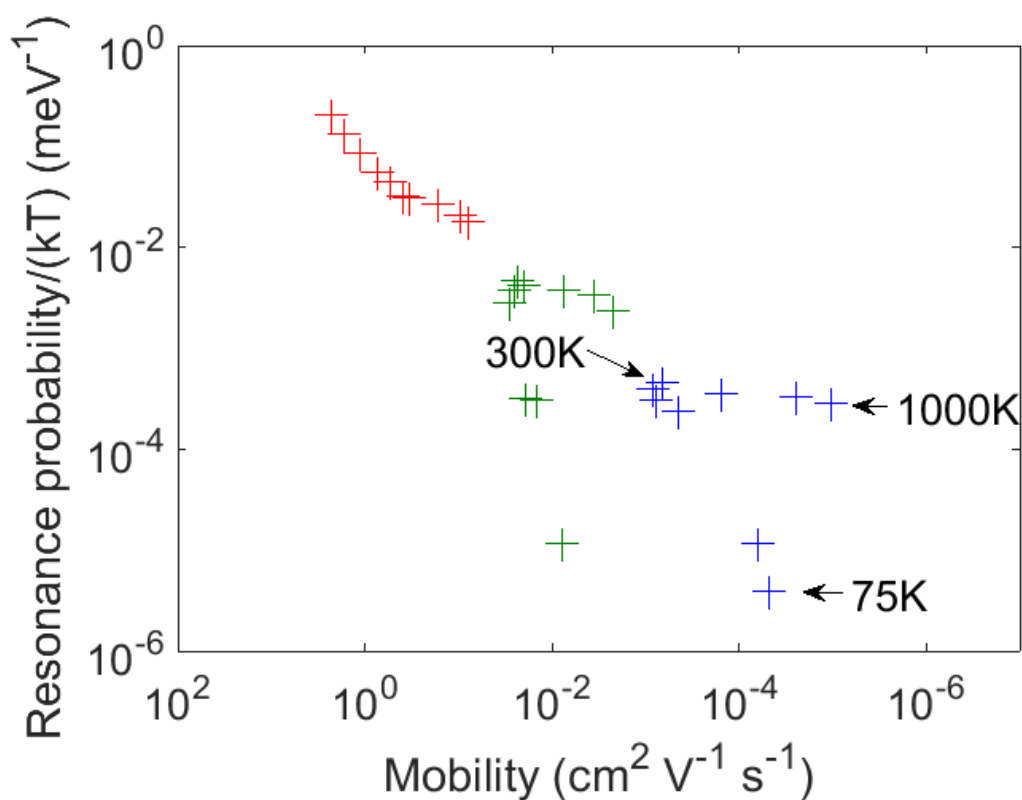


FIGURE 5.4: The probability of the first two molecules in the ELM chain being in resonance for charge transfer with each other, divided by  $k_B T$ , is plotted against the corresponding mobility value. The trends in the resonance probability for the lowest and highest coupling regimes clearly match with the mobilities. The intermediate coupling regime appears to contain a mixture of the two behaviours.



## Chapter 6

# Conclusions and Outlook

### 6.1 Conclusions

The goal of the work in this thesis has been to develop and then use for the first time a new surface hopping-based method which could study the problem of charge transport in organic semiconductors. As previously discussed, the method needs to be sufficiently computationally efficient to simulate large systems over long timescales, in order to accurately model the behaviour of materials relevant to organic electronic devices. This efficiency must not come at the expense of correctly portraying short-term ultrafast behaviour, which is relevant to charge transport in high coupling regimes such as can be found in organic semiconductors.

The FOB-SH method which I have derived in Chapter 2 promises to fulfill both of these requirements. There are a few crucial elements of the method which enable this. The first is the decision to use a classical force field and classical MD, from which I take the diagonal elements of the Hamiltonian  $H$  and the force matrix  $\nabla_I H$ . The second is the analytic overlap method, which has been discussed both here and in Ref. 149, and which allows the crucial off-diagonal elements of both  $H$  and  $\nabla_I H$  to be calculated accurately and quickly. The third is the derivation of a force expression, Eqs. 2.22 together with 2.29, which allows calculations of the forces on the adiabatic electronic surfaces for a system of any size.

The last of these is what makes the FOB-SH method specifically suited to broader simulations of organic semiconducting materials, but even without this advance I have been able to use the two-site donor-acceptor system to compare my method

to the predictions of standard ET theory and to begin to investigate regions where these theories are supposed to break down. Qualitatively I see strong agreement between the FOB-SH calculated rates and those predicted from Eq. 1.3 in all regimes where Eq. 1.3 should hold - i.e. where there is a clearly defined barrier to charge transfer. This is most clear in Figures 4.4 and 4.8, as well as to an extent in the low-coupling region of both Figures 4.6 and 4.7. As discussed in Chapter 4, Figure 4.8 deviates from this agreement somewhat with the 'anomalous' points at  $\Delta A = -300, -350, -400$  meV: as shown in Figure 4.9, removing these points from the inverted parabola fit allows this fit to correctly reproduce the reorganization energy. The nature of this deviation is currently unknown, as it does not appear to be a statistical error, and possibly hints at some additional effect on the rates here. I speculate that this may somehow be related to the irreversibility of the charge transfer for very negative values of  $\Delta A$ . It is also worth noting that for large negative values of  $\Delta A$ , the exponential fit fails to describe the long-term behaviour of the population decay. This could be related to the choice of description for the electronic state populations [119], although the short-term behaviour of all populations in Figure 4.8 fits the exponential decay very well so it is unclear if this would change any of the data points.

The charge transfer rates calculated from FOB-SH simulations in the high-coupling regime, demonstrated particularly in Figure 4.7, intriguingly suggest that even when the crucial assumption underlying ET theory is invalid such theories agree relatively well with methods that do not make this assumption. This may go some way to explaining why standard theories are capable of making good predictions of charge mobility in organic semiconductors, even if the validity of the theory cannot be guaranteed. It seems obvious that in such systems, the underlying mechanism of charge transport is not that which non-adiabatic ET theory describes, and so there is clear value in methods which do not make this assumption to further drive understanding of these systems and make future predictions of charge mobility.

With regard to the calculations discussed in Chapter 5, I think it further bolsters the method to demonstrate that it can reproduce qualitatively the same behaviour of mobility with temperature that was reported in Ref. 85 along a similar 1D chain. Crucially, in Figure 5.2 I observe both the crossover from low-coupling to high-coupling behaviour, where at high couplings there is no thermal activation for charge transport, and the crossover in the low-coupling regime from low temperature to high temperature, where mobility first increases with temperature and then fits into something akin to a band-like transport past the activated maximum. The exponent for this latter case (where  $\mu \propto T^{-3.5}$ ) seems to fall outside the standard range (-0.5 to -3.0). This exponent may be within error: choosing extreme values of the points at the end of the fit range suggested possible values of the exponent from -2.7 to -4.0. It may equally be suggestive of some additional effect for charge transport at very high temperature and very low coupling. This should be considered in any future simulations calculating the temperature dependence of charge mobility in a similar system.

## 6.2 Outlook

Work is progressing in our research group on the FOB-SH method, with the intention of re-implementing it in the CP2K molecular dynamics framework. It is hoped that this new implementation will be able to address a few potential shortcomings in the FOB-SH implementation reported herein, as I shall now enumerate.

### Velocity rescaling

Chapter 3 explains the velocity rescaling method that I have used to conserve energy in my surface hopping simulations: it simply rescales all the atomic velocities in the system by a constant factor when a surface hop occurs. This is cruder than the suggested rescaling approach in Tully's original publication on surface hopping for electronic transitions [110] which has generally been followed by other surface hopping implementations. An unfortunate drawback of the use of the NAMD molecular dynamics package is the lack of any finer control over the atomic velocities. It is

intended that the new implementation will rectify this, as well as making it easier to calculate the necessary non-adiabatic coupling vectors between adiabatic states (a task which would not be simple in the current implementation).

A possible consequence of my approach to velocity rescaling is that FOB-SH may not at present correctly reproduce the Boltzmann populations of the various adiabatic electronic states. It has been shown [120, 167, 168] that FSSH approximately reproduces these populations correctly, which is thought to rely on the existence of “forbidden hops” [139]. A hop is forbidden - i.e. does not take place - if the change in total energy is greater than can be accounted for with the velocity rescaling. Since my velocity rescaling approach rescales all the atomic velocities of the system, in principle any hop which results in a total energy change less than the total kinetic energy of the system is permitted. This allows the possibility that hops which my implementation allows would be forbidden under a different velocity rescaling approach: in the approach of Tully, only the component of atomic velocity that lies along the non-adiabatic coupling vector between adiabatic states can be rescaled, which would in general allow the system less energy for hops. It is therefore possible that this implementation of FOB-SH is too ‘permissive’ about hops to higher energy adiabatic states. I do not consider that this should qualitatively affect the results I have outlined in this thesis, though it may lead to FOB-SH predicting rates that are higher than they should be. An early goal for the new FOB-SH implementation will probably be a like-for-like comparison of rates for the ELM dimer to evaluate if this has indeed had any significant effect.

### **Decoherence correction**

Although there is no question that a decoherence correction of some sort must be applied to FSSH, I note that the correction applied in this implementation of FOB-SH is a very simple one, with a direct wavefunction collapse at decreed conditions. Figure 4.2 implies that the effect of this correction on the calculated rates is small, though finite. Changing the threshold below which the non-adiabatic coupling elements between adiabatic states need to fall before a wavefunction collapse is also

likely to have some small effect on charge transfer rates, simply through altering the rate of wavefunction collapse. I consider it possible in addition that there may be more detailed ways to correct for electronic overcoherence in a surface hopping framework: it is likely that these questions can be further explored by FOB-SH in the future.

### **Trivial crossings**

The trivial crossing problem in surface hopping [137] can occur when a molecular system has many densely-spaced adiabatic potential energy surfaces. The vanishing intermolecular interactions at larger distance can lead to two surfaces with almost zero energy splitting: the probability of hopping between these two surfaces may therefore be essentially 1 at the exact crossing point, but very small even close to it. Thus a finite time step may cause this crossing to be missed during a simulation, even though a surface hop should have occurred, leading to spurious long-term behaviour. Dealing with this problem becomes particularly crucial in large and complex molecular systems [85, 115, 169].

As currently implemented, the FOB-SH method does not have a way to deal with this issue. The two-state nature of the ELM dimer system means that in those simulations the trivial crossing problem should be essentially irrelevant. Although I assert that it is reasonable to ignore possible effects of trivial crossings on the larger 10-ELM system in a first implementation, I acknowledge that this needs to be dealt with in the method before it can be applied freely to larger and more realistic systems. It should be easy to apply the simple solution of Wang et al. [137], or a modified version, to the new implementation of FOB-SH.

### **Force field**

As the FOB-SH method is intended for the simulation of large molecular systems, it will be important for the classical MD force field to be able to accurately model various sorts of large-scale behaviour and thereby convincingly simulate the reaction of

the wider environment to the presence and motion of the excess charge. For example, a crucial element of this environmental reorganization is the induced dipole polarization as a result of excess charge [170]. The NAMD molecular dynamics package in this implementation does not have the ability to simulate this well: this is likely to be very important in future simulations (in particular ones modelled after physical materials) as the polarization response of the wider environment is the only mechanism available by which an excess charge may become relocalized on one or a few molecular sites. I do not think that the neglect of environmental polarization in this implementation has any effect on the results reported herein, as I have restricted myself to relatively small test systems: it is however something currently lacking from the method, which I hope the future CP2K-based implementation will add.

### **Parallelization**

While I consider it important to emphasise the relative computational efficiency of the current FOB-SH implementation, this does not preclude seeking ways to improve this even further. One obvious avenue to explore is parallelization, as at present the FOB-SH code is designed to run only on a single core. Computational tasks such as the site energy and electronic coupling calculations could be parallelized, for example in the case of the former simply assigning a single core to each molecule to calculate all the site energies alongside each other. As most if not all of the tasks in the FOB-SH routine are expected to scale with system size, parallelising the code according to the system size could offset this and hopefully speed up the method even further, making it possible to carry out the required simulations to study charge transport in large organic systems.

## **6.3 Final conclusion statement**

I conclude by saying that the work in this thesis has described the derivation, implementation and validation of a novel fragment-orbital-based surface hopping

method, which has demonstrated its applicability to the problem of charge transport in organic semiconductors. I have used it in a simple organic two-site test system to demonstrate that the method can reproduce established charge transfer theory in regimes where said theory is valid, and have begun to probe regimes where the theory should break down. I have additionally used it in a test system of a 1D chain to show that it is capable of and suited to calculations of charge mobility in large systems. I think that the results reported in this thesis are a valuable addition to the wider field, and that the method itself shows great promise to tackle the problem of charge transport in organic semiconductors in further future work.



# Bibliography

- [1] H. Kallmann and M. Pope, "Positive hole injection into organic crystals," *The Journal of Chemical Physics*, vol. 32, no. 1, pp. 300–301, 1960.
- [2] H. Kallmann and M. Pope, "Bulk Conductivity in Organic Crystals," *Nature*, vol. 186, no. 4718, pp. 31–33, 1960.
- [3] V. Coropceanu, R. S. Sanchez-Carrera, P. Paramonov, G. M. Day, and J.-L. Bredas, "Interaction of Charge Carriers with Lattice Vibrations in Organic Molecular Semiconductors : Naphthalene as a Case Study," *The Journal of Physical Chemistry C*, vol. 113, pp. 4679–4686, 2009.
- [4] V. Coropceanu, J. Cornil, D. A. da Silva Filho, Y. Olivier, R. Silbey, and J.-L. Bredas, "Charge transport in organic semiconductors," *Chemical Reviews*, vol. 107, no. 4, pp. 926–952, 2007.
- [5] M. E. Gershenson, V. Podzorov, and A. F. Morpurgo, "Colloquium: Electronic transport in single-crystal organic transistors," *Reviews of Modern Physics*, vol. 78, no. 3, pp. 973–989, 2006.
- [6] J. Nelson, J. J. Kwiakowski, J. Kirkpatrick, and J. M. Frost, "Modeling Charge Transport in Organic Photovoltaic Materials," *Accounts of Chemical Research*, vol. 42, no. 11, pp. 1768–1778, 2009.
- [7] M. J. Bedard-Hearn, F. Sterpone, and P. J. Rossky, "Nonadiabatic simulations of exciton dissociation in poly-p- phenylenevinylene oligomers," *Journal of Physical Chemistry A*, vol. 114, no. 29, pp. 7661–7670, 2010.
- [8] J. Ren, N. Vukmirović, and L.-W. Wang, "Nonadiabatic molecular dynamics simulation for carrier transport in a pentathiophene butyric acid monolayer," *Physical Review B*, vol. 87, no. 20, p. 205117, 2013.

- [9] J.-L. Brédas, D. Beljonne, V. Coropceanu, and J. Cornil, "Charge-transfer and energy-transfer processes in pi-conjugated oligomers and polymers: a molecular picture.," *Chemical Review*, vol. 104, no. 11, pp. 4971–5004, 2004.
- [10] D. L. Cheung and A. Troisi, "Modelling charge transport in organic semiconductors: from quantum dynamics to soft matter.," *Physical Chemistry Chemical Physics*, vol. 10, no. 39, pp. 5941–52, 2008.
- [11] S. Ciuchi and S. Fratini, "Electronic transport and quantum localization effects in organic semiconductors," *Physical Review B*, vol. 86, no. 24, p. 245201, 2012.
- [12] K. Myny, S. Steudel, S. Smout, P. Vicca, F. Furthner, B. Van Der Putten, A. K. Tripathi, G. H. Gelinck, J. Genoe, W. Dehaene, and P. Heremans, "Organic RFID transponder chip with data rate compatible with electronic product coding," *Organic Electronics: physics, materials, applications*, vol. 11, no. 7, pp. 1176–1179, 2010.
- [13] F. Ortmann, F. Bechstedt, and K. Hannewald, "Charge transport in organic crystals: interplay of band transport, hopping and electron–phonon scattering," *New Journal of Physics*, vol. 12, no. 2, p. 023011, 2010.
- [14] F. Ortmann, F. Bechstedt, and K. Hannewald, "Charge transport in organic crystals: Theory and modelling," *Physica Status Solidi (b)*, vol. 248, no. 3, pp. 511–525, 2011.
- [15] R. H. Friend, R. W. Gymer, A. B. Holmes, J. H. Burroughes, R. N. Marks, C. Taliani, D. D. C. Bradley, M. Lo, W. R. Salaneck, D. A. D. Santos, and J. L. Bre, "Electroluminescence in conjugated polymers," *Nature*, vol. 397, no. 6715, pp. 121–128, 1999.
- [16] M. Slawinski, M. Weingarten, M. Heuken, A. Vescan, and H. Kalisch, "Investigation of large-area OLED devices with various grid geometries," *Organic Electronics: physics, materials, applications*, vol. 14, no. 10, pp. 2387–2391, 2013.

- [17] C. Dimitrakopoulos and P. Malenfant, "Organic Thin Film Transistors for Large Area Electronics," *Advanced Materials*, vol. 14, no. 2, pp. 99–117, 2002.
- [18] G. Horowitz, "Organic field-effect transistors," *Advanced Materials*, vol. 10, no. 5, pp. 365–377, 1998.
- [19] K. Zhou, H. Dong, H.-L. Zhang, and W. Hu, "High performance n-type and ambipolar small organic semiconductors for organic thin film transistors.," *Physical Chemistry Chemical Physics*, vol. 16, no. 41, pp. 22448–57, 2014.
- [20] Y. Yuan, G. Giri, A. L. Ayzner, A. P. Zoombelt, S. C. B. Mannsfeld, J. Chen, D. Nordlund, M. F. Toney, J. Huang, and Z. Bao, "Ultra-high mobility transparent organic thin film transistors grown by an off-centre spin-coating method.," *Nature Communications*, vol. 5, p. 3005, 2014.
- [21] B. Kippelen and J.-L. Brédas, "Organic photovoltaics," *Energy & Environmental Science*, vol. 2, no. 3, p. 251, 2009.
- [22] G. Raos, M. Casalegno, and J. Idé, "An Effective Two-Orbital Quantum Chemical Model for Organic Photovoltaic Materials," *Journal of Chemical Theory and Computation*, vol. 10, no. 1, pp. 364–372, 2014.
- [23] M. Hiramoto, H. Fujiwara, and M. Yokoyama, "Three-layered organic solar cell with a photoactive interlayer of codeposited pigments," *Applied Physics Letters*, vol. 58, no. 10, p. 1062, 1991.
- [24] T. Kirchartz and J. Nelson, "Device Modelling of Organic Bulk Heterojunction Solar Cells," *Topics in Current Chemistry*, 2013.
- [25] D. Meissner, S. Siebentritt, and S. Günster, "Charge carrier photogeneration in organic solar cells," *Chemical Review*, vol. 110, pp. 6736–6767, 2010.
- [26] W. Tress, K. Leo, and M. Riede, "Optimum mobility, contact properties, and open-circuit voltage of organic solar cells: A drift-diffusion simulation study," *Physical Review B*, vol. 85, no. 15, p. 155201, 2012.

- [27] J. Nelson and C. Emmott, "Can solar power deliver?," *Philosophical Transactions of the Royal Society A*, vol. 371, 2013.
- [28] A. V. Akimov and O. V. Prezhdo, "Theory of solar energy materials," *Journal of Physics: Condensed Matter*, vol. 27, no. 13, p. 130301, 2015.
- [29] R. a. J. Janssen and J. Nelson, "Factors limiting device efficiency in organic photovoltaics," *Advanced Materials*, vol. 25, no. 13, pp. 1847–58, 2013.
- [30] M. a. Faist, S. Shoaee, S. Tuladhar, G. F. a. Dibb, S. Foster, W. Gong, T. Kirchartz, D. D. C. Bradley, J. R. Durrant, and J. Nelson, "Understanding the Reduced Efficiencies of Organic Solar Cells Employing Fullerene Multiadducts as Acceptors," *Advanced Energy Materials*, vol. 3, no. 6, pp. 744–752, 2013.
- [31] M. Irimia-Vladu, "'Green' electronics: biodegradable and biocompatible materials and devices for sustainable future.," *Chemical Society Reviews*, vol. 43, no. 2, pp. 588–610, 2014.
- [32] J.-L. Bredas, J. E. Norton, J. Cornil, and V. Coropceanu, "Molecular understanding of organic solar cells: the challenges.," *Accounts of Chemical Research*, vol. 42, no. 11, pp. 1691–1699, 2009.
- [33] G. H. Gelinck, H. E. a. Huitema, E. van Veenendaal, E. Cantatore, L. Schrijnemakers, J. B. P. H. van der Putten, T. C. T. Geuns, M. Beenhakkers, J. B. Giesbers, B.-H. Huisman, E. J. Meijer, E. M. Benito, F. J. Touwslager, A. W. Marsman, B. J. E. van Rens, and D. M. de Leeuw, "Flexible active-matrix displays and shift registers based on solution-processed organic transistors.," *Nature Materials*, vol. 3, no. 2, pp. 106–10, 2004.
- [34] A. Shah, J. Meier, A. Buechel, U. Kroll, J. Steinhauser, F. Meillaud, H. Schade, and D. Dominé, "Towards very low-cost mass production of thin-film silicon photovoltaic (PV) solar modules on glass," *Thin Solid Films*, vol. 502, pp. 292–299, 2006.

- [35] E. Frankevich, Y. Maruyama, and H. Ogata, "Mobility of charge carriers in vapor-phase grown C60 single crystal," *Chemical Physics Letters*, vol. 214, no. 1, pp. 39–44, 1993.
- [36] E. Frankevich, Y. Maruyama, H. Ogata, Y. Achiba, and K. Kikuchi, "Mobilities of charge carriers in C60 orthorhombic single crystal," *Solid State Communications*, vol. 88, no. 2, pp. 177–181, 1993.
- [37] Y. N. Li, P. Sonar, L. Murphy, and W. Hong, "High mobility diketopyrrolopyrrole (DPP)-based organic semiconductor materials for organic thin film transistors and photovoltaics," *Energy & Environmental Science*, vol. 6, no. 6, pp. 1684–1710, 2013.
- [38] W. Xie, K. A. McGarry, F. Liu, Y. Wu, P. P. Ruden, C. J. Douglas, and C. D. Frisbie, "High-mobility transistors based on single crystals of isotopically substituted rubrene-d28," *Journal of Physical Chemistry C*, vol. 117, no. 22, pp. 11522–11529, 2013.
- [39] P. K. Watkins, A. B. Walker, and G. L. B. Verschoor, "Dynamical Monte Carlo modelling of organic solar cells: the dependence of internal quantum efficiency on morphology," *Nano Letters*, vol. 5, no. 9, pp. 1814–8, 2005.
- [40] F. Ortmann, F. Bechstedt, and K. Hannewald, "Theory of charge transport in organic crystals: Beyond Holstein's small-polaron model," *Physical Review B*, vol. 79, p. 235206, 2009.
- [41] A. V. Akimov and O. V. Prezhdo, "Large-Scale Computations in Chemistry: A Bird's Eye View of a Vibrant Field," *Chemical Reviews*, vol. 115, no. 12, pp. 5797–5890, 2015.
- [42] V. Coropceanu, M. Malagoli, D. da Silva Filho, N. Gruhn, T. Bill, and J. Brédas, "Hole- and Electron-Vibrational Couplings in Oligoacene Crystals: Intramolecular Contributions," *Physical Review Letters*, vol. 89, no. 27, p. 275503, 2002.

- [43] N. Vukmirović, C. Bruder, and V. M. Stojanović, "Electron-Phonon Coupling in Crystalline Organic Semiconductors: Microscopic Evidence for Nonpolaronic Charge Carriers," *Physical Review Letters*, vol. 109, no. 12, p. 126407, 2012.
- [44] L. A. Girifalco, "Molecular Properties of C<sub>60</sub> in the Gas and Solid Phases," *Journal of Physical Chemistry*, vol. 96, no. 2, pp. 858–861, 1992.
- [45] P. A. Heiney, "Structure, Dynamics and Ordering Transition of Solid C<sub>60</sub>," *J. Phys. Chem. Solids*, vol. 53, no. 11, pp. 1333–1352, 1992.
- [46] F. C. Grozema and L. D. Siebbeles, "Mechanism of charge transport in self-organizing organic materials," *International Reviews in Physical Chemistry*, vol. 27, no. 1, pp. 87–138, 2008.
- [47] A. Troisi, "Charge transport in high mobility molecular semiconductors: classical models and new theories.," *Chemical Society Reviews*, vol. 40, no. 5, pp. 2347–58, 2011.
- [48] T. Holstein, "Studies of polaron motion: Part I. The molecular-crystal model," *Annals of Physics*, vol. 8, pp. 325–342, 1959.
- [49] T. Holstein, "Studies of polaron motion: Part II. The "small" polaron," *Annals of Physics*, vol. 8, pp. 343–389, 1959.
- [50] A. Heck, J. J. Kranz, T. Kubař, and M. Elstner, "Multi-Scale Approach to Non-Adiabatic Charge Transport in High-Mobility Organic Semiconductors," *Journal of Chemical Theory and Computation*, vol. 11, pp. 5068–5082, 2015.
- [51] H. Oberhofer and J. Blumberger, "Revisiting electronic couplings and incoherent hopping models for electron transport in crystalline C<sub>60</sub> at ambient temperatures," *Physical Chemistry Chemical Physics*, vol. 14, p. 13846, 2012.

- [52] F. Gajdos, H. Oberhofer, M. Dupuis, and J. Blumberger, "On the Inapplicability of Electron-Hopping Models for the Organic Semiconductor Phenyl-C61-butyric Acid Methyl Ester (PCBM)," *The Journal of Physical Chemistry Letters*, vol. 4, no. 6, pp. 1012–1017, 2013.
- [53] D. L. Cheung and A. Troisi, "Theoretical Study of the Organic Photovoltaic Electron Acceptor PCBM: Morphology, Electronic Structure, and Charge Localization," *The Journal of Physical Chemistry C*, vol. 114, no. 48, pp. 20479–20488, 2010.
- [54] Z. Shuai, L. Wang, and Q. Li, "Evaluation of charge mobility in organic materials: from localized to delocalized descriptions at a first-principles level," *Advanced Materials*, vol. 23, no. 9, pp. 1145–53, 2011.
- [55] A. Troisi and G. Orlandi, "Charge-Transport Regime of Crystalline Organic Semiconductors: Diffusion Limited by Thermal Off-Diagonal Electronic Disorder," *Physical Review Letters*, vol. 96, no. 8, p. 086601, 2006.
- [56] P. Brown, H. Sirringhaus, M. Harrison, M. Shkunov, and R. Friend, "Optical spectroscopy of field-induced charge in self-organized high mobility poly(3-hexylthiophene)," *Physical Review B*, vol. 63, no. 12, p. 125204, 2001.
- [57] M. T. Dang, G. Wantz, H. Bejbouji, M. Urien, O. J. Dautel, L. Vignau, and L. Hirsch, "Polymeric solar cells based on P3HT:PCBM: Role of the casting solvent," *Solar Energy Materials and Solar Cells*, vol. 95, no. 12, pp. 3408–3418, 2011.
- [58] W. David and R. Ibberson, "Structural phase transitions in the fullerene C<sub>60</sub>," *Europhysics Letters*, vol. 18, no. 3, pp. 219–225, 1992.
- [59] F. Frigerio, M. Casalegno, C. Carbonera, T. Nicolini, S. V. Meille, and G. Raos, "Molecular dynamics simulations of the solvent- and thermal history-dependent structure of the PCBM fullerene derivative," *Journal of Materials Chemistry*, vol. 22, no. 12, p. 5434, 2012.

- [60] L. Zheng and Y. Han, "Solvated crystals based on [6,6]-phenyl-C61-butyric acid methyl ester (PCBM) with the hexagonal structure and their phase transformation.," *The Journal of Physical Chemistry B*, vol. 116, no. 5, pp. 1598–604, 2012.
- [61] Y. Wang, M. Alcamí, and F. Martín, "Understanding the supramolecular self-assembly of the fullerene derivative PCBM on gold surfaces.," *ChemPhysChem*, vol. 9, no. 7, pp. 1030–5, 2008.
- [62] A. Heck, J. J. Kranz, and M. Elstner, "Simulation of Temperature-Dependent Charge Transport in Organic Semiconductors with Various Degrees of Disorder," *Journal of Chemical Theory and Computation*, vol. 12, pp. 3087–3096, 2016.
- [63] B. Blülle, A. Troisi, R. Häusermann, and B. Batlogg, "Charge transport perpendicular to the high mobility plane in organic crystals: Bandlike temperature dependence maintained despite hundredfold anisotropy," *Physical Review B*, vol. 93, no. 3, p. 035205, 2016.
- [64] N. Karl, "Charge carrier transport in organic semiconductors," *Synthetic Metals*, vol. 133-134, pp. 649–657, 2003.
- [65] H. Sirringhaus, T. Sakanoue, and J. F. Chang, "Charge-transport physics of high-mobility molecular semiconductors," *Physica Status Solidi (B)*, vol. 249, no. 9, pp. 1655–1676, 2012.
- [66] V. Podzorov, E. Menard, J. A. Rogers, and M. E. Gershenson, "Hall effect in the accumulation layers on the surface of organic semiconductors," *Physical Review Letters*, vol. 95, p. 226601, 2005.
- [67] Y. Okada, M. Uno, Y. Nakazawa, K. Sasai, K. Matsukawa, M. Yoshimura, Y. Kitaoka, Y. Mori, and J. Takeya, "Low-temperature thermal conductivity of bulk and film-like rubrene single crystals," *Physical Review B*, vol. 83, p. 113305, 2011.
- [68] K. Marumoto, S. I. Kuroda, T. Takenobu, and Y. Iwasa, "Spatial extent of wave functions of gate-induced hole carriers in pentacene field-effect devices

- as investigated by electron spin resonance," *Physical Review Letters*, vol. 97, p. 256603, 2006.
- [69] H. Y. Tsao and Y. J. Lin, "Electronic properties of annealed pentacene films in air at various temperatures up to 400 K," *Applied Physics Letters*, vol. 101, p. 113306, 2012.
- [70] T. Sakanoue and H. Sirringhaus, "Band-like temperature dependence of mobility in a solution-processed organic semiconductor," *Nature Materials*, vol. 9, no. 9, pp. 736–40, 2010.
- [71] J. F. Chang, T. Sakanoue, Y. Olivier, T. Uemura, M. B. Dufourg-Madec, S. G. Yeates, J. Cornil, J. Takeya, A. Troisi, and H. Sirringhaus, "Hall-effect measurements probing the degree of charge-carrier delocalization in solution-processed crystalline molecular semiconductors," *Physical Review Letters*, vol. 107, p. 066601, 2011.
- [72] J. Arago and A. Troisi, "Dynamics of the excitonic coupling in organic crystals," *Physical Review Letters*, vol. 114, p. 026402, 2015.
- [73] A. Troisi, "Dynamic disorder in molecular semiconductors: Charge transport in two dimensions," *The Journal of Chemical Physics*, vol. 134, p. 034702, 2011.
- [74] H. Imahori, N. V. Tkachenko, V. Vehmanen, K. Tamaki, H. Lemmetyinen, Y. Sakata, and S. Fukuzumi, "An Extremely Small Reorganization Energy of Electron Transfer in Porphyrin - Fullerene Dyad," *The Journal of Physical Chemistry A*, vol. 105, pp. 1750–1756, 2001.
- [75] R. Marcus, "Chemical and electrochemical electron-transfer theory," *Annual Review of Physical Chemistry*, vol. 15, pp. 155–196, 1964.
- [76] R. Marcus, "Electron transfer reactions in chemistry. Theory and experiment," *Reviews of Modern Physics*, vol. 65, no. 3, pp. 599–610, 1993.
- [77] A. Nitzan, *Chemical Dynamics in Condensed Phases*. Oxford University Press, 2006.

- [78] B. S. Brunschwig, J. Logan, M. D. Newton, and N. Sutin, "A semi-classical treatment of electron-exchange reactions. Application to the hexaaquoiron(II)-hexaaquoiron(III) system," *Journal of the American Chemical Society*, vol. 102, no. 18, pp. 5798–5809, 1980.
- [79] M. D. Newton and N. Sutin, "Electron Transfer Reactions in Condensed Phases," *Annual Review of Physical Chemistry*, vol. 35, no. 1, pp. 437–480, 1984.
- [80] R. P. Fornari, J. Aragón, and A. Troisi, "Exciton Dynamics in Phthalocyanine Molecular Crystals," *The Journal of Physical Chemistry C*, vol. 120, no. 15, pp. 7987–7996, 2016.
- [81] J. Idé, D. Fazzi, M. Casalegno, S. V. Meille, and G. Raos, "Electron transport in crystalline PCBM-like fullerene derivatives: a comparative computational study," *Journal of Materials Chemistry C*, vol. 2, pp. 7313–7325, 2014.
- [82] A. Troisi, "Prediction of the Absolute Charge Mobility of Molecular Semiconductors: the Case of Rubrene," *Advanced Materials*, vol. 19, no. 15, pp. 2000–2004, 2007.
- [83] A. Troisi, D. L. Cheung, and D. Andrienko, "Charge transport in semiconductors with multiscale conformational dynamics," *Physical Review Letters*, vol. 102, pp. 18–21, 2009.
- [84] L. Wang and D. Beljonne, "Charge transport in organic semiconductors: assessment of the mean field theory in the hopping regime," *The Journal of Chemical Physics*, vol. 139, no. 6, p. 064316, 2013.
- [85] L. Wang and D. Beljonne, "Flexible Surface Hopping Approach to Model the Crossover from Hopping to Band-like Transport in Organic Crystals," *The Journal of Physical Chemistry Letters*, vol. 4, no. 11, pp. 1888–1894, 2013.
- [86] T. Kubar and M. Elstner, "What Governs the Charge Transfer in DNA? The Role of DNA Conformation and Environment," *Journal of Physical Chemistry B*, vol. 113, no. 15, p. 5339, 2009.

- [87] T. Kubař and M. Elstner, "A hybrid approach to simulation of electron transfer in complex molecular systems," *Journal of The Royal Society Interface*, vol. 10, p. 20130415, 2013.
- [88] T. Kubař and M. Elstner, "Efficient algorithms for the simulation of non-adiabatic electron transfer in complex molecular systems: application to DNA," *Physical Chemistry Chemical Physics*, vol. 15, no. 16, pp. 5794–813, 2013.
- [89] G. Nan, L. Wang, X. Yang, Z. Shuai, and Y. Zhao, "Charge transfer rates in organic semiconductors beyond first-order perturbation: from weak to strong coupling regimes.," *The Journal of Chemical Physics*, vol. 130, p. 024704, 2009.
- [90] A. V. Akimov and O. V. Prezhdo, "The PYXAID program for non-adiabatic molecular dynamics in condensed matter systems," *Journal of Chemical Theory and Computation*, vol. 9, pp. 4959–4972, 2013.
- [91] A. V. Akimov and O. V. Prezhdo, "Advanced capabilities of the PYXAID program: Integration schemes, decoherence effects, multiexcitonic states, and field-matter interaction," *Journal of Chemical Theory and Computation*, vol. 10, pp. 789–804, 2014.
- [92] A. V. Akimov, R. Asahi, R. Jinnouchi, and O. V. Prezhdo, "What Makes the Photocatalytic CO<sub>2</sub> Reduction on N-Doped Ta<sub>2</sub>O<sub>5</sub> Efficient: Insights from Nonadiabatic Molecular Dynamics.," *Journal of the American Chemical Society*, vol. 137, pp. 11517–11525, 2015.
- [93] N. L. Doltsinis, "Nonadiabatic Dynamics : Mean-Field and Surface Hopping," in *Quantum Simulations of Complex Many-Body Systems: From Theory to Algorithms*, vol. 10, pp. 377–397, 2002.
- [94] J. C. Tully, "Perspective: Nonadiabatic dynamics theory," *The Journal of Chemical Physics*, vol. 137, p. 22A301, 2012.
- [95] J. C. Tully, "Nonadiabatic Dynamics," in *Modern Methods for Multidimensional Dynamics Computations in Chemistry*, pp. 34–71, 1998.

- [96] N. Doltsinis and D. Marx, "First principles molecular dynamics involving excited states and nonadiabatic transitions," *Journal of Theoretical and Computational Chemistry*, vol. 1, no. 2, pp. 319–349, 2002.
- [97] R. Kapral and G. Ciccotti, "Mixed quantum-classical dynamics," *The Journal of Chemical Physics*, vol. 110, no. 18, p. 8919, 1999.
- [98] J. C. Tully, "Mixed quantum-classical dynamics," *Faraday Discussions*, vol. 110, pp. 407–419, 1998.
- [99] J. C. Tully, "Mixed quantum-classical dynamics: mean-field and surface-hopping," in *Classical and Quantum Dynamics in Condensed Phase Simulations*, pp. 489–514, 1998.
- [100] L. Wang, O. V. Prezhdo, and D. Beljonne, "Mixed quantum-classical dynamics for charge transport in organics," *Physical Chemistry Chemical Physics*, vol. 17, no. 19, pp. 12395–12406, 2015.
- [101] A. Abedi, N. T. Maitra, and E. K. U. Gross, "Exact factorization of the time-dependent electron-nuclear wave function," *Physical Review Letters*, vol. 105, p. 123002, 2010.
- [102] A. Abedi, N. T. Maitra, and E. K. U. Gross, "Correlated electron-nuclear dynamics: Exact factorization of the molecular wavefunction," *The Journal of Chemical Physics*, vol. 137, no. 22, 2012.
- [103] F. Agostini, A. Abedi, and E. K. U. Gross, "Classical nuclear motion coupled to electronic non-adiabatic transitions," *The Journal of Chemical Physics*, vol. 141, no. 21, 2014.
- [104] O. Prezhdo and P. Rossky, "Mean-field molecular dynamics with surface hopping," *The Journal of Chemical Physics*, vol. 107, no. 3, pp. 825–834, 1997.
- [105] X. Li, J. C. Tully, H. B. Schlegel, and M. J. Frisch, "Ab initio Ehrenfest dynamics," *The Journal of Chemical Physics*, vol. 123, no. 8, p. 084106, 2005.

- [106] A. Ojanperä, V. Havu, L. Lehtovaara, and M. Puska, "Nonadiabatic Ehrenfest molecular dynamics within the projector augmented-wave method.," *The Journal of Chemical Physics*, vol. 136, no. 14, p. 144103, 2012.
- [107] X. Gao, H. Geng, Q. Peng, J. Ren, Y. Yi, D. Wang, and Z. Shuai, "Nonadiabatic Molecular Dynamics Modeling of the Intrachain Charge Transport in Conjugated Diketopyrrolo-pyrrole Polymers," *The Journal of Physical Chemistry C*, vol. 118, no. 13, pp. 6631–6640, 2014.
- [108] A. P. Horsfield, D. R. Bowler, A. J. Fisher, T. N. Todorov, and C. G. Sánchez, "Beyond Ehrenfest: correlated non-adiabatic molecular dynamics," *Journal of Physics: Condensed Matter*, vol. 16, no. 46, pp. 8251–8266, 2004.
- [109] J. C. Tully, "Nonadiabatic molecular dynamics," *International Journal of Quantum Chemistry*, vol. 40, pp. 299–309, 1991.
- [110] J. C. Tully, "Molecular dynamics with electronic transitions," *The Journal of Chemical Physics*, vol. 93, no. 2, p. 1061, 1990.
- [111] C. Craig, W. Duncan, and O. Prezhdo, "Trajectory Surface Hopping in the Time-Dependent Kohn-Sham Approach for Electron-Nuclear Dynamics," *Physical Review Letters*, vol. 95, no. 16, p. 163001, 2005.
- [112] G. Cui and W. Thiel, "Generalized trajectory surface-hopping method for internal conversion and intersystem crossing.," *The Journal of Chemical Physics*, vol. 141, p. 124101, 2014.
- [113] N. L. Doltsinis and D. Marx, "Nonadiabatic Car-Parrinello Molecular Dynamics," *Physical Review Letters*, vol. 88, no. 16, p. 166402, 2002.
- [114] E. Fabiano, G. Groenhof, and W. Thiel, "Approximate switching algorithms for trajectory surface hopping," *Chemical Physics*, vol. 351, pp. 111–116, 2008.
- [115] E. Fabiano, T. Keal, and W. Thiel, "Implementation of surface hopping molecular dynamics using semiempirical methods," *Chemical Physics*, vol. 349, pp. 334–347, 2008.

- [116] J. Y. Fang and S. Hammes-Schiffer, "Improvement of the internal consistency in trajectory surface hopping," *Journal Of Physical Chemistry A*, vol. 103, pp. 9399–9407, 1999.
- [117] A. V. Akimov, D. Trivedi, L. Wang, and O. V. Prezhdo, "Analysis of the trajectory surface hopping method from the markov state model perspective," *Journal of the Physical Society of Japan*, vol. 84, p. 094002, 2015.
- [118] G. Granucci and M. Persico, "Critical appraisal of the fewest switches algorithm for surface hopping," *The Journal of Chemical Physics*, vol. 126, no. 13, p. 134114, 2007.
- [119] B. R. Landry, M. J. Falk, and J. E. Subotnik, "Communication: The correct interpretation of surface hopping trajectories: How to calculate electronic properties," *The Journal of Chemical Physics*, vol. 139, no. 21, p. 211101, 2013.
- [120] J. R. Schmidt, P. V. Parandekar, and J. C. Tully, "Mixed quantum-classical equilibrium: Surface hopping," *The Journal of Chemical Physics*, vol. 129, no. 4, p. 044104, 2008.
- [121] W. Ouyang and J. E. Subotnik, "Estimating the entropy and quantifying the impurity of a swarm of surface-hopping trajectories: A new perspective on decoherence," *The Journal of Chemical Physics*, vol. 140, p. 204102, 2014.
- [122] E. Tapavicza, A. M. Meyer, and F. Furche, "Unravelling the details of vitamin D photosynthesis by non-adiabatic molecular dynamics simulations.," *Physical Chemistry Chemical Physics*, vol. 13, no. 47, pp. 20986–98, 2011.
- [123] U. Müller and G. Stock, "Surface-hopping modeling of photoinduced relaxation dynamics on coupled potential-energy surfaces," *The Journal of Chemical Physics*, vol. 107, no. 16, pp. 6230–6245, 1997.
- [124] Z. Lan, E. Fabiano, and W. Thiel, "Photoinduced nonadiabatic dynamics of pyrimidine nucleobases: On-the-fly surface-hopping study with semiempirical methods," *Journal of Physical Chemistry B*, vol. 113, no. 11, pp. 3548–3555, 2009.

- [125] A. V. Akimov, A. J. Neukirch, and O. V. Prezhdo, "Theoretical insights into photoinduced charge transfer and catalysis at oxide interfaces.," *Chemical Reviews*, vol. 113, no. 6, pp. 4496–565, 2013.
- [126] R. Jiang and E. L. Sibert, "Surface hopping simulation of vibrational predissociation of methanol dimer," *The Journal of Chemical Physics*, vol. 136, p. 224104, 2012.
- [127] D. Fazzi, M. Barbatti, and W. Thiel, "Modeling Ultrafast Exciton Deactivation in Oligothiophenes via Nonadiabatic Dynamics," *Physical Chemistry Chemical Physics*, vol. 17, pp. 7787–7799, 2015.
- [128] B. R. Landry and J. E. Subotnik, "Surface hopping outperforms secular Redfield theory when reorganization energies range from small to moderate (and nuclei are classical)," *The Journal of Chemical Physics*, vol. 142, no. 10, p. 104102, 2015.
- [129] E. R. Bittner and P. J. Rossky, "Quantum decoherence in mixed quantum-classical systems: Nonadiabatic processes," *The Journal of Chemical Physics*, vol. 103, no. 18, p. 8130, 1995.
- [130] G. Granucci, M. Persico, and A. Zocante, "Including quantum decoherence in surface hopping," *The Journal of Chemical Physics*, vol. 133, p. 134111, 2010.
- [131] B. R. Landry and J. E. Subotnik, "Communication: Standard surface hopping predicts incorrect scaling for Marcus' golden-rule rate: the decoherence problem cannot be ignored.," *The Journal of Chemical Physics*, vol. 135, no. 19, p. 191101, 2011.
- [132] B. R. Landry and J. E. Subotnik, "How to recover Marcus theory with fewest switches surface hopping: Add just a touch of decoherence," *Journal of Chemical Physics*, vol. 137, p. 22A513, 2012.

- [133] N. Shenvi, J. E. Subotnik, and W. Yang, "Simultaneous-trajectory surface hopping: a parameter-free algorithm for implementing decoherence in nonadiabatic dynamics.," *The Journal of Chemical Physics*, vol. 134, no. 14, p. 144102, 2011.
- [134] J. E. Subotnik, "Fewest-switches surface hopping and decoherence in multiple dimensions," *Journal of Physical Chemistry A*, vol. 115, pp. 12083–12096, 2011.
- [135] T. Nelson, S. Fernandez-Alberti, A. E. Roitberg, and S. Tretiak, "Nonadiabatic excited-state molecular dynamics: treatment of electronic decoherence.," *The Journal of Chemical Physics*, vol. 138, no. 22, p. 224111, 2013.
- [136] J. E. Subotnik and N. Shenvi, "Decoherence and surface hopping: when can averaging over initial conditions help capture the effects of wave packet separation?," *The Journal of Chemical Physics*, vol. 134, no. 24, p. 244114, 2011.
- [137] L. Wang and O. Prezhdo, "A Simple Solution to the Trivial Crossing Problem in Surface Hopping," *The Journal of Physical Chemistry Letters*, vol. 5, pp. 713–719, 2014.
- [138] T. Nelson, S. Fernandez-Alberti, A. E. Roitberg, and S. Tretiak, "Artifacts due to trivial unavoided crossings in the modeling of photoinduced energy transfer dynamics in extended conjugated molecules," *Chemical Physics Letters*, vol. 590, pp. 208–213, 2013.
- [139] J. E. Subotnik, A. Jain, B. Landry, A. Petit, W. Ouyang, and N. Bellonzi, "Understanding The Surface Hopping View of Electronic Transitions and Decoherence," *Annual Review of Physical Chemistry*, vol. 67, pp. 387–417, 2016.
- [140] M. J. Falk, B. R. Landry, and J. E. Subotnik, "Can surface hopping sans decoherence recover Marcus theory? Understanding the role of friction in a surface hopping view of electron transfer.," *The Journal of Physical Chemistry B*, vol. 118, no. 28, pp. 8108–17, 2014.

- [141] A. Jain, M. F. Herman, W. Ouyang, and J. E. Subotnik, "Surface hopping, transition state theory and decoherence. I. Scattering theory and time-reversibility," *The Journal of Chemical Physics*, vol. 143, no. 13, p. 134106, 2015.
- [142] L. Wang, D. Trivedi, and O. V. Prezhdo, "Global Flux Surface Hopping Approach for Mixed Quantum-Classical Dynamics," *Journal of Chemical Theory and Computation*, vol. 10, pp. 3598–3605, 2014.
- [143] A. E. Sifain, L. Wang, and O. V. Prezhdo, "Mixed quantum-classical equilibrium in global flux surface hopping," *The Journal of Chemical Physics*, vol. 142, no. 22, p. 224102, 2015.
- [144] S. Pal, D. J. Trivedi, A. V. Akimov, B. Aradi, T. Frauenheim, and O. V. Prezhdo, "Nonadiabatic Molecular Dynamics for Thousand Atom Systems: A Tight-Binding Approach toward PYXAID," *Journal of Chemical Theory and Computation*, vol. 12, no. 4, pp. 1436–1448, 2016.
- [145] S. Hammes-Schiffer and J. C. Tully, "Proton transfer in solution: Molecular dynamics with quantum transitions," *The Journal of Chemical Physics*, vol. 101, no. 6, p. 4657, 1994.
- [146] F. Plasser and H. Lischka, "Semiclassical dynamics simulations of charge transport in stacked  $\pi$ -systems," *The Journal of Chemical Physics*, vol. 134, no. 2011, 2011.
- [147] F. Plasser, G. Granucci, J. Pittner, M. Barbatti, M. Persico, and H. Lischka, "Surface hopping dynamics using a locally diabatic formalism: Charge transfer in the ethylene dimer cation and excited state dynamics in the 2-pyridone dimer," *The Journal of Chemical Physics*, vol. 137, no. 22, 2012.
- [148] F. Plasser, R. Crespo-Otero, M. Pederzoli, J. Pittner, H. Lischka, and M. Barbatti, "Surface Hopping Dynamics with Correlated Single-Reference Methods: 9H-Adenine as a Case Study," *Journal of Chemical Theory and Computation*, vol. 10, pp. 1395–1405, 2014.

- [149] F. Gajdos, S. Valner, F. Ho, J. Spencer, M. Breuer, A. Kubas, M. Dupuis, and J. Blumberger, "Ultrafast Estimation of Electronic Couplings for Electron Transfer between  $\pi$ -Conjugated Organic Molecules," *Journal of Chemical Theory and Computation*, vol. 10, pp. 4653–4660, 2014.
- [150] J. Spencer, F. Gajdos, and J. Blumberger, "FOB-SH: Fragment orbital-based surface hopping for charge carrier transport in organic and biological molecules and materials," *The Journal of Chemical Physics*, vol. 145, p. 064102, 2016.
- [151] J. Spencer, L. Scalfi, A. Carof, and J. Blumberger, "FDREACT16: Confronting Surface Hopping Molecular Dynamics with Marcus Theory for a molecular donor-acceptor system," *Faraday Discuss.*, vol. 195, pp. 215–236, 2016.
- [152] O. V. Prezhdo and P. J. Rossky, "Evaluation of quantum transition rates from quantum-classical molecular dynamics simulations," *The Journal of Chemical Physics*, vol. 107, no. 15, pp. 5863–5878, 1997.
- [153] P.-O. Lowdin, "On the Non-Orthogonality Problem Connected with the Use of Atomic Wave Functions in the Theory of Molecules and Crystals," *The Journal of Chemical Physics*, vol. 18, no. 3, p. 365, 1950.
- [154] L. Kalé, R. Skeel, M. Bhandarkar, and R. Brunner, "NAMD2: greater scalability for parallel molecular dynamics," *Journal of Computational Physics*, vol. 151, no. 1, pp. 283–312, 1999.
- [155] J. C. Phillips, R. Braun, W. Wang, J. Gumbart, E. Tajkhorshid, E. Villa, C. Chipot, R. D. Skeel, L. Kalé, and K. Schulten, "Scalable molecular dynamics with NAMD," *Journal of Computational Chemistry*, vol. 26, no. 16, pp. 1781–802, 2005.
- [156] S. Weiner and P. Kollman, "A new force field for molecular mechanical simulation of nucleic acids and proteins," *Journal of the American Chemical Society*, vol. 106, no. 3, pp. 765–784, 1984.

- [157] S. Weiner, P. Kollman, D. Nguyen, and D. Case, "An all atom force field for simulations of proteins and nucleic acids," *Journal of Computational Chemistry*, vol. 7, no. 2, pp. 230–252, 1986.
- [158] D. Tan and Z. Chen, "On A General Formula of Fourth Order Runge-Kutta Method," *Journal of Mathematical Science & Mathematics Education*, vol. 7, no. 2, pp. 1–10, 2012.
- [159] J. E. Subotnik and N. Shenvi, "A new approach to decoherence and momentum rescaling in the surface hopping algorithm.," *The Journal of Chemical Physics*, vol. 134, no. 2, p. 024105, 2011.
- [160] C. Zhu, S. Nangia, A. W. Jasper, and D. G. Truhlar, "Coherent switching with decay of mixing: An improved treatment of electronic coherence for non-born-oppenheimer trajectories," *The Journal of Chemical Physics*, vol. 121, no. 16, pp. 7658–7670, 2004.
- [161] C. Zhu, A. W. Jasper, and D. G. Truhlar, "Non-Born-Oppenheimer Liouville-von Neumann dynamics. Evolution of a subsystem controlled by linear and population-driven decay of mixing with decoherent and coherent switching," *Journal of Chemical Theory and Computation*, vol. 1, no. 4, pp. 527–540, 2005.
- [162] M. Casalegno, S. Zanardi, F. Frigerio, R. Po, C. Carbonera, G. Marra, T. Nicolini, G. Raos, and S. V. Meille, "Solvent-free phenyl-C61-butyric acid methyl ester (PCBM) from clathrates: insights for organic photovoltaics from crystal structures and molecular dynamics.," *Chemical Communications*, vol. 49, no. 40, pp. 4525–7, 2013.
- [163] T. Liu and A. Troisi, "What makes fullerene acceptors special as electron acceptors in organic solar cells and how to replace them.," *Advanced Materials*, vol. 25, no. 7, pp. 1038–41, 2013.
- [164] G. Paternò, A. J. Warren, J. Spencer, G. Evans, V. G. Sakai, J. Blumberger, and F. Cacialli, "Micro-focused X-ray diffraction characterization of high-quality

- [6,6]-phenyl-C61-butyric acid methyl ester single crystals without solvent impurities," *Journal of Materials Chemistry C*, vol. 1, no. 36, p. 5619, 2013.
- [165] J. Blumberger, "Recent Advances in the Theory and Molecular Simulation of Biological Electron Transfer reactions," *Chemical Reviews*, vol. 182, pp. 112–130, 2015.
- [166] S. Fratini and S. Ciuchi, "Bandlike Motion and Mobility Saturation in Organic Molecular Semiconductors," *Physical Review Letters*, vol. 103, no. 26, p. 266601, 2009.
- [167] M. C. Sherman and S. A. Corcelli, "Thermal equilibrium properties of surface hopping with an implicit Langevin bath," *The Journal of Chemical Physics*, vol. 142, p. 024110, 2015.
- [168] P. V. Parandekar and J. C. Tully, "Mixed quantum-classical equilibrium," *The Journal of Chemical Physics*, vol. 122, no. 9, p. 094102, 2005.
- [169] G. Granucci, M. Persico, and A. Toniolo, "Direct semiclassical simulation of photochemical processes with semiempirical wave functions," *The Journal of Chemical Physics*, vol. 114, no. 24, pp. 10608–10615, 2001.
- [170] P. Cieplak, F.-Y. Dupradeau, Y. Duan, and J. Wang, "Polarization effects in molecular mechanical force fields.," *Journal of Physics: Condensed Matter*, vol. 21, p. 333102, 2009.